Molecular Dynamics Simulations Study of Hydrophilic and Hydrophobic Interactions between Nanoscale Particles

Changsun Eun

A dissertation submitted to the faculty of the University of North Carolina at Chapel Hill in partial fulfillment of requirements for the degree of Doctor of Philosophy in the Department of Chemistry.

Chapel Hill
2010

Approved By:

Prof. Max Berkowitz

Prof. Chris Fecko

Prof. Andrew Moran

Prof. Lee Pedersen

Prof. Sergei Sheiko

ABSTRACT

Changsun Eun: Molecular Dynamics Simulations Study of Hydrophilic and Hydrophobic Interactions between Nanoscale Particles
(Under the direction of Max L. Berkowitz)

This dissertation presents our research on hydrophilic and hydrophobic interactions performed using molecular dynamics (MD) simulations with nanoscale model plates. Hydrophobic and hydrophilic interactions have been discussed in many places of chemistry and biology to explain water-involved phenomena such as solute aggregation and protein folding. However, until recently, the absence of appropriate methodology and insufficient computing power has prevented quantitatively detailed discussions of these phenomena. In this dissertation, we design model hydrophilic and hydrophobic plates and use MD methodology to study the nature of the hydrophobic and hydrophilic interactions. These plates are simple enough to be computationally accessible but still applicable for understanding the essence of hydrophobic and hydrophilic phenomena in nature. Since the hydrophobic and hydrophilic interactions are considered to be medium effects involving water molecules, we extract this medium contribution from the total interaction between two plates in water and analyze it. This analysis is applied to the case of two interacting model lipid plates across water and it demonstrates that the monotonic repulsive interaction between lipid bilayers, known as the hydration force, originates from the water-induced interaction, and not from the steric repulsions between the headgroups. Further detailed thermodynamic and hydrogen bonding analyses

indicate that strong plate-water interaction is responsible for the repulsive water-mediated interaction. Interestingly, when we remove electric charges from the model lipid plate, the repulsive character due to water changes to the attractive character and the overall shape of the total interaction is very similar to typical hydrophobic interaction. We investigate the hydrophobic property of the charge-removed model lipid plate by comparing it with other hydrophobic plates based on the graphene plate model. From this comparison, we find that the roughness of the surface enhances the hydrophobic interaction. The graphene plates are also used to study the fluctuation of water between hydrophobic plates, which is considered to be a signature of the hydrophobic interaction.

ACKNOWLEDGEMENTS

First of all, I would like to express my sincere gratitude to my advisor Prof. Max L. Berkowitz for his continuous support, guidance and encouragement through my Ph.D. study. He has always been a great advisor to me. I learned many things from him including a professional attitude in research, and how to think scientifically, to perform research and to write papers. Without him, none of this work presented in this dissertation would have been possible.

I would also like to thank my committee members, Prof. Chris J. Fecko, Prof. Andrew M. Moran, Prof. Lee G. Pedersen and Prof. Sergei S. Sheiko for useful suggestions and their help. They have been always friendly to me and I appreciate their encouragement.

Next, I would like to thank all past and present group members, especially Dr. Zhancheng Zhang and Dr. Charles Davis. I have always been pleased to discuss scientific problems with Zhancheng and Charles, and they always gave me many useful and insightful ideas. Above all, they have all been really good friends throughout my Ph.D. I would also like to thank Dr. Sheeba Irudayam and Dr. Jhuma Das. In addition to their help and useful suggestions on this dissertation, they have provided an enjoyable work environment and I have always enjoyed many pleasuble discussions with them. Also, I need to thank Dr. Lanyuan Lu for his generous help in setting up the simulations when I was getting my research started. I wish all of them the best in their future endeavors.

I would like to thank my close friends in Chapel Hill. Dr. Ralph House has always been a good friend and I really appreciate his friendship. I would also like to thank Will and Jessica Alexander. I have been very lucky to know them. They always support me and help me a lot in many ways. I will never forget my friendship with them. I also must thank my Korean friends in the chemistry department, particularly Dr. Chang Jun Lee, Dr. Sangwook Wu, Dr. Jae Ho Shin, Dr. Jinwoo Park, Dr. Doo-Hyun Ko, Dr. Wonhee Jeong, Dr. Sungjin Park, Myoung-Ryul Ok, Ahyeon Koh and Soo Yeon Sim. Without them, my life in here would not be the same. I thank all other people at Chapel Hill who have interacted with me.

Finally, I would like to express my sincere love and my deepest gratitude to my parents. They have always supported and encouraged me throughout my entire life. I would also like to thank my brother, Youngsun, for everything. Without the endless love and help of my family, I would never be able to complete this desertation.

To my Parents and my Brother

TABLE OF CONTENTS

LIST OF TABLES

Page

LIST OF FIGURES

Page

ABBREVIATIONS

Å	Angstrom
CNT	Carbon Nanotube
COM	Center of Mass
CP	Choudhury and Pettitt
CRPC	Charge-removed phosphatidylcholine-headgroup
DPPC	Dipalmitoylphophatidylcholine
fs	Femtosecond(s)
ΔG	Change in Gibbs Free Energy
ΔH	Change in Enthalpy
k (or k_B)	Boltzmann Constant
K	Kelvin
kJ	Kilojoule(s)
LJ	Lennard-Jones
MD	Molecular Dynamics
mol	Mole(s)
MR	Marcelja and Radic
nm	Nanometer(s)
NPT	Constant Pressure Simulation
ns	Nanosecond(s)
NVT	Constant Volume Simulation
PC	Phophatidylcholine

POPC	Palmitoyloleoylphosphatidylcholine
ps	Picoseond(s)
ΔS	Change in Entropy
SPC/E	Simple Point Charge/Extended
PMF	Potential of Mean Force
T	Temperature
WCA	Week-Chandler-Andersen

Chapter 1:

Introduction

Water is the most abundant molecule in living organisms and it is believed to be essential for all living systems. Molecular-level studies have shown that water plays a very crucial role as a solvent or a biomolecule in biological processes and structuring biological systems.[1-3] Microscopically, water can interact with individual biomolecules and affect their structure[4-6] or dynamic behavior.[7-10] It can also mediate the interaction between two biomolecules, as in protein-DNA[11] and protein-ligand interactions[12]. In particular the latter water-mediated interaction can induce large-scale molecular assemblies such as multiprotein complex[13] and micelle/cell membrane[14], which are very crucial components in living cells. However, the fundamental principles governing these water-involved interactions have not yet been fully understood at the molecular level. For example, the prediction of three-dimensional structure of proteins from amino acid sequences, in which water-involved interaction plays an important role,[6] is still a challenging problem.[15] The reason for this difficulty probably comes from the many-body feature of water-involved interaction. For example, the interaction between two particles in water is not simply a particle-particle interaction but a particle-water-particle interaction, where many water molecules are involved while making a hydrogen bonding network around the particles.

One of the ways to simplify this complication would be to define particles (or molecules) as hydrophobic ("water-fearing") or hydrophilic ("water-loving") particles. For example, instead of particle-water-particle interaction, we regard the interaction as hydrophobic particle-hydrophobic particle interaction, or hydrophilic particle-hydrophilic particle interaction and so on. In this way, we can reduce a many-body problem to a two-body problem. Thus, it is important to characterize whether a particle is hydrophobic or hydrophilic.

There are two common ways to determine the hydrophobicity/hydrophilicity of a particle. One way is to measure the contact angle of a water droplet on the surface of the particle and the other is to determine the solubility (or the solvation free energy) of the particles. If a particle is large and flat enough, it would be ideal to perform the contact angle measurement, but otherwise, the measurement of solubility would be ideal. These methodologies with the concept of hydrophobicity/hydrophilicity have proven to be useful, particularly in macroscale experiments. However, practically, when the size of the system is reduced to the nanoscale level as in biomolecules in water, it is hard to use the above methods to determine the hydrophobicity/hydrophilicity.[16,17] Thus, hydrophobic and hydrophilic concepts are not well-defined at the nanoscale level and the boundary between them is vague in some cases; for example, CNT (carbon nanotube), which is commonly believed to be hydrophobic because of the non-polar atoms, can be regarded as hydrophilic in that it can hold water molecules inside it.[18] Moreover, at such a microscopic scale, the interaction between a particle and water, determining hydrophobicity/hydrophilicity, is highly dependent on the molecular details such as the density of atoms, the roughness of particle's surface,[19] the spatial arrangement of polar

atoms,[20] and the local geometry of the particle.[21] Complicating maters further, the behaviors of a particle in water depend on the presence/absence of other particles in the system. For example, water molecules between two plates could be depleted as in hydrophobic cases, although each separate plate shows wetting next to the plates.[22]

The complex nature of hydrophobic and hydrophilic phenomena at the atomic scale raises many scientific issues and has broadened the research field. Finding out what molecular properties of a particle cause hydrophobic or hydrophilic behavior, as well as making more clear and explicit definitions of hydrophobic/hydrophilic interactions are some of the important issues in this field that have yet to be resolved. In this dissertation, we study these issues systematically with model systems.

1.1 Scope of our study

The research fields associated with water are very broad and each field is a huge subject. Even within the field of physical chemistry, for example, research areas include water structures in phase diagram, the dynamics of water next to a hydrophobic particle, the kinetics in the aggregation of hydrophobic particles, and other topics. Thus, we need to clarify the scope of our study. Here, we are mainly interested in the interaction between two nanoscale particles in water, as shown in Figure 1-1b. Although this type of interaction is associated with the interactions in other types of systems, the study of the cases presented in Figure 1-1a and Figure 1-1c is beyond our scope. For example, we focus on the hydrophobic interaction rather than the hydrophobic hydration.

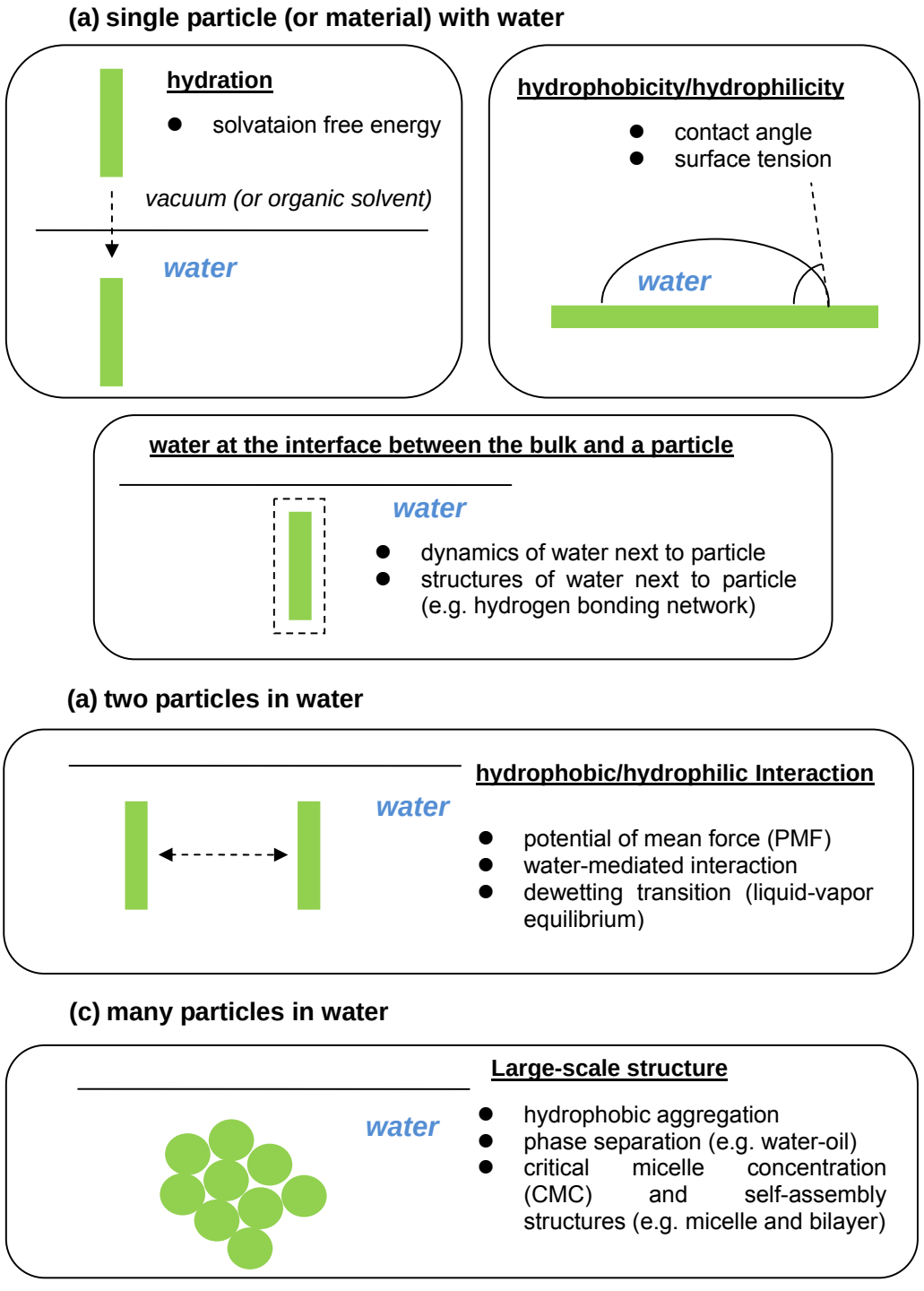

Figure 1-1. Schematic diagrams showing typical systems involving water. The list with bullet points indicates the physical properties or phenomena of interest from a physical chemist's viewpoint.

1.2 Goal of our study

Our primary goal is to understand the interaction between two nanoscale particles in water from a unified viewpoint. This requires the unification of the hydrophobic and hydrophilic interactions, which traditionally have been studied separately, into one single framework. In order to do that, we adopt Ben-Naim's definition of hydrophobic interaction defined by the attractive water-mediated interaction[23] and extend it to the discussion of hydrophilic interaction. We then apply this definition to our model study. As an example of hydrophilic interaction, we first reexamine an old problem about the origin of repulsive hydration force acting between two zwitterionic lipid bilayers.[24,25] This study also resolves the controversy in the origin of the repulsion as to whether it is due to the structured water or the molecular protrusion.[26,27] Then we devise a hydrophobic case derived from the lipid bilayers. This allows us to directly compare both cases of hydrophobic and hydrophilic interactions in one model system.

However, this hydrophobic model is not a typical hydrophobic particle in that the model surface is rough. Thus, we consider a second system, a smooth-surface graphene plate, as a more common type. The goal of the study with graphene is to systematically investigate the nature of hydrophobic and hydrophilic interactions between two plates as a function of the strength of water-graphene interaction. For this study, we use a smaller size of graphene plate, compared to the hydrophobic model lipid bilayer, to reduce the computational cost and to perform more MD simulations with different types of "graphene." Here, another objective is to consider the definition of hydrophobic interaction defined by the water number fluctuations in the space between two "graphene" plates.

The final objective is to understand the effect of the roughness of the surface on the hydrophobic interaction between two particles, by comparing the cases of the hydrophobic model lipid bilayer and the “graphene” plate.

1.3 Model systems in our study

In this dissertation, we design multiple model systems for different purposes of study. But basically, they can be categorized into two groups as demonstrated by the two columns of Figure 1-2. In Chapters 2 and 3, we use a model lipid bilayer named the PC(Phosphatidylcholine)-headgroup plate, a hydrophilic plate which has polar headgroups. This is shown in System A of Figure 1-2. This plate is used for the study of the origin of the hydration force. In Chapter 4, we use graphene-based carbon plates shown in Systems B, C and D of Figure 1-2 for the study of hydrophobic and hydrophilic interactions. In Chapter 5, along with the above systems, we additionally prepare the hydrophobic plate simply by removing charges from the PC-headgroup plate, as in System E of Figure 1-2. Detailed descriptions of the model systems are given in the methodology sections of the relevant chapters.

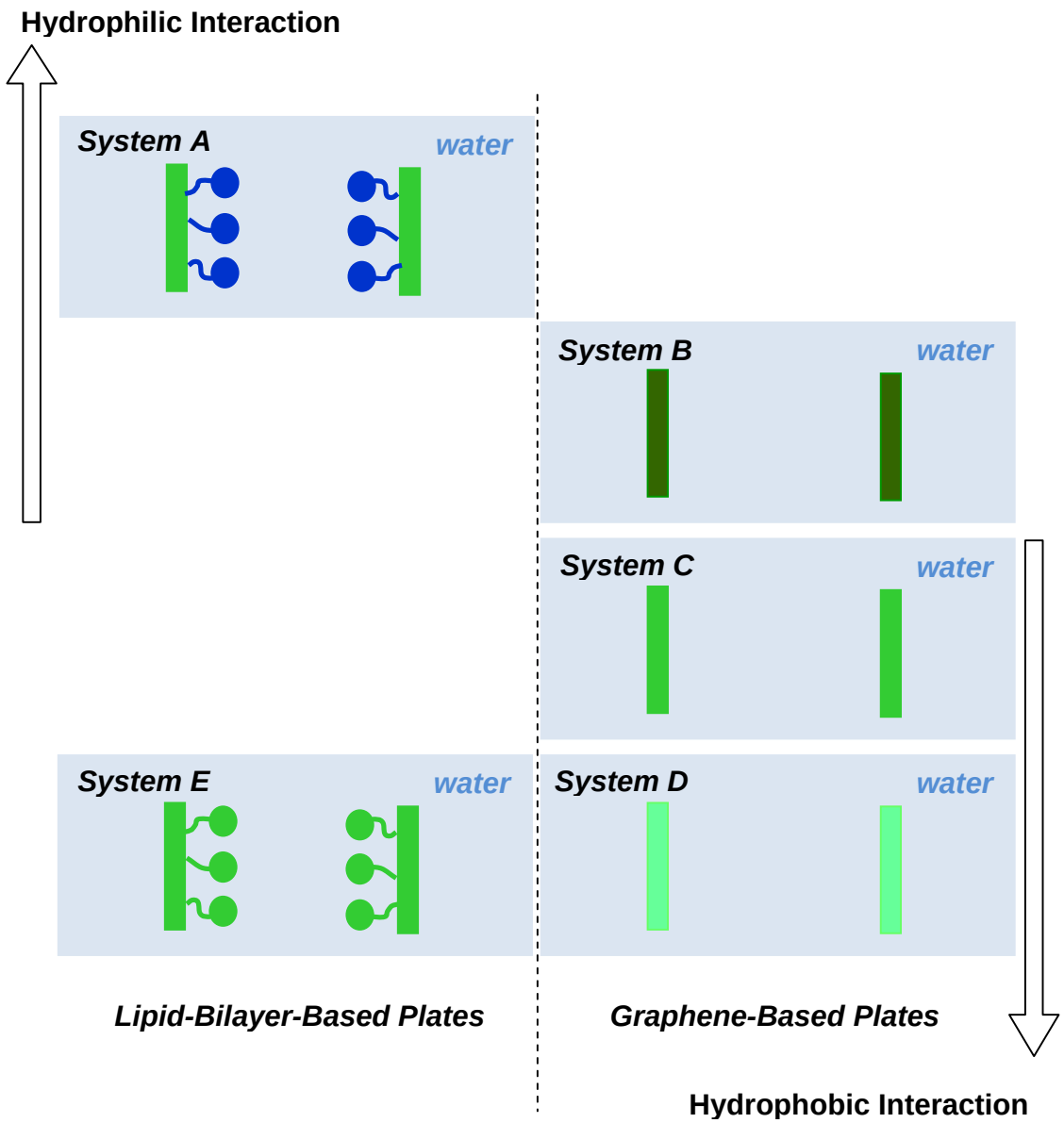

Figure 1-2. Schemactic of the model systems employed in our study. The plates in Systems A and E are based on a lipid biayer and the plates in Systems B, C and D are on graphene. Note that polar and non-polar parts are represented by blue and green colors, respectively. Here, the brightness of green colors in Systems B, C and D indicates the strength of interaction between water and plate, with the strongest interaction in System B and the weakest on in System D.

1.4 Outline of the dissertation

The initial motivation of our research is to understand the origin of the "hydration force," a repulsive interaction between zwitterionic lipid bilayers.[24,25] This origin has been explained by two prevailing theories. One theory is that the origin is due to the structured water molecules next to the lipid bilayers and the other one is that it is due to the protrusion of the headgroups of the lipid molecules. However, which one of these theories is correct still remains unclear, and only some indirect experimental evidence supporting the origin due to water exists.[28] Thus, to resolve this issue clearly and to get a more detailed molecular insight, we use molecular dynamics (MD) methodology. The recent advances in computational methodologies and computing power allow us to revisit this relatively old problem about the origin of the hydration force. Chapter 2 and Chapter 3 are devoted to this study.

In Chapter 2, we describe the details of our MD simulations and the model lipid bilayer plate used in the study, which is a simplified representation of the original lipid bilayers for computational advantage. First, we make sure that this model plate can reproduce the characteristics of repulsive interaction observed in experiments. Then to understand the origin, we separate the interaction, or the potential of mean force (PMF) as a function of the interplate distance, into water-mediated interaction and direct interaction. Also, we investigate the structure of the confined space between model plates by calculating the density profiles of water and lipid headgroups, as well as the structural changes of the confined water molecules by calculating the oxygen-hydrogen (OH) bond orientations of water molecules.

In Chapter 3, we continue to the discussion of the origin of hydration force in terms of thermodynamics. To determine if the origin is entropic or enthalpic, we perform thermodynamic analysis by decomposing the PMF into entropic and enthalpic components. Additionally, we consider the correlation between this thermodynamic change and the change in hydrogen bonding analysis by conducting hydrogen bonding analysis.

In another view, the interaction we study in Chapters 2 and 3 could be considered as the interaction between hydrophilic surfaces. Interestingly, this allows us to study another type of interaction, hydrophobic interaction. By noting that the hydrophilicity of model plate comes from strong electrostatic interaction between the plate and water, we are able to prepare a hydrophobic plate by simply removing all the charges from the plate. Thus, we study the hydrophobic interaction between charge-removed model lipid bilayer plates. However, since this charge-removed plate is unique in that it has non-polar lipid headgroups, we also study how the roughness of the surface due to the non-polar headgroups affects the hydrophobic interaction by comparing it to the interaction between the corresponding plates without the headgroups, or smooth plates. These smooth plates are graphene plates or the hydrophobic plates derived from the graphene plates by reducing the interaction parameter between water and the plate. However the hydrophobic or hydrophilic effect of these smooth plates has not been studied intensively in terms of the hydrophobic interaction. Therefore, in Chapter 4 we first systematically study the relation between hydrophobicity, defined by the water-plate interaction, and hydrophobic interaction, in terms of PMF and the fluctuation of water in the confined

space, before we discuss the hydrophobic interaction of charge-removed plate in Chapter 5.

Chapter 4 investigates the hydrophobic and hydrophilic nature of the interaction between "graphene" plates, by calculating the PMF and the average number of water molecules in the confined space between two plates. Particularly, the latter is associated with the phenomenon known as dewetting transition. For a systematic study, we prepare a series of "graphene" plates: strong hydrophobic, weak hydrophobic and weak hydrophilic plates by adjusting the strength of the interaction between water and the plate. Besides the attractive nature of water-mediated interaction, the large fluctuations in water structure next to hydrophobic solutes is known as one of the hydrophobic effects. In this chapter, we apply this idea to study the hydrophobic interaction and we examine this property of fluctuation of water molecules between two plates, as a possible measure of the hydrophobic interaction. We discuss and summarize the changes in the characteristics of the PMFs as well as water number fluctuations in the interplate space, as functions of the water-plate interaction.

In Chapter 5, we focus on the hydrophobic interaction between the model lipid plates when all the charges of the plates are removed. First, we carry out the PMF calculation to show that the (water-mediated) interaction is attractive, which is the signature of a hydrophobic interaction. Then by comparing this case of rough surface with the cases of smooth surface as in a "graphene" plate, we investigate if the roughness can enhance the hydrophobic effect as is known from the contact angle measurements. Also, we study the effect of flexibility of the surface on the interaction. Additionally, we

investigate the correlation between the change in water-mediated interaction and the change in the number of water molecules confined between two hydrophobic surfaces.

Chapter 2:

Origin of the Hydration Force: Water-Mediated Interaction between Two Hydrophilic Plates

Changsun Eun and Max L. Berkowitz

Department of Chemistry, University of North Carolina at Chapel Hill, Chapel Hill, North Carolina, 27599

Published in *the Journal of Physical Chemistry B*, 113, 13222-13228 (2009)

Abstract

We performed molecular dynamics simulations on systems containing phosphatidycholine headgroups attached to graphene plates (PC−headgroup plates) immersed in water to study the interaction between phosphatidylcholine bilayers in water. The potential of mean force (PMF) between PC−headgroup plates shows that the interaction is repulsive. We observed three distinct regimes in the PMF depending on the interplate distances: the small distance regime, intermediate distance regime, and large distance regime. We believe that the repulsive interaction in the intermediate interplate distance regime is associated with the hydration force due to the removal of water molecules adjacent to the headgroups

2.1 Introduction

Initial measurements of the interaction force acting between lecitin bilayers demonstrated that this force is repulsive and that it could be fitted by an exponential function with the characteristic exponential decay length, λ, which was in the range of 3 Å.[24] This length scale inspired the idea that the nature of the force originated from the presence of water molecules between the bilayers and that it was due to the induced orientational polarization of water. For this reason, the force was named the hydration force.[24] Subsequent experiments questioned the original idea that the total force has its origin in water only; instead, they indicated that just a part of the force has. Thus, according to McIntosh and Simon,[28] the repulsive force acting between phospholipid bilayers in water has three components: steric, hydration, and undulation. The steric component is dominant at short separations between membrane surfaces (when the fluid space between bilayers is below 0.4 nm), the hydration component is dominant at intermediate separation distances (0.4−0.8 nm), and the undulation component is dominant at larger separation distances (above 0.8 nm). The Marcelja and Radic phenomenological theory[29] initiated a series of theoretical papers where an attempt was made to clarify the nature of the hydration force.[25,30-35] In some of the work, the idea that the force has a hydration component has been completely abolished; instead, it was proposed that the repulsive force acting between lipid bilayers is due to the protrusion of lipid molecules.[26] Computer simulations were also performed to study the nature of the force.[36-38] Simulations of water next to lipid bilayers showed that indeed water in the vicinity of the bilayers was polarized and that this polarization did not propagate over a long distance.[36] Therefore, these simulations painted a qualitative picture that was similar

to the one obtained from the experiments of McIntosh and Simon. Simulations using the grand canonical Monte Carlo ensemble were performed to calculate the force as a function of distance at short distances.[38,39] Due to the complexity of the system, it was observed that it is not simple to separate the total force into components and that the values of the components were strongly depending on the force field used. To eliminate such complexity and in search for generic features related to the influence of water on the interaction between hydrophilic surfaces, Lu and Berkowitz proposed a simplified system where they represented a bilayer as a graphene plate and "dressed" up the plate with physical dipoles to represent the zwitterionic character of lipid molecules.[40,41] Although Lu and Berkowitz were able to illustrate some of the theoretical predictions that the force depends on the distribution of dipoles on the surface of the bilayer,[42] the major shortcoming in their model was the rigid character of the dipoles. In this chapter, we present simulations that, although again are performed on a simplified model of a bilayer, are done using a more realistic model, where the headgroups of lipids are faithfully reproduced and therefore allowed to move in response to the water motion, therefore avoiding the main handicap present in the model of Lu and Berkowitz.

2.2 System and Computation Details

We prepared our model phospholipid membrane surface by attaching 9 phosphatidylcholine (PC) headgroups to a graphene plate composed of 252 carbon atoms with a distance of 0.14 nm between the carbon atoms. The oxygen atom at the end of the phosphate group was bonded to the carbon atom of the graphene plate, but otherwise, the PC headgroup could freely move (see Figure 2-1). The graphene plate dimensions we used are 2.425 nm by 2.380 nm, so that the area per headgroup is 64 $Å^2$.

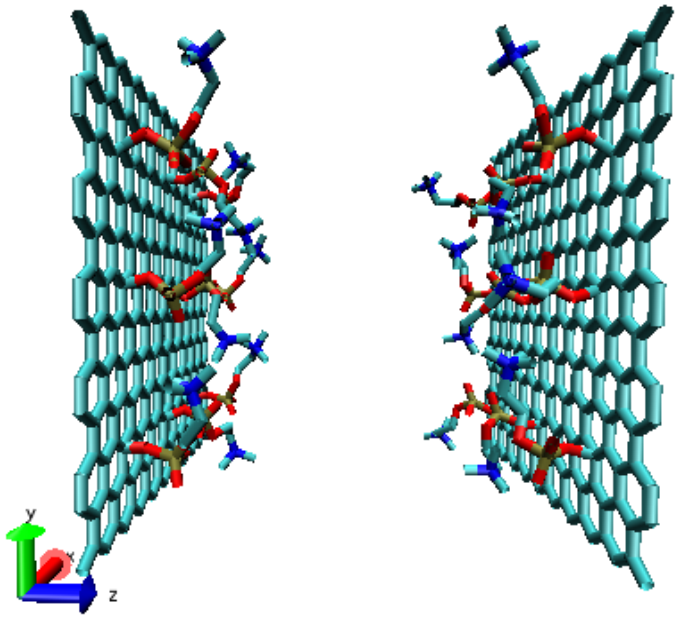

Figure 2-1. Snapshot of the two PC−headgroup plates in water at an interplate distance of 2.4 nm. For clarity, the two plates are only shown. Carbon and united carbon with hydrogen, nitrogen, phosphorus, and oxygen are colored in cyan, blue, tan, and red, respectively.

To calculate the potential of mean force (PMF) as a function of the distance *r* between the centers of two plates, we employed the thermodynamic perturbation method

previously used to calculate the PMF between two graphene plates in water.[43] Therefore, the states of the system were defined by this interplate distance, which was changed from 0.70 to 3.00 nm with an interval of 0.01 nm. The Gibbs free energy change between two adjacent states specified by r_1 and r_2 at a given temperature T was calculated on the basis of the following formula $\Delta g_1 = -k_B T \ln\langle e^{-(U(r_1)-U(r_2))/k_B T}\rangle_1$ assuming that the state of r_2 is slightly perturbed from the state of r_1. Here, k_B is Boltzmann's constant and U is the potential energy of the system. The bracket denotes an ensemble average with respect to the reference state of r_1. Since, equivalently, the r_1 state can be considered as a perturbed state from the state r_2, we also calculated Δg_2 and took an average of Δg_1 and Δg_2 for the final Gibbs free energy change between the two states. Finally, by summing up all of these changes from a reference state to a given state defined by the interplate distance r and assuming the PMF at the largest distance to have a value of zero, we obtained the PMF as a function of interplate distance. The relation between the free energy and the force acting between the plates is given by $f = -\partial g/\partial r$.

In order to evaluate the potential energies of each state and their perturbed states for the PMF calculation and to calculate other physical quantities such as density profiles of water, we carried out a series of MD simulations under NPT conditions. For each interplate distance, the two prepared PC−headgroup plates were placed around the center of a cubic simulation box at a designated interplate distance and subsequently solvated by 8800 water molecules. Periodic boundary conditions were applied to this system. The simulation time for each MD run was 1 ns, and the trajectories from 500 ps to 1 ns were used for the data analysis. During the runs, the box size was fluctuating around the values of 6.5 nm by 6.5 nm by 6.5 nm to maintain the target pressure. The coordinates were

saved every 1 ps, and a time step of 2 fs was used. The temperature and the pressure were maintained at 298 K by a Nose−Hoover thermostat[44,45] and 1.0 bar by a Parrinello−Rahman barostat,[46] respectively. The coupling time constants for both are 0.5 ps. The particle mesh Ewald method[47] with a cutoff length of 0.9 nm was used for the electrostatic interaction, and the same cutoff length was also used for the van der Waals interaction. The SPC/E model was employed for water.[48] The force field for the phosphatidycholine headgroup was based on the palmitoyl-oleoyl-phosphatidylcholine (POPC) force field from the Tieleman group (http://moose.bio.ucalgary.ca/index.php?page =Structures_and_Topologies), and that for the graphene was from the G43a1 force field defined in GROMACS.[49] For vacuum simulations, we used the NVT ensemble at the same temperature as in the NPT simulation. We used GROMACS 3.3.1 to perform all of our MD simulations.

2.3. Results and Discussion

The calculated PMF as a function of the interplate distance between the PC−headgroup plates is shown in Figure 2-2. As we can see from this figure, the plates repel as the distance between them decreases. We also display the curve for the interplate interaction when the water is not present in the system. In this case, the interaction has a minimum at a distance around 1 nm, predicting a stable associated state. The observed repulsive interaction between the plates immersed in water is opposite in character to the so-called hydrophobic interaction, the interaction between hydrophobic particles in water.[50] In our system, containing PC−headgroup plates in water, each headgroup is charge neutral, but the charge distribution produces a nonzero dipole moment. Because of the electrostatic interaction between the plates and water, the water density near the headgroups increased. Therefore, we can call our plates “hydrophilic” plates, and we can consider the interaction between them as an example of a water-mediated interaction between two hydrophilic bodies.

(a)

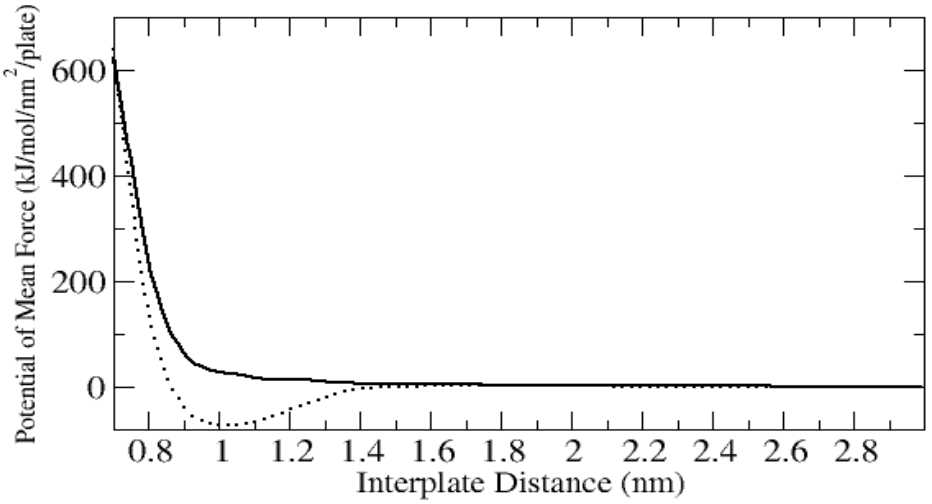

(b)

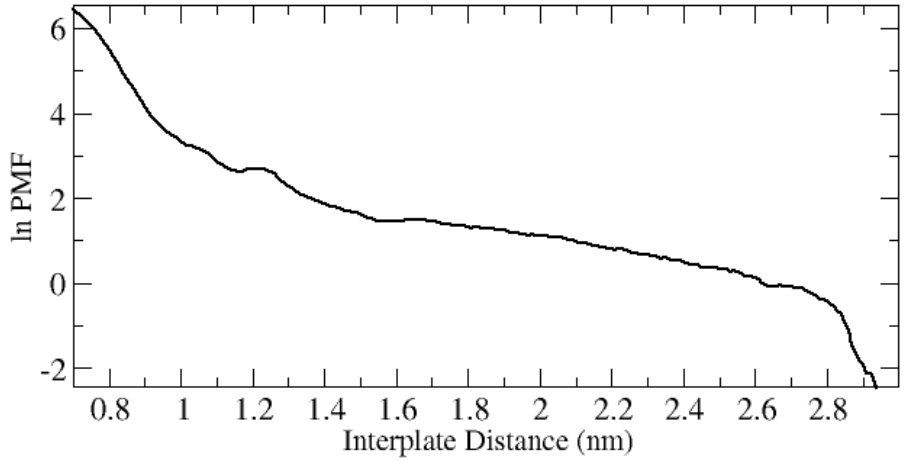

Figure 2-2. (a) PMFs between two PC−headgroup plates in water (solid line) and in a vacuum (dotted line) as a function of the interplate distance defined as the distance between two graphene plates. The PMFs at the largest separation of 2.99 nm are set to zero. The original PMF values are rescaled by dividing them by the area of the plate and the number of plates. (b) Logarithm of the PMF in water against the interplate distance.

From Figure 2-2, we can see that our PMF curve can not be fitted to a single exponential function. Following the ideas from the experiment, we attempted to fit it piece-wise and noticed that three distinct fitting regimes exist, as illustrated in Figure 2-3: a regime at small interplate distances (0.75−1.00 nm), intermediate interplate distances (1.00−1.60 nm), and large interplate distances (1.70−2.40 nm). In the small interplate distance regime, the PMF can be fitted to an exponential function $\exp(-x/\lambda)$ with a characteristic constant λ = 0.809 Å. In the intermediate interplate distance regime, the PMF is also well fitted with an exponential function, but with a larger lambda, 2.95 Å. In the third, large distance regime, the PMF can also be fitted to an exponential with λ = 7.82 Å. Since the relationship between the force f and the PMF g is $f = -\partial g/\partial r$, the forces in the corresponding regimes are also exponential.

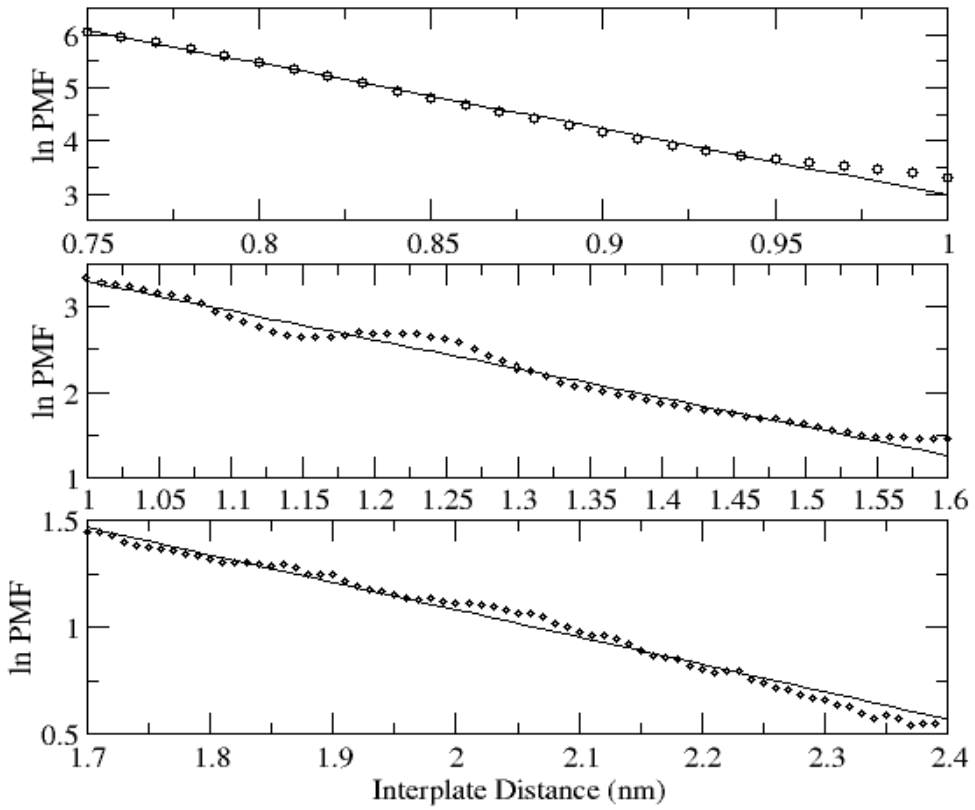

Figure 2-3. Best fits for the three distinct regimes of the logarithm of PMF obtained by a nonlinear curve fitting. The circles are the log PMF values for each interplate distance. To get high correlation coefficients, we considered the data from 0.75 nm for the small interplate distance regime (top panel) and we did not include the data between 1.6 and 1.7 nm, which corresponds to the boundary region between the intermediate interplate distance regime (middle panel) and the large interplate distance regime (bottom panel). In addition, we excluded the data beyond 2.40 nm for the large interplate distance regime. The correlation coefficients for the small, intermediate, and large interplate distance regimes are 0.99, 0.98, and 0.99, respectively. From the fitting curves, the characteristic exponents (λ) for the small, intermediate, and large interplate distances are 0.809, 2.95, and 7.82 Å, respectively.

Because water plays such an important role in determining the shape of the PMF, we also calculated the number of water molecules in the interplate space as a function of the distance between plates (see Figure 2-4) and found that the average water density, which is a slope of this curve, is a constant for the interplate distances above ~1.05 nm and it corresponds to the normal water density of 1 g/cm^3. The figure displays a clear break in the slope for distances below ~1.05 nm. This confirms that the origin of the force at distances above ~1.0 nm is quite different from the origin of the force below ~1.0 nm of the interplate space. Moreover, the reduction of water density at distances below 1.0 nm indicates that at these distances the headgroups may already engage in steric interactions.

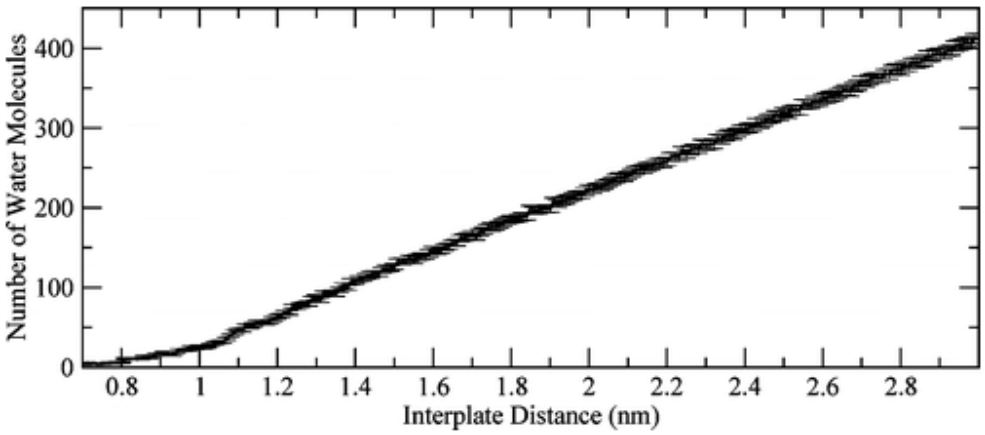

Figure 2-4. Number of water molecules in the interplate space, as a function of the interplate distance. The value at each interplate distance represents the average number of water molecules over the trajectory, and the corresponding error bar is calculated from the standard deviation.

To get more detailed information on densities, we calculated density profiles at certain interplate distances. The water density profiles are displayed in Figure 2-5. From the top panel of this figure, the water density profile at an interplate distance of 2.9 nm clearly shows that there are three kinds of water molecules in the interplate space: water molecules bound to the phosphates with the corresponding density peaks at −1.1 and 1.1 nm (we call this water phosphate water or inner water), water molecules next to choline moieties of the phoshatidylcholine headgroups with the corresponding density peaks at −0.85 and 0.85 nm (interfacial water), and water molecules interacting mostly with the other water molecules occupying space between −0.7 and 0.7 nm. The latter shows no density oscillations and has bulk-like density, and therefore, we call it bulk-like water. As the second panel of Figure 2-5 clearly shows, when we start reducing the spacing between plates, but still remain in the large interplate distance regime, bulk-like water molecules are getting removed as the plates are brought together. When the distance reaches a value of ~1.6 nm, most of the bulk-like water molecules are already removed and the remaining water molecules are interfacial. These molecules significantly interact with the phoshatidylcholine headgroups, and therefore, the free energy cost for removing these water molecules is different from the one when the bulk-like water is removed. The removal of mostly interfacial water molecules between the two PC−headgroup plates, that occurs when the interplate distance is in the interval from 1.6 to 1.0 nm, is responsible for the shape of the PMF at this distance interval. The profiles of water density in this regime are displayed in the third panel of Figure 2-5. In this regime, we observe that water density undergoes very substantial changes, from three peaks corresponding to layering of the interfacial water to no interfacial water. When the

interplate distance reaches a value of ~1.0 nm, only the phosphate waters remain in the system (the last panel of Figure 2-5), and therefore, we expect that direct interactions between headgroups significantly increase, as is also seen for the PMF in a vacuum (Figure 2-2). Notice that, in the small interplate distance regime, as the interplate distance decreases, the phosphate water molecules are removed and the two peaks in the water density corresponding to this water are merged into one peak that eventually disappears. Our water density plots clearly display a layering structure next to PC plates and their headgroups, and this layering is reflected in the small oscillation we observe in the PMF for the intermediate interplate distance regime (see the middle panel of Figure 2-3).

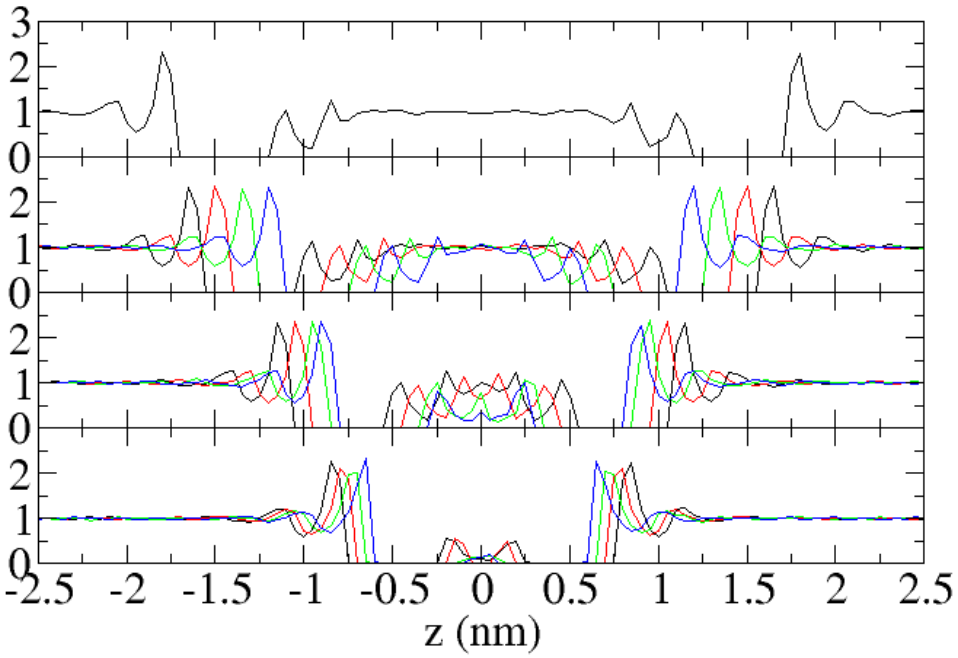

Figure 2-5. Number of water molecules in the interplate space, as a function of the interplate distance. The value at each interplate distance represents the average number of water molecules over the trajectory, and the corresponding error bar is calculated from the standard deviation.

Since we expect that the origin of the repulsive force in the small interplate distance regime is due to the strong steric interaction between the headgroups from each plate, and also for the purpose of comparison between the experiments and our simulations, we calculated the distribution of the *z* positions of the headgroups of each plate, specifically, the positions of the center of mass (COM) of the phosphate group and the COM of three end carbons of the choline group. The distributions of these coordinates are shown in the upper panels of Figure 2-6a−d. Generally, the distributions for phosphate groups are narrow, whereas the ones for choline are broad. From these panels, we observe that the overlap of *z* coordinates between the three carbons of choline is significantly increasing when the situation changes from the intermediate interplate distance regime to the small interplate distance regime. This suggests that the steric repulsion between the headgroups belonging to the different plates might be responsible for the exponential decay of the PMF in the small interplate distance regime. At the same time, the removal of the inner water molecules can still contribute to the interaction between the plates at this regime.

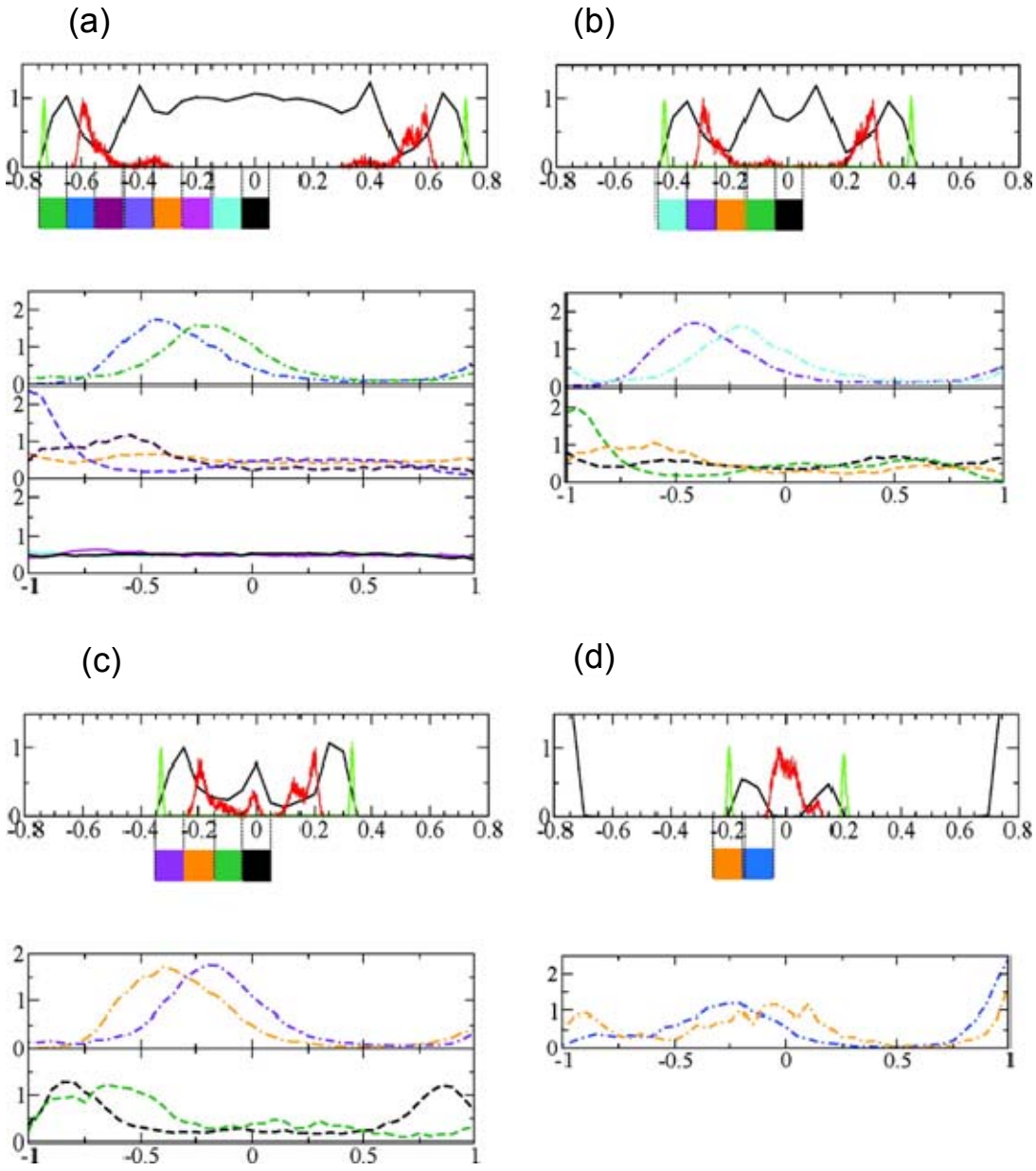
(a)
(b)
(c)
(d)

Figure 2-6. Superposition of the density profile of water (black) and the distributions of COM of three end carbons of choline (red) and COM of phosphate (green) are shown in the top panels at different interplate distances of 2.00 nm (a), 1.40 nm (b), 1.20 nm (c), and 0.90 nm (d) and the distributions of the OH bond orientation of water molecules in the bottom panels at the corresponding distances. The water density is normalized by the density of bulk water and the distributions for choline and phosphate are normalized to the value of unity. In the top panels, the abscissa corresponds to the *z* axis defined in the same way as in Figure 2-5; units are in nanometers. The bottom panels depict a series of the distributions for water in different regions, represented by different colors assigned below the density profiles (the same color is used to depict the distribution of the color-matched region). The distributions are grouped according to the characteristics of water: phosphate water (dot−dashed line), interfacial water (dashed line), and bulk-like water (solid line). The abscissa in the lower panels of part a−d corresponds to $\cos\theta$.

From the distributions shown in Figure 2-6, we estimated the values for the average distance along the *z* axis from the COM of the three carbons of the choline group of one plate to those of the other plate. Also, we did the same estimate for the phosphate groups. This analysis showed that the phosphate group is located 0.27 nm away from the plate, and the COM of choline is 0.45 nm away from the plate. For the purpose of comparison between the experiments and our simulations, we assume that the bilayer edge is located at the COM of choline, i.e., at a distance ~0.45 nm from the plate location. That means that when the interplate distance is 1.6 nm, the fluid interbilayer distance is 0.7 nm.

To get a deeper understanding of the origin of the hydration force acting between PC−headgroup plates, we calculated the orientational distributions of OH bonds of water molecules (see Figure 2-6) and looked at the snapshots taken from the simulations (Figure 2-7). To calculate the orientational distributions depending on the location of water molecules in the space between plates, we sliced the interplate space into intervals of 0.1 nm each along the *z* axis; the slice for the central bin corresponds to the interval from −0.05 to 0.05 nm. In the distributions, θ is the angle between the *z* axis (parallel to the normal vectors of the plates) and the direction vector from the oxygen atom of a water molecule to its hydrogen atom. Therefore, there are two θ's for each water molecule. We calculated $\cos\theta$ for the water molecules in a designated space (each slice) and then computed a distribution. Here, $\cos\theta = 0$ indicates that the OH bond is perpendicular to the *z* axis. In a large interplate distance regime, Figure 2-6a, the phosphate water molecules are roughly parallel to the PC plate rather than perpendicular, while the interfacial water molecules are situated in the opposite way. For the bulk-like water molecules, there is no orientational preference displayed, as we expected. These conclusions can also be confirmed by an inspection of the snapshot picture made at 1 ns of the trajectory (Figure 2-7). In an intermediate interplate distance regime, we consider the situation at distances in the middle of this regime, i.e., at distances of 1.4 and 1.2 nm. As Figure 2-6b shows, the distributions for the phosphate and the interfacial water molecules display the same tendency as for the corresponding waters from Figure 2-6a. Note that in this case there is no bulk-like water present in the system. In the intermediate interplate distance regime with one layer of interfacial water (1.2 nm), as Figure 2-6c shows, the pattern of the distribution for the phosphate water molecules is the same as

seen in Figure 2-6a and b, but the one for the interfacial water is different from those of Figure 2-6a and b. The presence of a single peak in the density profile of this water implies that interfacial water molecules strongly interact with both plates, whereas interfacial water molecules in cases described by Figure 2-6a and b mostly interact with only one of the plates. This can be clearly seen from the snapshots in Figure 2-7b and c. In a small interplate distance regime, Figure 2-6d, the pattern of distribution for the phosphate water molecules is different from those of the Figure 2-6a, b, and c cases. This is because some water molecules are interacting with both plates, as it is in the case of the interfacial water molecules from Figure 2-6c. Also, since the main properties of water are due to the presence of the hydrogen bonding network, we represent hydrogen bonds in Figure 2-7. At a large interplate distance case, the left panel of Figure 2-7a clearly shows that, while the bulk-like water molecules are oriented without any preferential direction, one OH bond of the interfacial waters is likely to be oriented perpendicular to the plate. The two OH bonds of the phosphate water molecules are situated almost parallel to the plate in order to maximize hydrogen bonding interactions with the phosphates. The right panel of Figure 2-7a presents the hydrogen bonding network between the phosphate water molecules and the phosphates of PC headgroups. As we see, the phosphate water molecules are located in between the PC headgroups and are interacting with the phosphates. Figure 2-7b, which depicts the case of an intermediate interplate distance regime at a separation of 1.4 nm, clearly demonstrates that the phosphate water molecules (yellow) are almost parallel to the plates and the OH bonds of the interfacial water molecules (green) are oriented perpendicular to the plates. Note that the interfacial water molecules form two water layers and the orientations of the water molecules are

symmetrical with respect to $z = 0$ (middle of the two plates). Contrary to the case of Figure 2-7b, at an intermediate interplate distance regime at separation of 1.2 nm, shown in Figure 2-7c, there is only one layer of the interfacial water molecules. These interfacial water molecules (circled with cyan) are interacting with both interfaces, while the water molecules in the case of Figure 2-7b are interacting with only one interface. For the case of the small interplate distance regime in Figure 2-7d, some of the OH bonds of the phosphate water molecules (circled with cyan) also make hydrogen bonds with the molecules from the other plate.

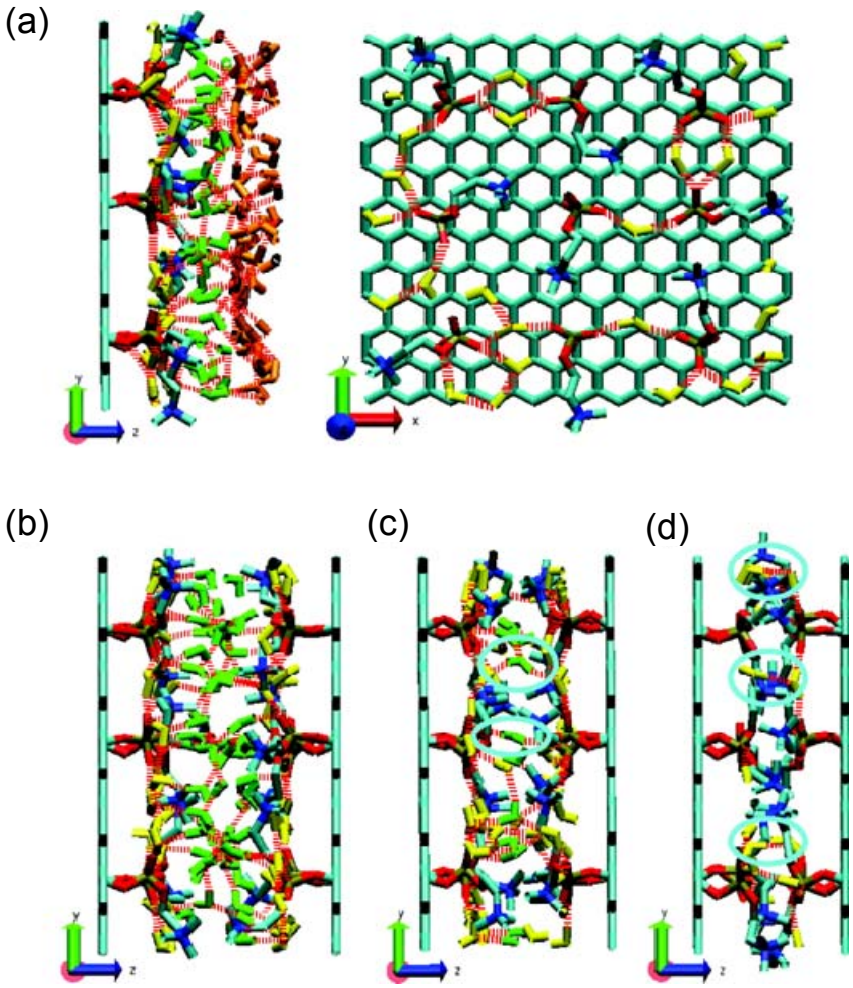

Figure 2-7. Snapshots of the interplate space at 1 ns of the trajectory at an interplate distance of 2.00 nm (a), 1.40 nm (b), 1.20 nm (c), and 0.90 nm (d). The phosphate water molecules, the interfacial water molecules, and the bulk-like water molecules are colored in yellow, green, and orange, respectively. The red dotted lines represent hydrogen bonds; we used for their definition a cutoff distance of 0.35 nm between a hydrogen bond donor atom and a hydrogen bond acceptor atom and a cutoff angle of 30° for the hydrogen−donor−acceptor angle. Due to the symmetry, we omit the right part of the interplate space in the left panel of part a. The highlighted molecules with the cyan circles in parts c and d are discussed in the text.

Finally, we would like to compare the observations from our simulations and from the experiments. The force in our MD simulations and the measured force from experiments have similar features: their action can be divided into three regimes fitted by exponential functions. Even the location of the regimes is somewhat similar. In the experiments of McIntosh and Simon, the hydration force regime appeared over distances from 0.4 to 0.8 nm in the fluid thickness which is basically the distance from the edge of one bilayer to the edge of the other bilayer.[28] In our simulations, the hydration force regime appeared when the range of interplate distances was from 1.0 to 1.6 nm. Since the fluid thickness is very close to the *z* directional distance between the choline groups, and these were 0.45 nm from the plates, our hydration force regime is corresponding to the region from 0.1 to 0.7 nm in the fluid thickness. Despite some difference in the fluid distance interval, which might come from the uncertainty in determining the fluid thickness in both simulations and experiment and also the truncation of lipid tails and absence of small scale protrusions in our model, the agreement on this issue between our result and the experiment is quite good. The agreement on the value of the exponent may depend on the quality of the fit of the curve to a multiexponential function, but for the hydration region of the force, we get a value of $\lambda \sim 0.3$ nm, the value often quoted as the exponent of the decay in this force.[25]

2.4 Conclusion

We model lipid bilayers as graphene plates decorated with flexible phosphatidylcholine headgroups attached to them and study the behavior of the free energy of interaction between these plates immersed in water as a function of distance between plates. The interaction energy displays three regions similar to the regions observed in the experiments, and like in the experiments, these regions can be fitted to exponential curves. For the region when the fluid spacing between plates is large (in our case, this happens when the fluid thickness is above 0.9 nm) and when there is bulk-like water in the fluid space, the force is small. In the experiments, this force is mostly due to the membrane undulations. In our simulations, the bilayer undulations, although present due to the flexible nature of the headgroups, have very different character compared to the ones in experimental bilayers. Our simulations clearly show the presence of the force correlated to the removal of water structures, the so-called hydration force, when we remove two to three layers of interfacial water, when the fluid space thickness is changed from 0.7 to 0.1 nm. Once all of the interfacial water is removed, the steric factor due to the overlap of the headgroups is mostly contributing to the interaction force, although water is also still contributing, because some inner water remains in the system.

The main goal in this chapter is to show that even a simple model, as the one we chose, is able to display the same features in the behavior of the interfacial force, as observed in experiments measuring the force acting between lipid bilayers. Specifically, the force is not a simple exponential force, but it can be represented as a force where different regions are dominated by forces of different origin. We observed that the hydration force is correlated to the removal of structured water in the interfacial space, and also observed

the restructuring of the hydrogen bonding network, as plates move toward each other and therefore the contributions to the force will have energetic and entropic components. These can be estimated by performing simulations at different temperatures, although the results will be very sensitive to the numerical noise in the calculations. Direct interactions between our surfaces that include the electrostatic interactions between the headgroups and also van der Waals interactions between the opposing graphene plates and also headgroups contribute to the force in the intermediate region, and the value of their contributions to the total free energy can be calculated. We describe how to perform such calculations in the Appendix. In Figure 2-8, we display the decomposition of the PMF into the contributions from the direct interaction and from the water-mediated interaction. As we can see from this decomposition, the direct interaction which consists of the van der Waals and electrostatic interactions is attractive, and therefore, the water contribution is repulsive for all separation distances. This means that even the long-ranged repulsive character of the force, which is due to undulations in experiments, is due to water in our simulations. From the form of the curve for the water-mediated interaction, we also can conclude that water-mediated force is mostly active at the interval between 1.6 and 1.0 nm, in agreement with our previous conclusion obtained from the consideration of the PMF. One should also understand that water indirectly influences the direct force by changing the character of the fluctuations of the headgroups on the plates, and therefore, it makes sense to call the total force in the intermediate interval the hydration force.

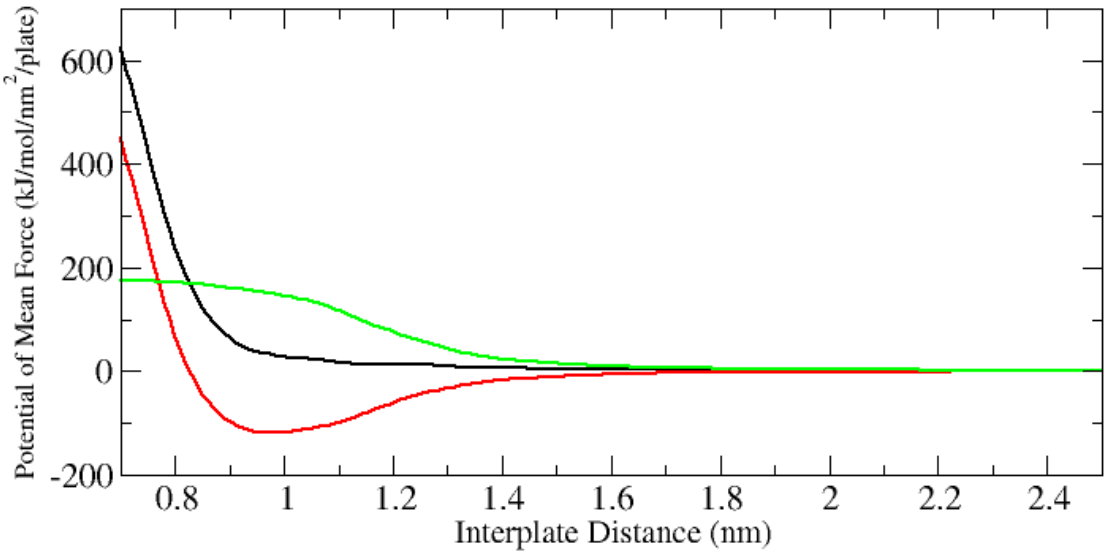

Figure 2-8. Decomposition of the PMF (black) into the contributions from direct interaction (red) and from water-mediated interaction (green)

Our simulations also show that protrusions are not needed to obtain the hydration force, since the model excludes protrusions. Comparison of the results from this simulation and previous work of Lu and Berkowitz also shows that flexibility of the headgroups plays an important role. Due to this flexibility, proper boundary conditions can be created to establish a nice hydrogen bonding network in water, while rigid dipoles on the plates can produce frustrations for creation of the hydrogen bonding network which results in a small hydration force. As we can see, although our model is still relatively simple, it provides a useful insight into the phenomenon of the hydration force.

Appendix

The Gibbs free energy change between two adjacent states specified by r_1 and r_2 at a given temperature T was calculated on the basis of the following formula $\Delta g_1 = -k_B T \ln\langle e^{-(U(r_1)-U(r_2))/k_B T}\rangle_1$ assuming that the state of r_2 is slightly perturbed from the state of r_1.

Since the potential is a sum of pairwise additive interactions, we can separate $U(r_1)$ into two terms, that is, $U(r_1) = u(r_1) + w(r_1)$. Here, $u(r_1)$ represents the interaction between the atoms belonging to PC−headgroup plates, which does not explicitly depend on the coordinates of water molecules, whereas $w(r_1)$ is dependent on the coordinates of water molecules. Using this separation, we get

$$\Delta g_1 = -k_B T \ln\langle e^{-(U(r_1)-U(r_2))/k_B T}\rangle_1 = -k_B T \ln\langle e^{-(u(r_1)+w(r_1)-u(r_2)-w(r_2))/k_B T}\rangle_1$$
$$= -k_B T \ln\langle e^{-(u(r_1)-u(r_2))/k_B T} e^{-(w(r_1)-w(r_2))/k_B T}\rangle_1$$
$$= -k_B T \ln\langle e^{-(u(r_1)-u(r_2))/k_B T}(1 + e^{-(w(r_1)-w(r_2))/k_B T} - 1)\rangle_1$$
$$= -k_B T \ln\langle e^{-(u(r_1)-u(r_2))/k_B T} + e^{-(u(r_1)-u(r_2))/k_B T}(e^{-(w(r_1)-w(r_2))/k_B T} - 1)\rangle_1$$
$$= -k_B T \ln\{\langle e^{-(u(r_1)-u(r_2))/k_B T}\rangle_1 + \langle e^{-(u(r_1)-u(r_2))/k_B T}(e^{-(w(r_1)-w(r_2))/k_B T} - 1)\rangle_1\}$$
$$= -k_B T \ln(\langle A\rangle + \langle B\rangle) = -k_B T \ln\left(\langle A\rangle\left(1 + \frac{\langle B\rangle}{\langle A\rangle}\right)\right)$$
$$= -k_B T \ln\langle A\rangle - k_B T \ln\left(1 + \frac{\langle B\rangle}{\langle A\rangle}\right)$$

where we denoted $\langle e^{-(u(r_1)-u(r_2))/k_B T}\rangle_1$ and $\langle e^{-(u(r_1)-u(r_2))/k_B T}(e^{-(w(r_1)-w(r_2))/k_B T} - 1)\rangle_1$ by $\langle A\rangle$ and $\langle B\rangle$, respectively. The first term in the result above is the contribution from the direct interactions, and the second term is the contribution from the water-mediated interactions. Therefore, we can define the first and second terms as $\Delta g_{1,d}$ and $\Delta g_{1,w}$, respectively, and get $\Delta g_1 = \Delta g_{1,d} + \Delta g_{1,w}$

$$\Delta g_{1,\mathrm{d}} \equiv -k_{\mathrm{B}}T \ln\langle \mathrm{e}^{-(u(r_1)-u(r_2))/k_{\mathrm{B}}T}\rangle_1$$

$$\Delta g_{1,\mathrm{w}} \equiv$$

$$-k_{\mathrm{B}}T \ln\left(1 + \frac{\langle \mathrm{e}^{-(u(r_1)-u(r_2))/k_{\mathrm{B}}T}(\mathrm{e}^{-(w(r_1)-w(r_2))/k_{\mathrm{B}}T} - 1)\rangle_1}{\langle \mathrm{e}^{-(u(r_1)-u(r_2))/k_{\mathrm{B}}T}\rangle_1}\right)$$

This result shows that the contribution from the direct interactions can be calculated by using the same trajectories obtained from our calculations of the total PMF. Note that, in the absence of water, $\Delta g_{1,w} = 0$, since $w(r_1) = w(r_2) = 0$. The water contribution can be obtained as a difference between the total PMF and the direct contribution.

Chapter 3:

Thermodynamic and Hydrogen-Bonding Analyses of the Interaction between Model Lipid Bilayers

Changsun Eun and Max L. Berkowitz

Department of Chemistry, University of North Carolina at Chapel Hill, Chapel Hill, North Carolina, 27599

Published in *the Journal of Physical Chemistry B*, 114, 3013-3019 (2010)

Abstract

We present further analysis of a system containing two graphene plates with attached phosphatidylcholine lipid headgroups embedded in water, which models a lipid bilayer. In Chapter 2, we performed molecular dynamics simulations on this system, calculated the potential of mean force (PMF) between plates (Eun, C.; Berkowitz, M. L. *J. Phys. Chem. B* **2009**, *113*, 13222−13228), and also performed a structural analysis of water in the confined space between the plates. Here, we perform thermodynamic analysis of the PMF and, in addition to the previous analysis of water that considered density plots and the OH bond orientational profiles, we perform hydrogen bonding analysis of water. We show that the structural analysis of water is consistent with the thermodynamic results we obtained for the PMF

3.1 Introduction

The hydration force acting between neutral lipid bilayers was first measured by LeNevue et al. in 1976.[24] While initially it was assumed that the force is exponentially decaying over the whole distance interval, more detailed measurements[51] showed that the force of interaction between neutral lipid bilayers in the liquid crystalline phase has three regimes: a long-range regime when the fluid spacing between membranes exceeds ~1 nm due to bilayer undulations, a short-range regime (when fluid spacing is below ~0.4 nm) due to steric repulsion of bilayers, and, finally, the intermediate-range regime, which is actually due to water and represents the proper "hydration" force. In addition to experimental work, a large amount of theoretical and simulation work[25,29,30,32,34-36,38-40,52-55] has been done to explain the nature of the hydration force. In Chapter 2, we performed molecular dynamics simulations on a model system, where the neutral lipid bilayer was represented as a graphene plate with attached phosphatidylcholine (PC) lipid headgroups, which we called PC-headgroup plates.[56] We used a model system to be able to efficiently calculate the free energy (or the potential of mean force, PMF) of plate interaction as a function of distance between plates and also to determine general principles related to the structure of water that induces the hydration force.

Lately, a lot of attention has been devoted to understanding the nature of interaction between hydrophobic particles.[50,57,58] To study characteristics of a possible hydrophobic interaction between nanoscale particles, Choudhury and Pettitt performed simulations on a system containing two graphene plates immersed in water.[22,43,59] To study the interaction between model hydrophilic particles, Lu and Berkowitz[40,41] used the graphene plates from the Choudhury and Pettitt simulations and assigned charges to

certain carbon atoms, so that the plates, while being neutral, had charges distributed on them. To connect their study to the problem of the hydration force acting between lipid bilayers, Lu and Berkowitz assigned charges in such a way that the charges, in a coarse-grained fashion, represented the zwitterionic character of lipid bilayers, such as dipalmitoylphosphatidylcholine (DPPC). The major shortcoming of the model used by Lu and Berkowitz was the rigid character of the dipoles. In our previous work,[56] we again studied the interaction between model hydrophilic surfaces, though, this time, the headgroups of lipids were faithfully represented and were allowed to move. Thus, our system contained two graphene plates (2.425 nm × 2.380 nm) with nine phosphatidylcholine (PC) headgroups attached to these plates, so that the area per headgroup is 0.64 nm^2, a value typical of the PC area observed in lipid bilayer experiments[60] and computer simulations.[61,62] The two plates separated by a certain distance were immersed into a large simulation box containing 8800 SPC/E water[48] molecules. The schematic picture of the system simulated, including a more detailed representation of the hydrophilic model plates and of the headgroup, is given in Figure 3-1.

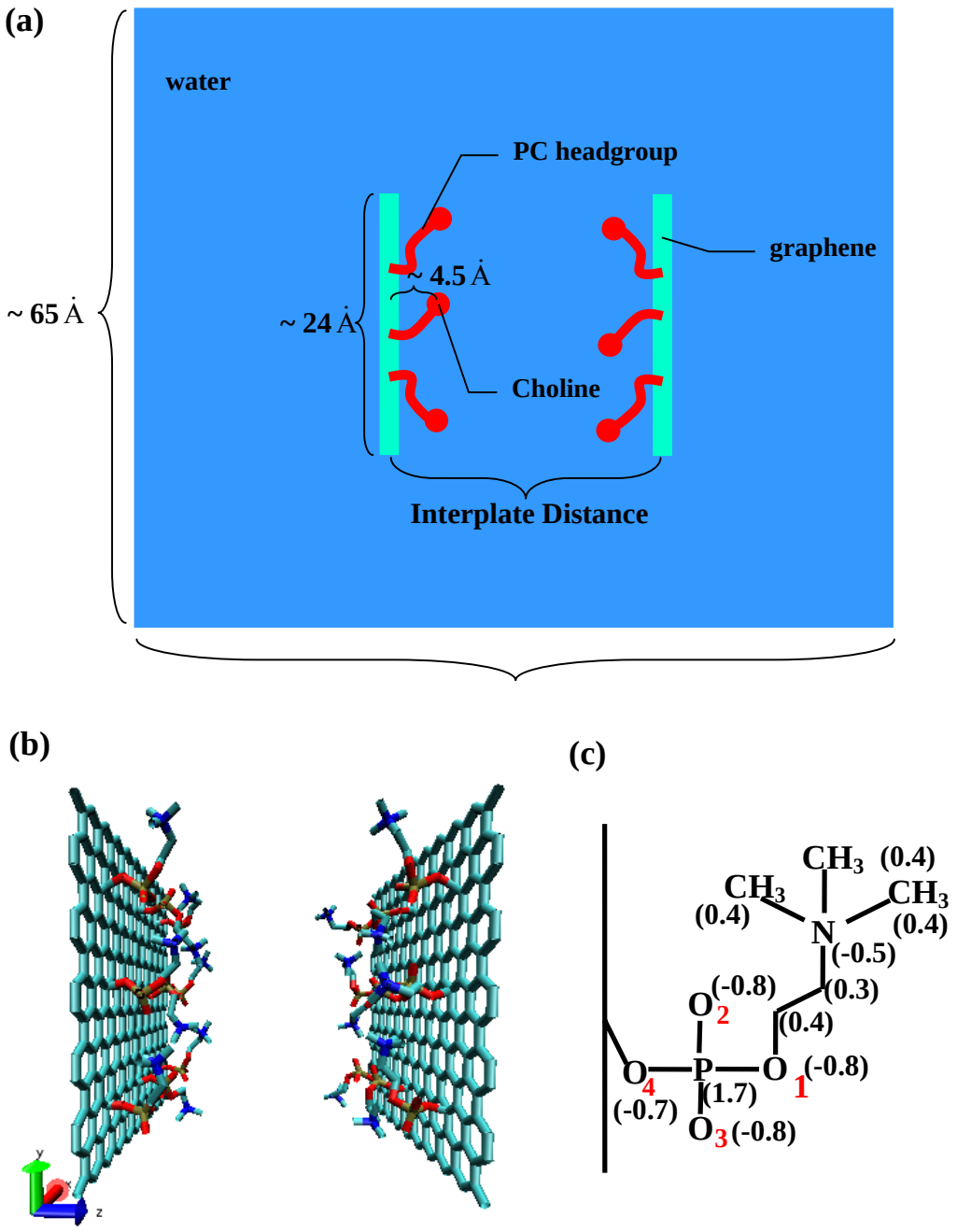

Figure 3-1. (a) Schematic diagram of our model system with associated length scales. (b) Snapshot of the PC-headgroup plates. (c) Detailed structure of the PC headgroup. The numbers in parentheses represent the magnitudes of partial charges (in units of the elementary charge, *e*).

Our previous calculations showed that the PMF has a repulsive character over all interplate distances. We also determined that the PMF has three regimes, and we were able to fit each of these to an exponential function. In parallel to the total PMF calculation, we also calculated the contributions to the free energy change due to the direct interaction between the plates and the water-mediated interaction. The total PMF, the direct contribution, and the water-mediated contribution are shown in Figure 3-2. We determined that the small distance regime of the interaction, when the plates are at distances below 1 nm and the fluid spacing below 0.1 nm, is due to steric repulsion between the headgroups. The intermediate distance regime, when the interplate distance is between 1 and 1.6 nm and the fluid spacing between 0.1 and 0.7 nm, is due to the removal of water structured by the surfaces. Finally, the large distance regime was also determined to be due to water in our simulation. In both the intermediate and large distance regimes, the water-mediated contribution acts in opposition to the direct contribution while the water-mediated contribution dominates. While both the water-mediated and direct contributions are small and nearly cancel in the large distance regime, the inset of Figure 3-2 with displayed error demonstrates that the total PMF in the large distance regime is due to water, which indicates that water is still slightly disturbed when the distance between the plates is in the range 1.6 to ~2.2 nm with a fluid spacing of 0.7 to ~1.3 nm. Since the long-range membrane undulation modes were not present in our simulations due to computational restrictions, our PMF could not have an undulation contribution. We also studied water properties by analyzing density profiles and orientational distributions of OH bonds of water in the confined region and showed that

structure of water is connected to the length scales of the three regimes observed in the PMF.

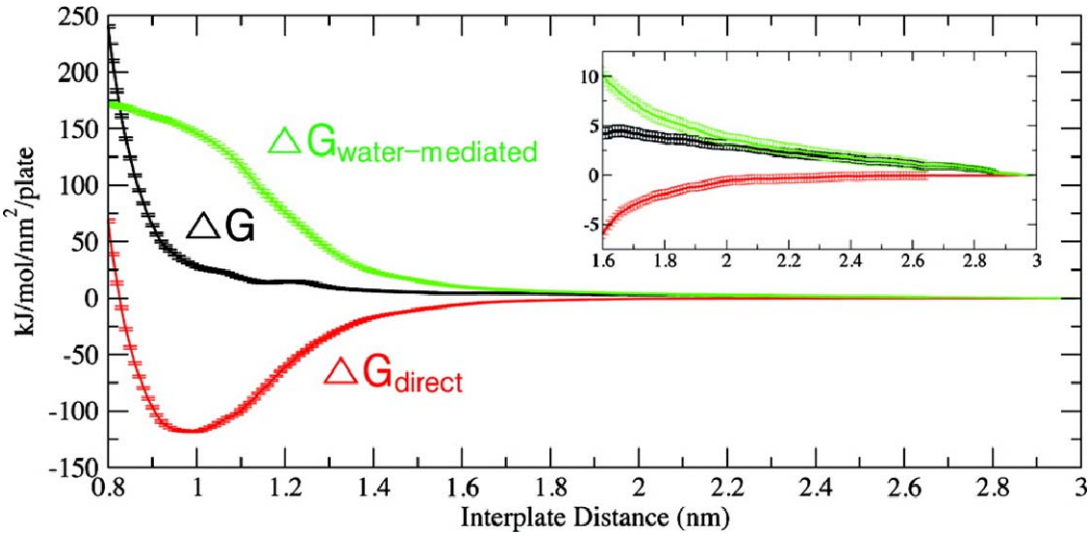

Figure 3-2. Decomposition of the PMF (black) into contributions from the direct interaction (red) and from the water-mediated interaction (green). Inset is for large interplate distances. Errors are represented by bars.

In this chapter, we further pursue our study of the nature of the PMF acting between lipid bilayers by performing a thermodynamic analysis of this PMF. We also perform an analysis of the hydrogen bonding network for water in confined space and show that this analysis may explain why water contributes to the PMF in the long-range regime. Our present work should be considered as complementary to our previous work that used the same model.

3.2 System and Computational Details

The same arrangement of the system as described in Chapter 2 is used in this work, with a depiction of the system provided in Figure 3-1. Previously we calculated the potential of mean force (PMF) between the two plates at thermodynamic conditions of P = 1 bar and T = 298 K. For this purpose, we performed molecular dynamics (MD) simulations on the system with plates fixed at a set of different interplate distances and used thermodynamic perturbation method[43] to obtain the PMF curve. The interplate distance was defined by the distance between two graphene plates. During the simulations the box size fluctuated around values of 6.5 nm × 6.5 nm × 6.5 nm. For our NPT simulations we used Nose−Hoover[44,45] temperature coupling and Parrinello−Rahman[46] pressure coupling algorithms. Electrostatic interaction was calculated through the particle mesh Ewald method.[47] More details about the preparation of the system and molecular dynamics simulations were described in the previous chapter.

To separate the PMF into the enthalpy−entropy contributions, we used the thermodynamic definition of entropy and employed the finite difference method[59,63] for its calculation:

$$-\Delta S(r) \equiv \left(\frac{\partial \Delta G(r)}{\partial T}\right)_{N,P} \cong \left(\frac{\Delta G(r, T + \mathrm{d}T) - \Delta G(r, T)}{\mathrm{d}T}\right)_{N,P} \qquad (3\text{-}1)$$

where $\Delta S(r)$ and $\Delta G(r)$ are the entropy and the Gibbs free energy changes from the reference state (r = 2.99 nm, where the free energy was assumed to have a zero value), to the state when the interplate distance had a value of r. In our calculation, the temperature difference, dT, was 10 K, thus requiring us to carry out an additional simulation at 308 K. Once we determined the entropy change, we calculated the enthalpy change, $\Delta H(r)$, by using the equation

$$\Delta H(r) = \Delta G(r) + T\Delta S(r) \tag{3-2}$$

Since PMF can be decomposed into contributions originating from the direct interaction between plates and water-mediated interaction,[56] as shown by eq 3-3:

$$\Delta G(r) = \Delta G_{\text{direct}}(r) + \Delta G_{\text{water-mediated}}(r) \tag{3-3}$$

we applied the finite difference method to each type of interaction and calculated enthalpic and entropic contributions for both direct and water-mediated interactions as well. In addition, to obtain a better understanding for the details involved in the enthalpy change, we calculated the potential energy change with respect to the reference state ($\Delta U(r)$), directly from the MD simulation at each interplate distance r, and further decomposed $\Delta U(r)$ into multiple terms:

$$\Delta U(r) = \Delta U_{\text{direct}}(r) + \Delta U_{\text{water-mediated}}(r) = \Delta U_{\text{direct}}(r) + \Delta U_{\text{water-water}}(r) + \Delta U_{\text{PC plate-water}}(r) \tag{3-4}$$

where $\Delta U_{\text{direct}}(r)$ and $\Delta U_{\text{water-mediated}}(r)$ are, respectively, the interaction potential energy between the PC-headgroup plates and the potential energy involving water molecules, which can be further separated into a water−water interaction ($\Delta U_{\text{water-water}}(r)$) and a water−plate interaction ($\Delta U_{\text{PCplate-water}}(r)$). All terms except $\Delta U_{\text{PCplate-water}}(r)$ are computed directly from the simulations, and $\Delta U_{\text{PCplate-water}}(r)$ is determined from eq 3-4.

Analysis of the hydrogen bonding network is a key ingredient for understanding the water−water and water−plate interactions. Therefore, we performed hydrogen bonding analysis using the standard geometry criterion for hydrogen bonds (H-bonds). According to this criterion, when the distance between oxygen atoms of the H-bond donor and the H-bond acceptor ($|\overrightarrow{OO}|$) is less than 0.35 nm and the angle between $|\overrightarrow{OH}|$ of the H-bond donor and $|\overrightarrow{OO}|$ is less than 30° and the hydrogen−oxygen (H-bonded) distance is less

than 0.245 nm, a hydrogen bond is considered to be formed.[64] Based on this criterion, we calculated the profiles of the number of H-bonds per water molecule and the number of H-bond donors/acceptors per water molecule. In that calculation, the position of the oxygen atom in a water molecule is considered as the position of the water molecule.

Errors for the PMF and the enthalpy−entropy calculation were estimated by using the block averaging method[65] and the standard error propagation method. For potential energy calculations and hydrogen bond calculations, we simply considered the standard deviation as an error.

All MD simulations were performed using the GROMACS 3.3.1[49] and GROMACS 3.3.3[49] suite of programs.

3.3 Results and Discussion

3.3.1 Thermodynamics

Enthalpic and Entropic contributions

To understand the thermodynamic basis behind the repulsive character of the interaction between our two hydrophilic plates immersed in water, we carried out entropy−enthalpy analysis of the PMF curve through the use of eq 3-1. The result is shown in Figure 3-3a. As we can see from this figure, while the enthalpic contribution is unfavorable when we squeeze the water out from the space between the plates, the entropic contribution is favorable (note that we plot the negative of the entropy change in units of energy ($-T\Delta S(r)$)).

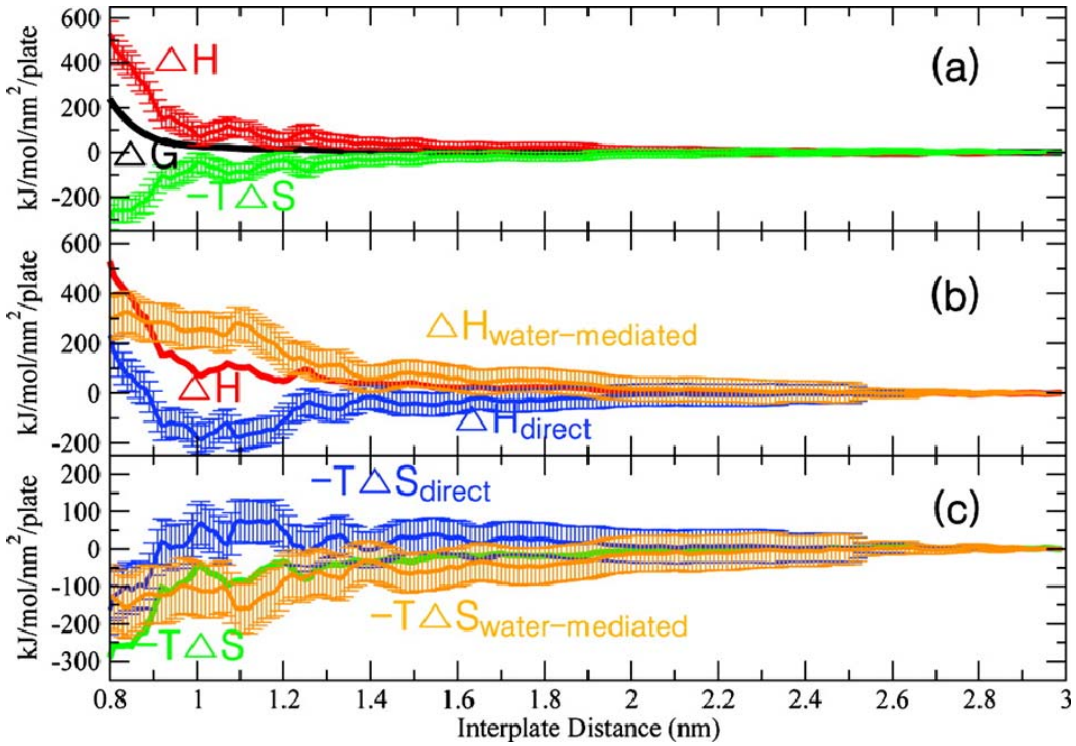

Figure 3-3. (a) Enthalpic (red) and entropic (green) contributions to the PMF (black). (b) Decomposition of the enthalpic contribution (red) into the direct interaction (blue) and the water-mediated interaction (orange). (c) Decomposition of the entropic contribution (green) into the direct interaction (blue) and the water-mediated interaction (orange). Errors are represented by bars.

For a more detailed understanding of the enthalpic and entropic parts of the PMF, we separated the entropic and enthalpic contributions further into direct and water-mediated contributions as depicted in Figures 3-3b and 3-3c. Figure 3-3b illustrates that the enthalpy change is dominated by the water-mediated contribution that is unfavorable due to removal of water from the interplate space. The direct contribution to the enthalpy change is favorable for large and intermediate distances and unfavorable for small distances; in its shape it is reminiscent of a van der Waals interaction as can be expected. The behavior of the direct and the water-mediated components contributing to the entropic part of the free energy change is shown in Figure 3-3c. As the figure shows, due to the release of water into the bulk-like environment, the water-mediated contribution is favorable at both intermediate and small distances. The direct contribution to entropy change is unfavorable at intermediate distances, but it is favorable at small. This likely is happening because, at intermediate distances, water restricts the conformational motion of the headgroups to support its hydrogen bonding network. Release of water, when the distance between plates decreases, removes the conformational constraints on these headgroups; as a result, the entropy increases. It is very hard to judge what is happening

in the large distance regime (at distances above 1.6 nm), since the error bars on Figure 3-3c are large in this regime.

Overall, the results displayed in Figures 3-2 and 3-3 show that the enthalpy change dominates the repulsive nature of the PMF. The results also show that the water-mediated contribution determines the repulsive nature of the PMF in the intermediate regime and that the water-mediated contribution is dominant for both entropy and enthalpy changes in this regime.

Potential Energy Change

Why is the water-mediated contribution into enthalpy change positive as the distance between plates decreases? To address this question, we need to perform a more detailed investigation of $\Delta H(r)$. Since enthalpy has two components (internal energy and a PV-work term, where P and V are pressure and volume of the system), we need to consider the internal energy change ($\Delta E(r)$) and the PV change (ΔPV) with respect to the reference state. The internal energy change can be directly calculated from the simulations. Regarding the PV term, it can be determined either by subtracting $\Delta E(r)$ from $\Delta H(r)$ or by direct calculation from the simulation. Since our simulations were done at constant P, and since we observed that the volume change is very small, the ΔPV term can be neglected. Furthermore, since the temperature of the system is constant, the kinetic energy change is zero and, thus, the internal energy change is equal to the potential energy change. In summary, $\Delta H(r) \approx \Delta E(r) \approx \Delta U(r)$. Therefore, the enthalpy change can be numerically calculated either from a difference between the free energy change and entropy change or directly from the energy change; in fact, Zangi and Berne[66] used the

latter method to calculate $\Delta H(r)$. Because our calculations contain numerical noise the results for enthalpy change from the two methods are not identical, but are still quite similar. Therefore, to examine the details of the enthalpy change, we examined the details of the potential energy change.

The total potential energy can be considered to be a sum of two terms: the first term due to the potential energy of interaction between two PC-headgroup plates (ΔU_{direct}) and the second term involving water molecules ($\Delta U_{\text{water-mediated}}$). For more detailed analysis, we also performed a separation of $\Delta U_{\text{water-mediated}}$ into contributions from $\Delta U_{\text{PCplate–water}}$ and $\Delta U_{\text{water–water}}$ according to eq 3-4; these are depicted in Figure 3-4. We observed that, as the interplate distance decreases, $\Delta U_{\text{PCplate–water}}$ begins to increase at ~1.6 nm and is saturated ~1 nm, whereas $\Delta U_{\text{water–water}}$ decreases until the interplate distance is ~1 nm and then increases. The increase of $\Delta U_{\text{PCplate–water}}$ with the decrease of the distance in the intermediate regime, especially in the distance interval from ~1.6 to ~1.3 nm, is somewhat unexpected as the number of hydrogen bonds between water and plates is not expected to change in this regime (see below). This increase, therefore, must be due to the decrease in the number of water molecules that interact with the PC-headgroups, but not through hydrogen bonding.

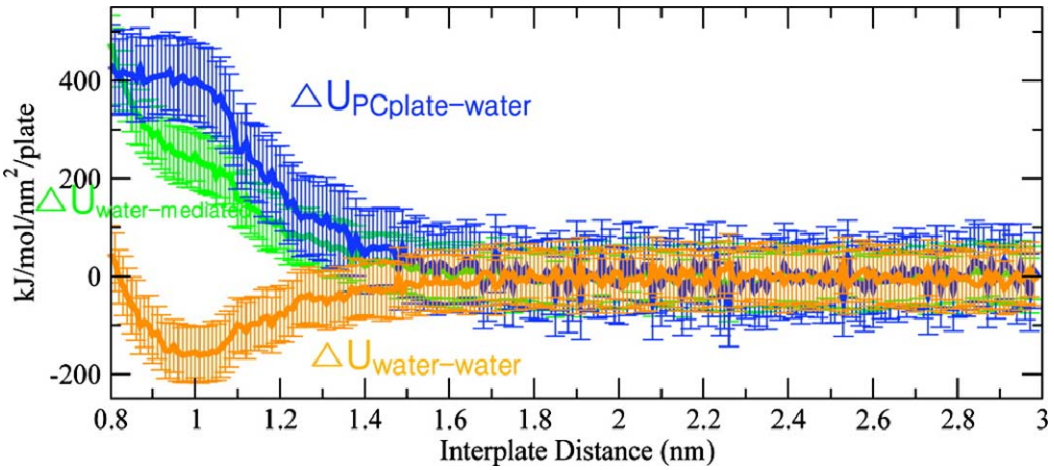

Figure 3-4. Potential energy contribution involving water molecules (green), further decomposed into the following two terms: potential energy of interaction between the PC-headgroup plates and water (blue) and potential energy of interaction between water molecules (orange). Error bars are obtained from standard deviation.

The observed behavior for the $\Delta U_{\text{water-water}}$ is not difficult to explain. At the intermediate separations, when the confined water molecules leave the interplate space for the bulk, the potential energy for water−water interaction decreases because the escaped water molecules interact with more water molecules in the bulk-like environment. At small separations, the water−water potential energy increases, as some water molecules (especially, waters next to phosphate groups) stay in the confined space due to a strong interaction between water and the plate, and these water molecules are more and more isolated from the water network as the interplate distance decreases.

From our analysis, we therefore conclude that in the intermediate distance regime the increase in energy of water−plate interaction dominates over the decrease in

water−water interaction energy: this balance is responsible for the observed positive change in the water-mediated contribution into the enthalpy as the distance between plates diminishes in the intermediate distance regime.

3.3.2 Hydrogen bonding analysis

In Chapter 2, we demonstrated that three different groups of water molecules exist in the confined space between PC-headgroup plates. The first group contains water molecules that are hydrogen bonded to phosphate groups of lipid headgroups and located in close proximity to phosphates; thus these molecules were named accordingly as phosphate waters. The second group contains water molecules around choline groups of the headgroups, i.e., molecules at the headgroup/water interface, and therefore these water molecules are named interfacial waters. Finally, the rest of the water molecules situated further from the surfaces were named bulk-like waters, although, as we will see, not all of them display bulk-like properties. We connected the different interaction regimes to changes in the water structure and the amount of water in the different groups mentioned above. It is clear that the thermodynamic changes we discussed in section are also associated with the change of the hydrogen bonding network. Below, we present an analysis of changes in the water hydrogen bonding network as the distance between plates changes, and we also present the connection between these changes and the thermodynamics of the system.

Number of Hydrogen Bonds

Based on the criteria presented in section, we calculated the average numbers of hydrogen bonds between the plates and water molecules, and between water molecules themselves as functions of interplate distance. Note that this calculation was performed for the entire space, and not only for the confined space, because the thermodynamic changes discussed in section result from changes which occurred in and out of the confined space. The results are reported in Figure 3-5. As we can see, the behavior of an average number of hydrogen bonds formed between plates and water in Figure 3-5a and the number of water−water hydrogen bonds from Figure 3-5b is consistent with the behavior of water-mediated potential energy change from Figure 3-4. Indeed, in the interval 1.6−1.3 nm, the number of water−plate hydrogen bonds does not change; therefore, the increase in water−plate interaction energy in this interval is due to non-hydrogen bonding energy change. The number of water−plate hydrogen bonds starts diminishing when the distance gets below 1.3 nm, and consequently, the water−plate interaction energy increases due to the loss of water−plate hydrogen bonding. The number of water−water hydrogen bonds also does not change before the distance between plates reaches 1.3 nm; it is the change in the strength of hydrogen bonding that decreases the energy of water−water interaction when the distance between plates is above 1.3 nm. Below the distance of 1.3 nm, the number of water−water bonds increases, and therefore, the corresponding energy decreases. When the interplate distance becomes smaller than 1 nm, the number of water−water hydrogen bonds decreases and the energy correspondingly increases.

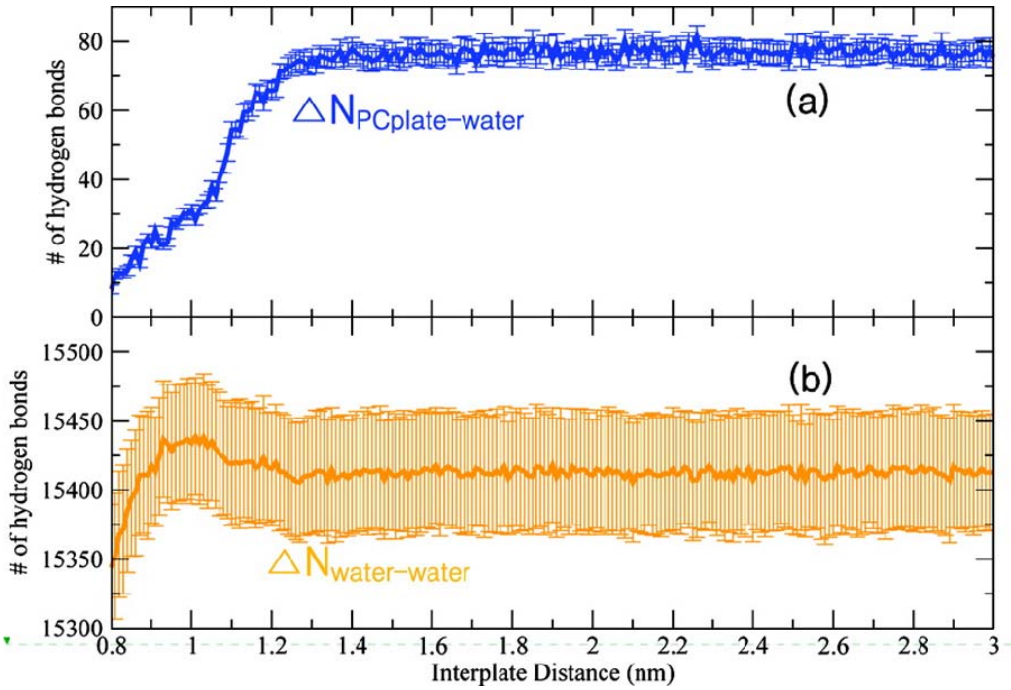

Figure 3-5. (a) Average number of hydrogen bonds between the PC-headgroup plates and water as a function of interplate distance. (b) Average number of hydrogen bonds between water molecules as a function of interplate distance. For direct comparison with Figure 3-3 we used the same colors. Error bars are obtained from standard deviation.

As we observed from Figure 3-5a, the decrease in the number of hydrogen bonds begins at ≈1.3 nm. This implies that some of the interfacial water molecules can also make hydrogen bonds with the phosphate groups of the plates, as phosphate waters do. Moreover, the fact that the strength of hydrogen bond between phosphates of the plate and water molecules is stronger than that between water molecules[67] can explain why the contribution of $\Delta U_{\text{PCplate–water}}$ into $\Delta U_{\text{water-mediated}}$ at distances below 1.3 nm is larger than the contribution of $\Delta U_{\text{water–water}}$. This shows that the presence of PC headgroups strongly

influences the structure of the water network; similar perturbation by polar headgroups to the water hydrogen bond network is also observed in solutions containing micelles[68] and reverse micelles.[69,70]

Hydrogen Bond Density Profiles

In Chapter 2 we performed density and orientational analyses of water between the PC-headgroup plates. We observed that water has bulk-like properties in the middle of the interplate space when the distance between plates is above 1.6 nm. At the same time, we observed that the repulsive interaction is present at the distances beyond 1.6 nm and it is also due to water. To understand the properties of water in the confined space between the plates and in the hope to observe that confined water is different from bulk water even when the interplate distance is beyond 1.6 nm, we calculated the average number of hydrogen bonds per water molecule in the confined space. In this calculation, all hydrogen bonds were taken into account, irrespective of whether the bonds were made with the PC headgroups or with other water molecules. The results are displayed in Figure 3-6. Here, the abscissa depicts the *z* axis of the system, which is perpendicular to both plates. The *z* coordinate of the point at the center between the two plates is set to zero and serves as a reference point. Thus, for example, if the two plates are at an interplate distance of 2.0 nm, one plate is situated at −1.0 nm and the other is at 1.0 nm. For comparison with the bulk water, water outside the plates (but confined in the *xy* dimensions to the plate size) is also considered.

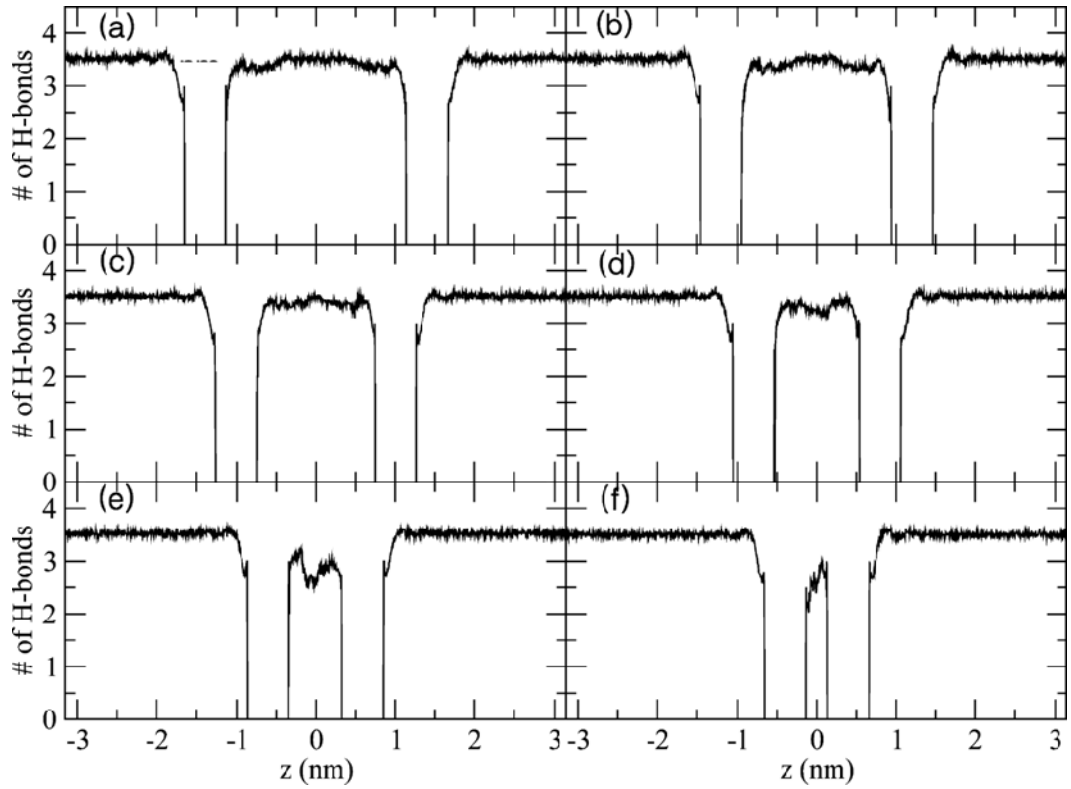

Figure 3-6. Profiles of the number of hydrogen bonds per water molecule at the interplate distances of 2.8 nm (a), 2.4 nm (b), 2.0 nm (c), 1.6 nm (d), 1.2 nm (e), and 0.8 nm (f).

Figure 3-6 indicates that the average number of hydrogen bonds per water molecule in the bulk (outside the confined space) is around 3.5, which is consistent with the previous calculation by Choudhury and Pettitt.[43] However, the number of hydrogen bonds per water molecule in the confined space is generally less than 3.5, especially at the intermediate and small separations (Figure 3-6d−f). We observed that the closer the plates are and the more confined the water is, the more the structure of water deviates from the bulk-like arrangement with its characteristic ~3.5 hydrogen bonds per water molecule. We can also compare the shapes of the profiles in the interplate space obtained

in this work with profiles obtained for the case of hydrophobic plates.[43] Although in both cases the heights of the profiles in the confined region decrease as the interplate distance decreases, in our case the decreasing height displays an undulating character, absent in the hydrophobic case. Clearly, in our case, as in the hydrophobic case, the confined water is restructured, but the water structure itself is different from the structure present in the hydrophobic case due to the different boundary conditions provided by hydrophilic and hydrophobic plates, respectively.

To better understand the details of the hydrogen bonding network in the confined water, we performed an additional analysis by specifying the donor or acceptor character of the hydrogen bond, i.e., by decomposing the number of hydrogen bonds per water molecule into two components: number of donor bonds and number of acceptor bonds. These numbers are equal for bulk water, but in the confined space between the plates, due to a specific structure of the network, we cannot expect them to be equal. Moreover, we expect the numbers to depend on the position along the *z* axis between the plates. Indeed, since our PC-headgroup plates have H-bond acceptors due to phosphates, water molecules next to the plates are mostly H-bond donors. However, for the confined water molecules that are situated further away, the opportunity to make hydrogen bonds with the phosphates decreases and, therefore, we expect the number of H-bond donors to decrease, while the number of H-bond acceptors per water molecule increases. This is indeed the situation, as one can see from Figure 3-7.

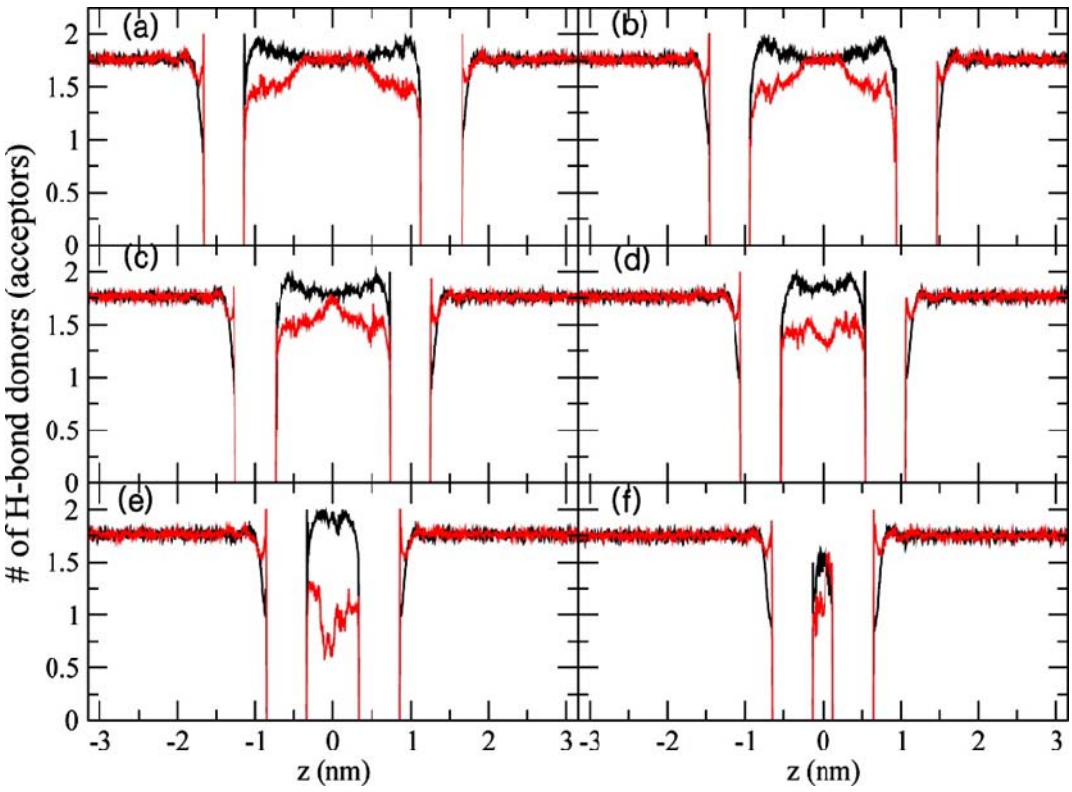

Figure 3-7. Profiles of the numbers of hydrogen bond donors (black) and acceptors (red) per water molecule at the interplate distances of 2.8 nm (a), 2.4 nm (b), 2.0 nm (c), 1.6 nm (d), 1.2 nm (e), and 0.8 nm (f).

Interestingly, the plots from Figure 3-7 allow us to perform a comparison of the H-bond donor/acceptor character of water molecules next to either hydrophobic or hydrophilic plates, since our PC-headgroup plate has both hydrophobic (outward with respect to the confined space) and hydrophilic (inward) sides. Both sides have a common feature in that they disturb the adjacent water structure, but in a very different way. The disparity in acceptor/donor character for water next to the hydrophobic side is short ranged (~0.25 nm), while the hydrophilic side has a longer range (~0.8 nm). From Figure

3-7 we observed that, next to the hydrophobic side, the average number of H-bond acceptors per water molecule is larger than the average number of H-bond donors. This occurs because, as it was observed previously, one of the OH bonds of the water molecule has a tendency to point toward the hydrophobic surface,[71] therefore diminishing its possibility to engage in hydrogen bonding as a H-bond donor. Contrary to this effect, near the hydrophilic side of the plate (the side with the PC headgroups), the average number of H-bond donors per water molecule is larger than the average number of H-bond acceptors, because, as was already explained above, of the presence of phosphate groups that accept hydrogen bonds from water. As we observed in Chapter 2, phosphate waters are nearly parallel to the plates and, therefore, can donate both of their hydrogen bonds to the plates; this is why the shoulders of hydrogen bond donor curves in Figure 3-7a−c reach the value of ~2.

The hydrogen bonding density plots presented in Figure 3-7 from this chapter are complementary to the number density and the orientational profile plots from the previous chapter. Together, the plots provide a qualitative description of the water structure in the interplate space. At large separations, such as the ones depicted in Figures 3-7a and 3-7b, real bulk-like water is present in the middle of the confined region. However, when the distance between plates is reduced below 2.1 nm (Figure 3-7c), the discrepancy in the number of donors and acceptors per water molecules appears, indicating that water starts deviating from having truly bulk-like characteristics. Note that both density profiles and orientational properties of water in Chapter 2 showed visible deviation from bulk-like properties only when the distance between plates was below 1.6 nm. The deviation of water from having true bulk properties at distances above 1.6 nm

that hydrogen bonding profiles in Figure 3-7 display is consistent with our observation of the large distance regime in the PMF. When the interplate distance is further reduced to 1.6 nm (see Figure 3-7d) and the intermediate distance regime of the PMF begins, the water molecules in the confined space are strongly perturbed, as the OH bond orientation and density profiles of water,[56] as well as hydrogen bonding profiles, show. The hydrogen bonding profile in Figure 3-7d is quite distinct from the profile of Figure 3-7c in that the average number of H-bond acceptors per water molecule is significantly reduced, while the number for H-bond donors per water molecule is slightly increased. Moreover, in the case when an interplate distance has a value of 1.2 nm, which also belongs to the intermediate regime, further reduction in the number of H-bond acceptors takes place, as shown in Figure 3-7e. This behavior can be understood by referring to the results obtained in Chapter 2 by performing analyses of OH bond orientation of the confined water and investigating the snapshots displaying the hydrogen bonding network (see Figures 2-6 and 2-7). The large reduction in the number of H-bond acceptors and the increase in the number of donors for water molecules in the middle of the confined space are due to the spatial arrangement of waters that serve as "bridging" molecules between phosphates from opposing plates. As the distance between plates is further reduced and the small distance regime is reached (see Figure 3-7f), all interfacial water molecules are expelled from the confined space. In this case, the hydrogen bonds between phosphates and phosphate water molecules become unstable, and as a result, some OH bonds tend to orient perpendicular to the plates (Figures 2-6d and 2-7d). Therefore, at the small distance regime, some of the hydrogen bonds between the phosphate water molecules and phosphates are broken, and the relative difference between the numbers of H-bond

acceptors and donors per water molecule is reduced, compared to the cases depicted in Figure 2-7d or 2-7e. However, the number of H-bond donors is still large because phosphate groups from the opposing plates play also the role of a H-bond acceptor.

PC Headgroups and Hydrogen Bonding

We also studied in some detail the role of the phosphate of the PC headgroups in the hydrogen bonding network. To determine which oxygen atoms (H-bond acceptors) of the phosphate moiety are contributing the most to the hydrogen bonding network, we calculated the contribution of each of the four oxygen atoms in the moiety to the formation of hydrogen bonds with water molecules. The results are summarized in Table 3-1. We assigned them numbers from 1 to 4 according to their positions in the backbone, which results in the equivalency of oxygen atoms 2 and 3 (see Figure 3-1c). Table 3-1 shows that oxygen atoms 2 and 3 of the phosphate contribute the most (~80%) to hydrogen bonding, while the contribution of oxygen atom 1 is small (~20%) and the contribution of the oxygen atom 4 is negligible. This is consistent with our previous observation that the phosphate water molecules are positioned between phosphate groups and make hydrogen bonds with the two oxygen atoms of the group (see Figure 2-7).

Interplate distance (nm)	oxygen atom 1	oxygen atom 2	oxygen atom 3
2.8	18.8 (±3.0)	80.8 (±4.8)	0.4 (±0.7)
2.4	19.9 (±2.7)	79.5 (±4.8)	0.6 (±0.7)
2.0	19.2 (±2.7)	80.5 (±4.9)	0.3 (±0.7)
1.6	19.1 (±3.0)	80.6 (±5.4)	0.3 (±0.7)
1.2	13.1 (±2.7)	86.5 (±4.6)	0.4 (±0.7)
0.8	16.6 (±9.4)	83.4 (±16.4)	0

Table 3-1. Contribution (in percentage) of each oxygen atom of the phosphates that are involved in the hydrogen bonding network as a function of interplate distance.

3.4 Summary and Conclusions

In summary, to explore the interaction between two zwitterionic lipid bilayers, we modeled the bilayers as graphene plates decorated with phosphatidylcholine lipid headgroups and calculated the PMF for the interplate interaction. As we showed in Chapter 2, this simple model can qualitatively reproduce the interaction between lipid bilayers. In this work, using MD simulations, we calculated the enthalpic and entropic contributions to the PMF. Our result demonstrated that the enthalpic contribution ($\Delta H(r)$) to the PMF is dominant over the entropic contribution ($-T\Delta S(r)$). Perhaps one of the key results from the thermodynamic analysis performed in this work is that the repulsive interaction in the intermediate regime, which is associated with the proper "hydration" force, is due to the loss of water involved in energetically favorable water−surface interaction. We also performed a hydrogen bonding analysis of water in the confined space between our surfaces. This analysis was complementary to our previous analysis in Chapter 2, wherein we studied the orientational and density profiles of water in the confined space. The present analysis produced results consistent with the previously reported results on the structure of water between plates. In general, the results from three different types of analysis involving water density plots, OH bond orientational plots, and hydrogen bonding profiles were consistent with our calculated thermodynamic results. Our detailed hydrogen bond analysis also revealed that water is still slightly perturbed when the interplate distance is beyond 1.6 nm. This explains why we observed a long-range regime in the PMF due to water, although it is important to mention here that, in experiments, this regime will be dominated by the undulation force.

Our previous results, together with the results of this chapter, show that during the three regimes present in the PMF different types of water are removed from the space between the plates. When the plates approach each other in the long-range regime, we remove the "bulk-like" water, but, as we showed in this work not all of this water is really bulk-like. In the midrange regime, or the proper "hydration force" regime, the water organized by the surfaces is removed. Finally, when we reach the small-range regime, the headgroups interact with directly each other and dominate the interaction, forcing some of the remaining water in the headgroups to be expelled. Although water most directly influences the interaction in the midrange regime, it also influences the interaction in other regimes through its influence on the headgroup configurations.

The initial theoretical treatment of the hydration force performed by Marcelja and Radic (MR)[29] had a phenomenological character and predicted an exponential decay for the order parameter. While the original paper by MR did not specify the microscopic origin of the order parameter, it was presumed that the order parameter was likely the orientational polarization of water. We calculated the two types of orientational polarization profiles for water, $\{\cos\theta(z)\}$ and $\{\cos\theta(z)\}n(z)$, where n(z) is the normalized (to bulk value) local density of water along the axis perpendicular to the plates. For the large interplate regime, both profiles could be fitted to the functional form predicted by the MR theory, but the fitting exponents were far out of the range observed in the decay of the PMF. For the intermediate regime, the polarization profiles displayed oscillations and the fit was poor. Moreover, the exponent of the fit also was not in agreement with the one from the PMF. We conclude that the MR theory with orientational polarization as an order parameter cannot explain the behavior of the interaction between our plates. The

conclusion that orientational polarization cannot explain the interaction between zwitterionic lipid bilayers has already been obtained previously, based on the results from earlier simulations[54,72] and also on theoretical analysis.[34] Our present calculations confirm this.

As we already mentioned, the main cause of the repulsive interaction between two bilayers in the intermediate distance regime (or proper hydration force regime) is due to reduction in the favorable interactions between the plate and water molecules, especially due to breaking strong hydrogen bonds between phosphates and water molecules. This suggests that the ability of the phosphate moiety of PC headgroups to make hydrogen bonds with water molecules is very crucial to generating the repulsive interaction between two bilayers. Thus, besides removing water, we expect that a decrease in the polarity of the phosphate moiety can also reduce the repulsive interaction in the hydration force regime. For this reason, and considering the importance of understanding of the role of electrostatic interaction, the direct comparison between the current system and the charge-removed system is very interesting. This investigation is performed in Chapter 5.

Chapter 4:

Fluctuations in Number of Water Molecules Confined between Nanoparticles.

Changsun Eun and Max L. Berkowitz

Department of Chemistry, University of North Carolina at Chapel Hill, Chapel Hill, North Carolina, 27599

Published in *the Journal of Physical Chemistry B*, 114, 13410-13414 (2010)

Abstract

We used molecular dynamics computer simulations to study the character of interactions between two nanoscale graphene plates in water and also between plates made of “carbon” atoms that have different interaction strength with water. Fluctuations in the number of water molecules in the confined space between plates are qualitatively similar when the plates are made of graphene or when the plates contain “carbon” atoms with weaker “carbon”−water interaction strength. We also observed that these fluctuations are strongly enhanced compared to the fluctuations observed next to a single plate. If the character of water fluctuations in the confined space determines the character of interactions, then it is possible to conclude that the interaction between graphene plates in water is hydrophobic.

4.1 Introduction

A while ago it was suggested that, while the hydrogen bonding in water around a small hydrophobic region is maintained, it is disrupted around a large hydrophobic region.[73] Recent studies[2,20,21,43,50,57,74-77] of the hydrophobicity effect demonstrated that, indeed, its manifestations including hydrophobic hydration and hydrophobic interactions depend on the sizes of hydrophobic solute particles. If the size of the solute is small, so that the hydrogen bonds around the solute are not significantly disrupted, one can use information theory and scaled particle ideas to model hydrophobic hydrations and interactions.[74-76,78] In this case, the solvation free energy of the solute is proportional to the solute volume and the hydrophobic interaction is determined by the entropic component. When the size of hydrophobic particles is substantially large, so that the particle disrupts the water hydrogen bonding network, the hydration free energy is proportional to the area of the particle and the hydrophobic interaction free energy is dominated by the enthalpic component.[50,57,58] The crossover from one regime to the other occurs at a certain particle size and it strongly depends on pressure and temperature of the system: it is around 1 nm at ambient conditions.[79,80] Whereas the small-scale solute hydration is explained by mostly considering statistical properties of cavities in bulk water,[75] the large-scale solute hydration is explained by the change in the properties of the particle−water interface.[50] In cases when the larger solute−water interaction is strongly dominated by a hard-core repulsion, the number of water molecules at the interface is reduced and the interface is similar to the one between water and its vapor; dewetting occurs next to the particle and it can be seen by inspecting the average water density at the interface.[81] If the strength of the attractive force acting between the larger

scale particle and water increases, the average water density at the interface also increases and the surface of the particle is becoming wet. Nevertheless, the character of fluctuations in the number of water molecules in a volume next to the surface is different from the character of fluctuations in the same volume of bulk water.[17,81,82] In bulk water and next to hydrophilic surfaces, the fluctuations have a Gaussian character, whereas next to hydrophobic surfaces these fluctuations display a fat tail toward a small number of water molecules,[82] pointing out that it is easier to create cavities at the interface and that the interface is softer. The increased ability to create cavities at the water interface was previously demonstrated in simulations that studied water/nonpolar liquid interfaces.[83] The softness of the water/hydrophobic particle interface can be also measured by the magnitude of the second moment of fluctuations,[84] which is proportional to the compressibility when the probing volume is very large. Therefore, it was proposed that the presence of large fluctuations in the number of water molecules at the interface can serve as a signature of a *hydrophobic hydration* of the particle.[84] Can the same criterion, related to the fluctuation in number of water molecules, be used to study the phenomenon of *hydrophobic interaction* when two nanoscale particles approach each other in water?

To determine if the interaction between small-scale particles is hydrophobic, one can study the behavior of different properties relevant to the interactions, such as osmotic virial coefficients and its temperature dependence, although they provide an indirect way to understand the solvent structure near apolar solutes and also are very sensitive to the details of the effective solute−solute interaction at large separations.[85] But, perhaps, the simplest and the most intuitively appealing definition of the hydrophobic interaction follows from considering the work (free energy change), $\Delta G(R)$, of bringing two particles

from an infinite separation to a distance R between fixed locations in particles, like their centers of mass. If $\Delta G(R)$ in water has a notably deeper minimum at distance $R \approx \sigma$ (σ is the diameter of the solute) than the minimum in other solvents, the interaction can be considered to be hydrophobic.[23] To eliminate the effect of direct interaction between particles, one subtracts the potential of interaction between particles from the total work, and obtains a quantity that measures the effect of the solvent on interaction, that is

$$\delta G(R) = \Delta G(R) - U(R) \tag{4-1}$$

Therefore, one can define hydrophobic interaction as the interaction that results in a condition that $\delta G(\sigma) < 0$. It is also possible to adopt the same definition of hydrophobic interaction to the case of larger scale particles, assuming that R is the distance between surfaces, which is well defined when, for example, we consider interaction between rigid model surfaces such as graphene plates. To study possible hydrophobic interaction between two graphene plates, Choudhury and Pettitt[43] calculated the potential of mean force between these plates interacting in water. The simulations showed that δG was positive at a large range of distances R including distance $R = \sigma$, thus indicating that the interaction between graphene plates is not hydrophobic, according to the definition given above that uses eq 4-1. It is interesting that the value of $\delta G(\sigma)$ allows the determination of the surface tension and therefore the hydration character of the plate. δG, the solvation part of the free energy, is equal to $4\gamma_{ws}A$ when two plates are at infinite separation (because four surfaces are solvated) and it is equal to $2\gamma_{ws}A$ when the surfaces are at distance σ in their contact, where A is the area of the plate and γ_{ws} is the water−solid plate surface tension. The difference in these free energies, which is $\delta G(\sigma)$, is equal to $-2\gamma_{ws}A$. From this result we conclude that γ_{ws} is negative, because $\delta G(\sigma) > 0$, and therefore the

graphene plates are hydrophilic. The hydrophobic (or hydrophilic) character of a graphene or any other surface can be also determined by considering the angle that a water droplet makes with a surface, but as was pointed out, this is very hard to do when the particle is nanoscopic in size.[17] In this case it was shown that the hydrophobic character of a surface can be determined by the fluctuation character of water next to the surface and that next to hydrophobic surfaces the fluctuations in number of water molecules are large.[17] To follow up on this idea, we decided to check if the fluctuations in the number of water molecules between surfaces can determine the character of the *interaction* between such surfaces, that is, determine if the interaction is hydrophobic or hydrophilic.

Therefore, we studied the potential of mean force (PMF) between two graphene plates immersed in water and compared it to the PMF between two plates with strongly reduced "carbon"–water interaction, so that the plates have a hydrophobic character.

4.2 Methods

To calculate the PMFs and changes in the fluctuations of water molecules in the confined space between the plates, we performed molecular dynamics (MD) simulations on seven different systems. In every system, we considered two plates of size 1.09 nm ×1.12 nm consisting of 60 "carbon" atoms in hexagonal arrangement immersed in a bath of water containing 1800 water molecules. This size of the plates was chosen to be identical with the size used in the simulation from ref [43] so that we can perform a comparison with that work. A choice of larger-sized plates would be more desirable but would require much larger simulation effort due to the need to increase substantially the number of water molecules in the simulations. We calculated the potential of mean force (PMF or $\Delta G(R)$) acting between plates as a function of the interplate distance, R. To calculate the PMF we followed the procedure described in the article by Choudhury and Pettitt (CP).[43] As we already mentioned, one of our seven systems we considered was exactly the system from the CP article: two graphene plates in water. The other system had the same geometric arrangement but differed in the strength of "carbon"−water interaction, described by the Lennard−Jones potential. To modify the strength of this interaction, we followed the strategy adopted in another work of CP[22] and modified the strength of the "carbon"−"carbon" interaction parameter, ε_{cc}. Because the value of the "carbon"−water interaction parameter is obtained by using the Lorentz−Berthelot combination rule $\varepsilon_{co} = (\varepsilon_{cc}\varepsilon_{oo})^{1/2}$, the change in ε_{cc} produces a change in ε_{co} (notice that the value of ε_{oo}, the parameter for water oxygen−water oxygen interaction, remains fixed in all cases). To make it possible to compare our results with the results reported in the literature, we report the strength of the "carbon"−water interaction parameter in the

values of the "carbon"−"carbon" interaction parameter. Thus, for the case of graphene we used the value of ε_{cc} = 0.3598 kJ/mol. In six other cases, the strength of "carbon"−water interaction was different: it was stronger than for graphene−water in one case (ε_{cc} = 1.0 kJ/mol), in four cases it was weaker (ε_{cc} = 0.20, 0.15, 0.10, and 0.05 kJ/mol). For the remaining case, when the potential of "carbon"−water interaction was considered to be purely repulsive, we used the WCA scheme for potential separation[86] based on ε_{cc} = 0.3598 kJ/mol. For water, we used the SPC/E model.[48]

In our simulations, we used the NPT ensemble with Nose−Hoover temperature[44,45] and Parrinello−Rahman pressure[46] coupling algorithms for maintaining 298 K and 1 bar. Electrostatic interaction was calculated through the particle mesh Ewald method[47] with a cutoff length of 0.9 nm. The same length was used for the van der Waals interaction cutoff. Periodic boundary conditions were employed. For the PMF calculation, we carried out a series of simulations with different interplate distances from 0.3 to 1.4 nm. The system at an interplate distance of 1.4 nm was considered as the reference state in the calculation. The total simulation time for each MD run was 2 ns and the trajectories from 500 ps to 2 ns were used for data analysis. The coordinates were saved every 1 ps and a time step was 2 fs. All MD simulations were carried out using the *GROMACS* 3.3.1 and 3.3.3 packages.[49]

4.3 Results and Discussion

In part a of Figure 4-1, we present the plots that show how the free energies $\Delta G(R)$ and $\delta G(R)$, and the plate−plate interaction energy $U(R)$ change as a function of distance between the plates as the strength of the "carbon"−water dispersion interaction changes. We observe that the minimum of all $\Delta G(R)$ is at a distance ~0.34 nm, which coincides with the value of $\sigma_{cc} = 0.34$ nm. As one can clearly see from part b of Figure 4-1, the value at the minimum of $\Delta G(R)$ at $R \approx \sigma$ is smaller than the minimum for $U(R)$ (and correspondingly $\delta G(\sigma) > 0$) in case of graphene plates, when the value for "carbon"−water interaction is relatively high. Therefore, using the criteria based on the sign of the solvent part of the PMF we may conclude that the interaction between graphene plates is not hydrophobic, but weakly hydrophilic. In other cases, when "carbon"−water interaction is weak the criterion based on the sign of $\delta G(R)$ predicts that the interaction between "carbon" plates is hydrophobic. Do the fluctuations in number of water molecules between plates confirm these conclusions about the character of the interaction between plates?

(a)

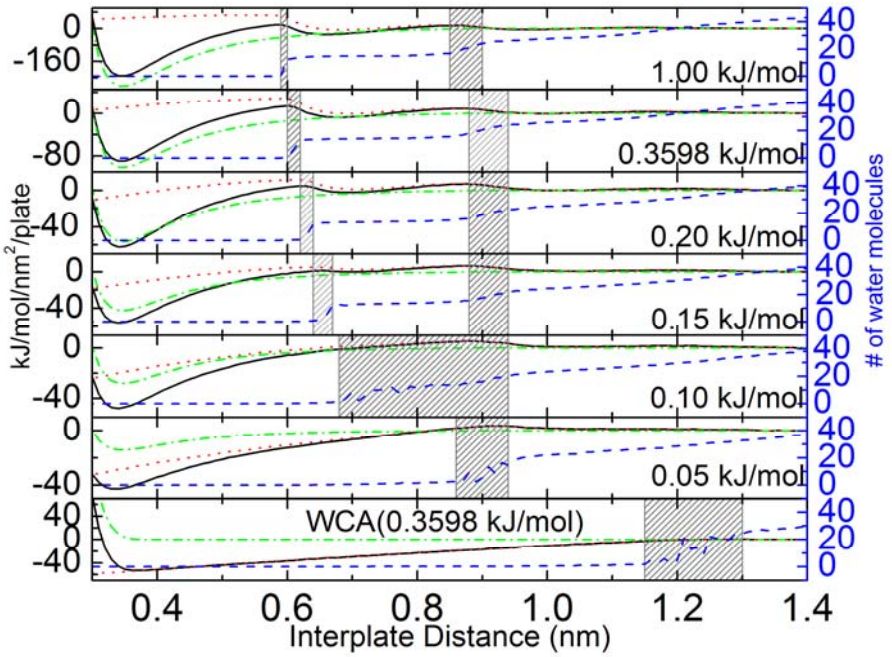
1.00 kJ/mol
0.3598 kJ/mol
0.20 kJ/mol
0.15 kJ/mol
0.10 kJ/mol
0.05 kJ/mol
WCA(0.3598 kJ/mol)
kJ/mol/nm2/plate
# of water molecules
Interplate Distance (nm)

(b)

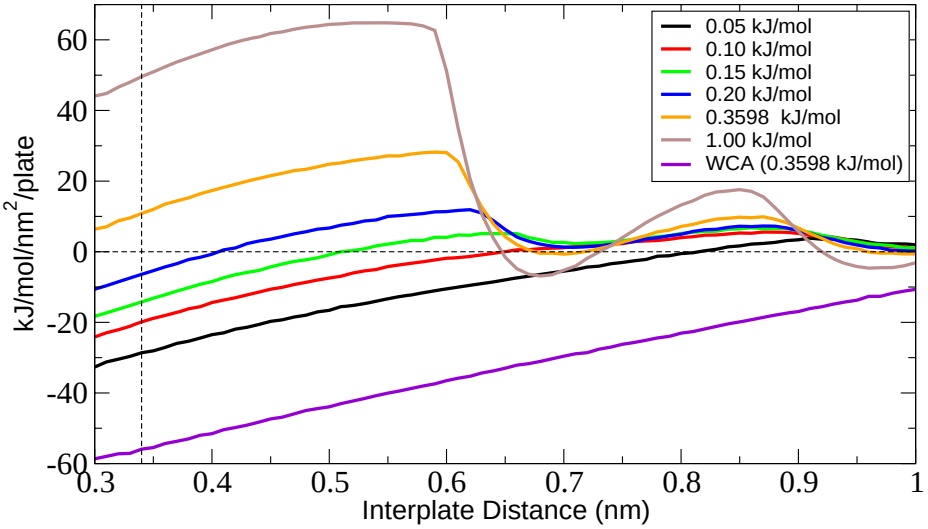
0.05 kJ/mol
0.10 kJ/mol
0.15 kJ/mol
0.20 kJ/mol
0.3598 kJ/mol
1.00 kJ/mol
WCA (0.3598 kJ/mol)
kJ/mol/nm2/plate
Interplate Distance (nm)

Figure 4-1. (a) Total PMF $\Delta G(R)$ (black solid line), direct interaction contribution $U(R)$ (green dot-dashed) and water-mediated interaction contribution $\delta G(R)$ (red dotted) as a function of distance between "carbon" plates. Also shown is the average number of water molecules (blue dashed) in the confined space. The numbers in each panel represent ε_{CC}. (b) Water-mediated interaction contributions into the PMFs. The vertical line represents σ_{CC} = 0.34 nm. The PMFs display their minima at R = ~0.34 nm (above figure). The intersection of $\delta G(R)$ curves with the vertical line at 0.34 nm gives the value of the surface tension between the water and the "carbon" surface when the surface is wetted.

To study the fluctuations in the number of water molecules, in Figure 4-1a we also present plots for the average number of water molecules ($\{N(R)\}$) in the rectangular space between plates as a function of the interplate distance. We observe that for ε_{cc} having values between 1.00 and 0.15 kJ/mol the $\{N(R)\}$ plots display changes in slopes at two different locations. When plates approach each other from a larger distance, the first change in slope occurs in a region when the distance between plates is ~0.9 nm. The water density plots (not shown) demonstrate that this happens when two water layers confined between "carbon" surfaces are reduced to one water layer. After that region, no change in slope is observed, and, therefore, the number of water molecules in the confined space remains constant. The next change in slope occurs at distances between 0.59 and 0.67 nm, depending on the strength of attraction between water and "carbon" atoms. This region is followed up by a region where the number of water molecules in the confined space is zero, corresponding to an absence of water from the space between surfaces; this is consistent with the size restrictions imposed by water and "carbon" atoms,

modulated by the presence of attractive interactions between them. The length interval over which the final change in slope occurs is very small. For ε_{cc} = 1.0 kJ/mol, the transition from the situation when the space between plates is occupied by water to an empty space is rather abrupt. The length of the transition region broadens, as the attractive interaction decreases to a value of ε_{cc} = 0.15 kJ/mol. The observation of water trajectories in the space between plates shows that the disappearance of the last water layer is accompanied by the instability of this layer, that is, large fluctuations in the number of water molecules are present in the intervals around 0.6−0.65 nm. The instability is present for ε_{cc} = 0.3598, 0.20, and 0.15 kJ/mol but is absent for ε_{cc} = 1.00 kJ/mol. Large fluctuations in the number of waters in the space between plates indicate that this space can be dewetted. Indeed, this can be seen in Figure 4-2, where we show the number of water molecules between plates as a function of time. We observe that at a certain distance (which depends on the strength of the "carbon"−water interaction) the space is filled up with water or it is empty. From part a of Figure 4-1 and parts a and b of Figure 4-2, we observe that qualitative behavior of water molecules in cases with ε_{cc} = 0.3598, 0.20, and 0.15 is very similar.

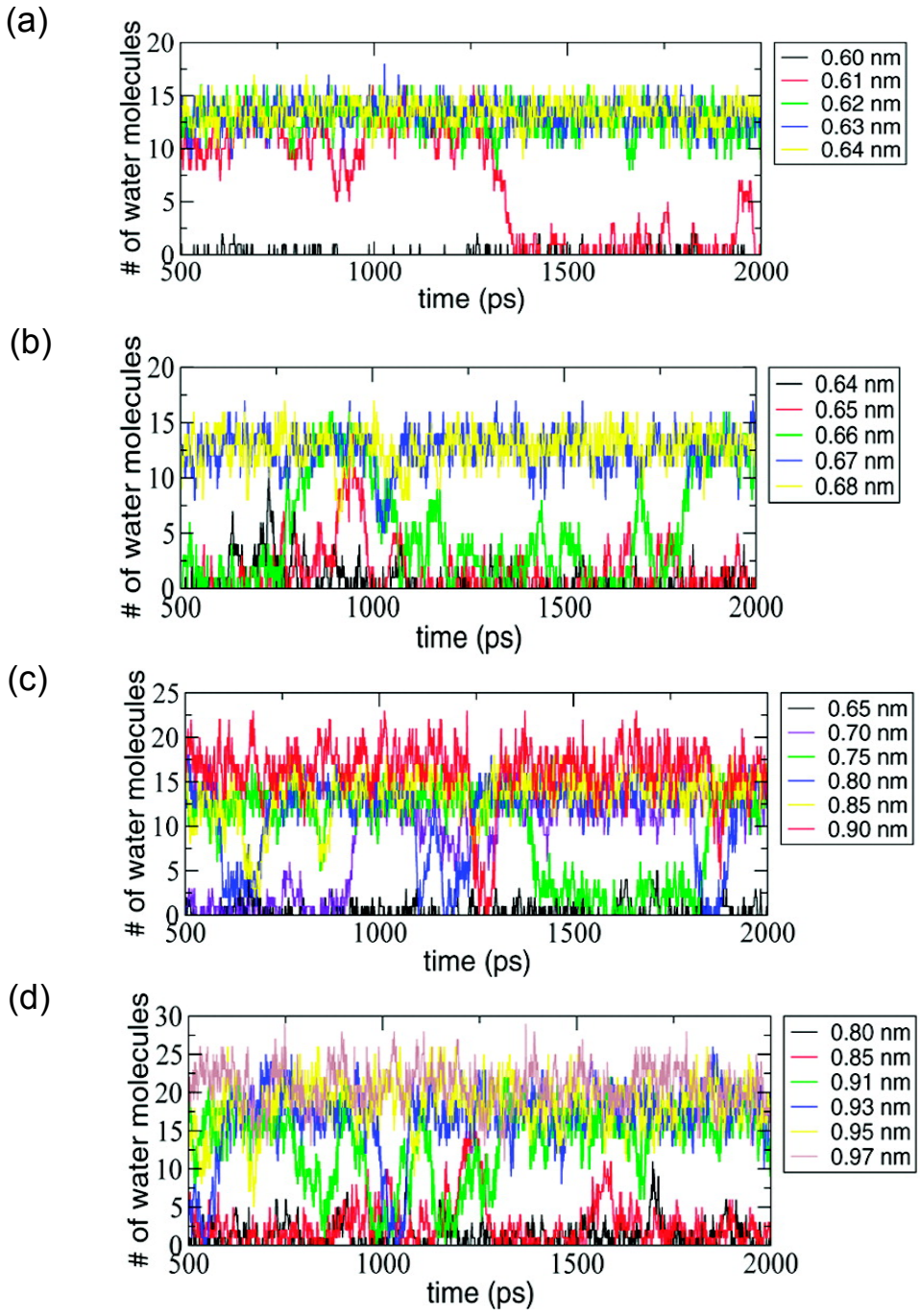

Figure 4-2. Number of water molecules as a function of time for the cases of ε_{cc} =0.3598 (a), 0.15 (b), 0.10 (c) and 0.05 kJ/mol (d) for different values of the interplate distance.

When the value of ε_{cc} is reduced to 0.1 kJ/mol, the stable region corresponding to one water layer between plates is not present any more. Once the interplate distance reaches the value of R = ~0.9 nm, the onset of a broad instability region with a width corresponding to the size of a water molecule is observed. Interestingly enough, dewetting for certain time intervals is observed in the interplate space for any value of R belonging to the instability region (part c of Figure 4-2). When the value of ε_{cc} is further reduced to 0.05 kJ/mol, the instability region is narrowed and now corresponds to the location where a transition between two layers to one water layer occurred at higher ε_{cc} (like ε_{cc} corresponding to graphene plates). For ε_{cc} = 0.05 kJ/mol the dewetting is nearly complete when the distance between plates is 0.8 nm, as one can see from part d of Figure 4-2. In case when the "carbon"−water attractive interaction is absent (this situation is described by WCA repulsive part of the potential), the instability region is pushed further away toward interplate distances in the interval of 1.15−1.3 nm, corresponding to distances when three water layers can be found between two graphene plates. Thus we see that strongly hydrophobic surfaces indeed dehydrate the space between them, as can be expected. Comparison between the results obtained for "carbon" plates with WCA potential and plates with ε_{cc} = 0.05 kJ/mol shows that a weak attraction between water and the surface does not eliminate dehydration, only reduces its range. We find that even a relatively strong "carbon"−water interaction, like in case of graphene, does not eliminate dehydration between two graphene plates, although a single graphene plate is hydrophilic.

It was recently suggested that the hydrophobic character of the surface can be determined by the character of fluctuations in the number N of water molecules in the volume adjacent to the surface.[17] Therefore we calculated the variance in these fluctuations, $\sigma^2(N) = \langle N^2 \rangle - \langle N \rangle^2$, next to the surface and, furthermore, in the confined space between two surfaces. Initially, we calculated the values of the variance in the volume next to one plate. These numbers are displayed in part a of Figure 4-3. Because the volume where we calculate the variance is given by expression $V = Ad$ that is just proportional to distance d from the plate, we present the normalized variance $\sigma^2/\langle N \rangle$ as a function of a distance d. This normalized variance may be also considered as a measure of local water compressibility. As we can see from part a of Figure 4-3, the character of fluctuations next to the WCA plate differs substantially from fluctuations in water number next to other plates, thus pointing out the strong hydrophobic character of the WCA plate. The most interesting, of course, is to investigate the fluctuations in the number of water molecules located in the space between plates. We present these calculations in part b of Figure 4-3, where we show the normalized variance as a function of interplate distance. As we can see from this figure, the values of local compressibility are strongly enhanced in the region. Note that local compressibility values in the instability regions are similar for graphene plates and plates with lower values of ε_{cc} = 0.20 or 0.15 kJ/mol.

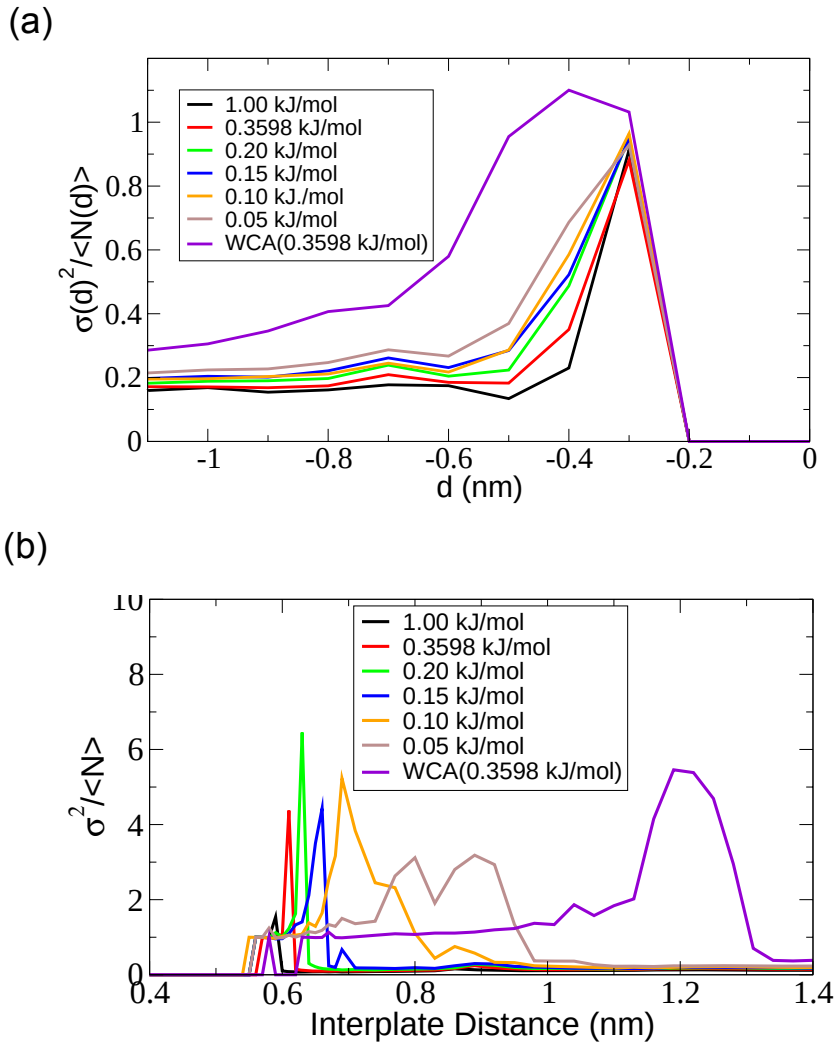

Figure 4-3. (a) Normalized water number fluctuations in the space next to a single plate for different values of ε_{cc}. Negative sign for *d* indicates that the volume where fluctuations are calculated is on the left side of one of the plates. From the water density profiles we determined that when *d* = 0.5 nm, the probe volume includes the first layer of water molecules next to the plate. (b) Normalized water number fluctuations in the confined space between plates. The numbers in the legend represent ε_{CC} values.

4.4 Conclusion

We present the summary of the results obtained from our seven simulations in Table 4-1. As we can see the difference in the interpretation of the interaction between plates exists for the case of graphene plates only. If we determine the character of interactions between the plates by the sign of $\delta G(\sigma)$ we need to conclude that graphene plates containing "carbon" atoms with relatively strong attraction between these atoms and water have a hydrophilic character. The calculation of the free energy at contact between plates when ε_{cc} is equal or below 0.20 kJ/mol shows that in these cases the plate interaction is hydrophobic. When we consider the fluctuations of water between two "carbon" plates, we observed that the character of these fluctuations is very similar when the plates are graphene or when ε_{cc} = 0.20 or 0.15 kJ/mol. Therefore, we may conclude that interaction between graphene plates is hydrophobic.

ε_{cc} (kJ/mol)	Water-mediated Interaction		Water Fluctuations		
	$\delta G(\sigma)$	Character of interaction based on the sign of $\delta G(\sigma)$	Large water fluctuations at the transition region (two-state equilibrium)	Transition region (nm)	Character of interaction based on water fluctuations
1.0	> 0	Hydrophilic	No	N/A	Hydrophilic
0.3598	> 0	Hydrophilic	Yes (1 layer ↔ 0 layers)	0.61	Hydrophobic
0.20	< 0	Hydrophobic	Yes (1 layer ↔ 0 layers)	0.62 ~ 0.63	Hydrophobic
0.15	< 0	Hydrophobic	Yes (1 layer ↔ 0 layers)	0.64 ~ 0.67	Hydrophobic
0.10	< 0	Hydrophobic	Yes (2 layers ↔ 0 layers)	0.68 ~ 0.90	Hydrophobic
0.05	< 0	Hydrophobic	Yes (2 layers ↔ 0 layers)	0.86 ~ 0.94	Hydrophobic
WCA (0.3598)	< 0	Hydrophobic	Yes (~ 2 layers ↔ 0 layers)	1.15 ~ 1.30	Hydrophobic

Table 4-1. Summary of the main results from our simulations related to the character of interaction between “carbon” plates in water and liquid-vapor equilibrium in the confined space between the plates.

Why are strong fluctuations in water number present between graphene plates? They are happening due to the collective effect, when the tendency to display fluctuations next to one surface is strongly enhanced as surfaces approach each other. Therefore, two graphene plates, each possibly hydrophilic as a separate plate, can be considered to be engaged in a hydrophobic interaction when approaching each other.

We also carefully searched for the existence of vapor−liquid equilibrium for water in the space between “carbon” plates and observed that it exists even in the case when plates are made of graphene. When the interaction between a “carbon” plate and water is weaker than the interaction between a graphene plate and water, the vapor−liquid equilibrium is easier to observe and it shifts to larger interplate separation distance as the plates are brought together. Clearly, the existence of liquid−vapor equilibrium and presence of large fluctuations in water number between plates are closely related to each other.

We also want to mention that although the systems studied by us are very similar to the systems studied by CP,[22,43] we reached different conclusions about the behavior of water between graphene plates. In ref [22], CP considered cases when the interplate distance was fixed at a particular value of R = 0.68 nm, whereas they changed the strength of “carbon”−water interaction. They concluded that when the interaction strength was such that ε_{cc} was in the region between 0.10 and 0.20 kJ/mol the space

between plates was oscillating between dry and wet states. For graphene plates, they concluded that the space between them was wet. In this chapter, by investigating the transitions over the range of interplate distances, we found that the oscillations between wet and dry states of the interplate region occur also in case of graphene plates, only at slightly smaller separations (part a of Figure 4-2). This equilibrium between the vapor and liquid states of water in the interplate space between graphene plates is exactly the reason why we may designate the interaction between the plates to be hydrophobic.

Finally, we want to emphasize that hydrophobic phenomena are multifaceted, and all their aspects, perhaps, cannot be adequately considered by one definition. In this article, we demonstrated that using different definitions of hydrophobic interaction we can conclude that interaction between graphene plates may be described either as hydrophobic or as hydrophilic. If the behavior of the fluctuations in water between plates can serve as a more appropriate criterion of the interaction hydrophobicity, we must conclude that graphene interaction in water is hydrophobic.

Chapter 5:

Molecular Dynamics Simulation Study of Interaction between Model Rough Hydrophobic Surfaces.

Changsun Eun and Max L. Berkowitz

Department of Chemistry, University of North Carolina at Chapel Hill, Chapel Hill, North Carolina, 27599

Abstract

We study some aspects of hydrophobic interaction between molecular rough and flexible model surfaces. The model we use in this work is based on a model we used previously (Eun, C.; Berkowitz, M. L. *J. Phys. Chem. B* **2009**, *113*, 13222-13228), when we studied interaction between model patches of lipid membranes. Our original model consisted of two interacting plates across water, containing polar headgroups of lipids attached to graphene surfaces. The interaction between such plates can be considered to be an example of a hydrophilic interaction. The modification into the model plates we study here consist of a charge removal from the zwitterionic headgroups attached to the plates. We observe that as a result of this procedure the plate character changes; it becomes hydrophobic. We also observe from separating the total interaction (or potential of mean force, PMF) between plates into the direct and the water-mediated interactions that the latter changes from repulsion to attraction, clearly emphasizing the important role of water as a medium. We investigate the effect of roughness and flexibility of the headgroups on the interaction between plates and observe that in our case roughness enhances the character of the hydrophobic interaction, consistent with other work that studies roughness effect on hydrophobic hydration. In addition, we observe a dewetting transition in a confined space between charge-removed plates, which serves as another evidence for presence of a strong hydrophobic interaction. We also notice that there is a shallow local minimum in the PMF in case of charge-removed plates, and we find that this is associated with the configurational changes that flexible headgroups undergo as two plates are brought together.

5.1 Introduction

The properties of molecules solvated in water are greatly influenced by water molecules surrounding them. For example, water induces creation of self-organized assemblies such as micelles, monolayers and bilayers of amphiphilic molecules. A large amount of effort was devoted to understanding the effect of water on the behavior of solutes. Many useful ideas and concepts emerged as a result of this effort, including such concepts as hydrophobicity ("water fearing") and hydrophilicity ("water loving").[2] If molecules are considered to be hydrophobic, their solubility in water is low; such molecules generally have a tendency to aggregate. If molecules are hydrophilic, the trend is opposite. The hydrophobic interaction is attractive and the origin of this interaction is due to water, and not the molecules themselves. This implies that to understand the nature of hydrophobic interactions we need to separate the total interaction into the contributions due to water and the contribution due to direct interaction; the latter may induce aggregation of molecules even without the presence of water, e.g. in vacuum.[23] This strategy should be also applied to the hydrophilic case, when one wants to understand hydrophilic interactions. Since the interaction between two particles is usually described by the potential of mean force (PMF), which is the free energy change along a certain reaction coordinate, this PMF can be decomposed into the aforementioned two contributions, whether the particles are rigid[23] or flexible.[56]

Recently, we used this separation method of the PMF to study hydration force, the monotonic repulsive interaction acting between lipid bilayers,[24,25,28] by performing simulations on a simplified model of lipid bilayers.[56] Since the surfaces of these model bilayers contained polar headgroups that can be identified as hydrophilic, the interaction

between them is an example of a hydrophilic interaction. In our study we found that the origin of the hydration force is a repulsive water-mediated interaction, and not the direct interaction due to the repulsion between bilayers originating from lipid protrusions.[26,87] In our follow-up work[88] we observed that the repulsive interaction between our model lipid bilayers is due to a strong attractive interaction between water and the bilayer. We also observed that this attaction is correlated with the change in the hydrogen bonding network formed between water and polar headgroups and also the change in the hydrogen bonding network between water molecules. Notice that in our work, the hydrophilic charged groups were flexible and that direct interaction between these headgroups was attractive. Previously, Lu and Berkowitz used molecular dynamics (MD) simulations[40] to calculate the water-mediated contributions to the PMFs for the interaction between two rigid model plates with different fixed charge distributions on them. They observed that water-mediated interaction depended on the charge-charge correlation between the plates and that water-mediated interaction was repulsive for the cases when the interaction between plates in vacuum was attractive. More recently, Hua et al.[89] studied similar systems and they also observed similar repulsive water-mediated interaction. Overall, all the previously mentioned studies illustrated that water-mediated contribution to the typical hydrophilic interaction is repulsive.

What about the nature of the water-mediated contribution to the hydrophobic interaction? Previous studies showed that water mediated interaction is monotonically attractive when the interaction between water and the model rigid plate containing "carbon"-like atoms in graphene geometry is purely repulsive.[43,90] Even some addition of a weak attraction to "carbon"-water interaction does not change the character of the

water-mediated interaction. When moderate attraction between "carbon" and water is present it can change the character of the water mediated interaction substantially: it starts oscillating and the interaction between plates may be considered as being hydrophilic.[90]

As we mentioned above, according to our study of hydrophilic interactions using model lipid bilayers,[88] the strong interaction between polar headgroups and water molecules is the reason for the repulsive water-mediated interaction. Thus, it is reasonable to consider that the polarity of headgroups, responsible for the strong plate-water interaction, is a key element in determining the character of water-mediated interaction. In this chapter, we explicitly test this idea by removing charges from the original hydrophilic plate, and by comparing the original water-mediated interaction with the one from this charge-removed case. In fact, a similar idea of changing polarity by adjusting the magnitude of charges has been used to study the effect of surface polarity on water contact angle and interfacial water structure[91]; however, not on the inter-surface interaction.

Besides polarity, other factors could be important in characterizing hydrophobic/hydrophilic properties; such as density and arrangement of polar/non-polar particles[40,89] and surface morphology and/or surface roughness. It is now well-established that roughness enhances the hydrophobicity of surfaces.[92-98] Remarkably, roughness can induce superhydrophobicity, a state that the flat surface of the same material cannot achieve. Nature uses roughness to achieve superhydrophobicity, as has been observed in cases of lotus leaves[99,100] or water striders' legs.[101] This roughness effect is usually

measured through contact angle; in particular, when the contact angle is above 150°, the surface is normally considered to be superhydrophobic.[102]

Two microscopic states for describing a water droplet on the rough surface were suggested, called the Wenzel[92] and Cassie-Baxter[93] states. To understand molecular details related to description of these states, some MD simulations were performed.[19,94,103-106] Most of MD simulation studies on rough hydrophobic surfaces have been focused on dewetting at a single rough hydrophobic surface, in particular, calculating the contact angle of a water nanodroplet on the surface.[19,94,103-106] Moreover, the model surfaces used in those studies were rigid and displayed no flexibility. However, to the best of our knowledge, the effect of roughness on the hydrophobic interaction has rarely been discussed in a context of water properties in the confined space between two rough surfaces, i.e. in terms of inter-surface interaction and dewetting transition. Performing model studies of wetting/dewetting behavior of water on single rigid rough surfaces is perhaps sufficient to study wetting of solid materials. However, in many situations especially in a biological environment, roughness of hydrophobic surfaces, such as protein surfaces, influences the hydrophobic interaction or dewetting transition between two particles. In addition, many materials in nature are soft, so their surfaces are flexible. Thus, by investigating hydrophobic interactions between our charge-removed PC-headgroup plates we also study interactions between rough and flexible surfaces in water. In addition, since the dewetting transition can be a signature of a hydrophobic interaction,[57] we will study the trajectories of molecular dynamics simulations to see if a dewetting transition takes place in our hydrophobic model.

In order to address the above mentioned issues, this chapter is organized in the following way. In the Methodology section we describe the details of our systems and of our molecular dynamics (MD) simulations. In the section after that we discuss the effect of the headgroup polarity on the water-mediated interaction between two model lipid bilayers and directly compare hydrophilic and hydrophobic interactions observed to act between plates with charged and uncharged headgroups, correspondingly. After that we study the hydrophobic behavior of our charge-removed model and compare the hydrophobic interaction of the plates with flexible groups and the interactions between smooth hydrophobic plates. Also, we consider the effect of roughness and flexibility on hydrophobic interaction. In the final section, we summarize our findings with some conclusions.

5.2 Methodology

To discuss the water-mediated interaction acting between two hydrophilic surfaces, we have used the results we obtained from our previous study of the hydration force.[56] In that study, a model hydrophilic surface contained nine polar phosphatidylcholine (PC) lipid headgroups were attached to a nanoscale graphene plate (252 carbon atoms; 2.425 nm by 2.380 nm). We named the plate the PC-headgroup plate and the details about this PC-headgroup plate are given in our previous paper.[56] However, to study water-mediated hydrophobic interaction between flexible surfaces we constructed a hydrophobic plate closely related to the original PC-headgroup plate. This hydrophobic plate, named the charge-removed PC-headgroup plate (CRPC plate), was prepared by removing all the electric charges from the lipid headgroups in the original PC-headgroup plate. Therefore, the interaction between the plate and water in this case was just Lennard-Jones interaction.

To calculate the water-mediated interaction for the CRPC plates, we performed MD simulations and employed the same methodology we used in our previous work.[56] Thus we calculated the potential of mean force (PMF) as a function of the interplate distance by using thermodynamic perturbation method.[43,107] Again, as in the previous work, the interplate distance is defined as the distance from one graphene plate to the other graphene plate. As previously, we decomposed the PMF into direct and water-mediated contributions.[56] The errors in the calculations were estimated using the block averaging method[65] and the standard error propagation method.[108,109]

In our MD simulations of the system with CRPC plates, we placed the plates into a simulation box separated by a certain interplate distance and solvated them with 8800

water molecules. We used the NPT ensemble. The Nose-Hoover temperature[44,45] and the Parrinello-Rahman pressure[46] coupling algorithms (both with a coupling constant of 0.5 ps) were utilized for maintaining temperature at 298 K and pressure at 1 bar, respectively. Electrostatic interaction was calculated through the particle mesh Ewald method.[47] The SPC/E model[48] was used for water. Periodic boundary conditions were employed. The same interaction and the same simulation parameters from our previous study[56] were also used, except for the length of the simulation time. That is, when the interplate distances were in a region between 1.68 nm and 1.82 nm the total simulation time for each distance was 10 ns, to permit enough sampling, because we observed that a dewetting transition is happening inside this region; otherwise the time of simulation runs was 1 ns. In our calculations of the PMF and other physical quantities the data from the first 500 ps were discarded.

To characterize the hydrophobic interaction between CRPC plates, we compared the calculated PMF and its components with the calculations we performed previously on a series of cases with simple graphene-like "carbon" plates that had no flexible headgroups attached.[90] All these "carbon" plates had the geometry of a graphene plate. We considered a series of simulations with "carbon" plates, where every simulation differed from the other by the strength of the Lennard-Jones (LJ) potential acting between the "carbon" of the plate and water.[22,90] Seven systems where the LJ interaction was moderately strong or weak were investigated. For these systems the water- "carbon" interaction strength was determined through the use of the Lorentz-Berthelot combination rules for the LJ parameters of "carbon"-"carbon" and oxygen-oxygen interaction, i.e. $\varepsilon_{CO} = \sqrt{\varepsilon_{CC} \cdot \varepsilon_{OO}}$ and $\sigma_{CO} = (\sigma_{CC} + \sigma_{OO})/2$. As was mentioned previously,[90] we

fixed the values of ε_{OO} and σ_{OO}, taken from the SPC/E water model, and $\sigma_{CC} = 3.4\text{Å}$. Note that for a realistic graphene plate, the LJ parameter ε_{CC} was 0.3598 kJ/mol[43] and for the other cases, ε_{CC} was 0.05, 0.10, 0.15, 0.20 and 1.00 kJ/mol. In addition, we considered the case in which the LJ potential was purely repulsive as a limiting hydrophobic case. For this, we used Weeks-Chandler-Andersen (WCA) separation scheme[86] based on ε_{CC} =0.3598 kJ/mol.

For all types of "carbon" plate the reference state for the PMF (the state where the value of the PMF is assumed to be zero) was at an interplate distance of 1.40 nm, whereas the reference state for the PMF of PC-headgroup plates was at 2.99 nm. The simulation time for systems with "carbon" plates for each interplate distance was 2 ns. In these cases we also disregarded the first 500 ps of trajectories for the data analysis. For the PMF calculations in "carbon" plate systems we used the 60-atom graphene-like plate as Choudhury and Pettitt did.[43]

All MD simulations were carried out using the GROMACS 3.3.1 and 3.3.3 packages.[49]

5.3 Discussion

5.3.1 Role of the electrostatic interaction in hydrophilic interaction

From our previous study of the interaction between model lipid bilayer plates we concluded that the repulsion between neutral lipid bilayers originates from the water-mediated interaction[56] (see Figure 5-1a), and that this interaction is mainly due to the increase of the potential energy of interaction between the model lipid plates and water molecules, as two plates are brought together.[88] In addition, the hydrogen bonding analysis showed that this potential energy change is inversely correlated with the change in the number of hydrogen bonds between the plates and water.[88] All this implies that the electrostatic interaction between the polar headgroup and water plays an important role in the origin of repulsive or hydration force.

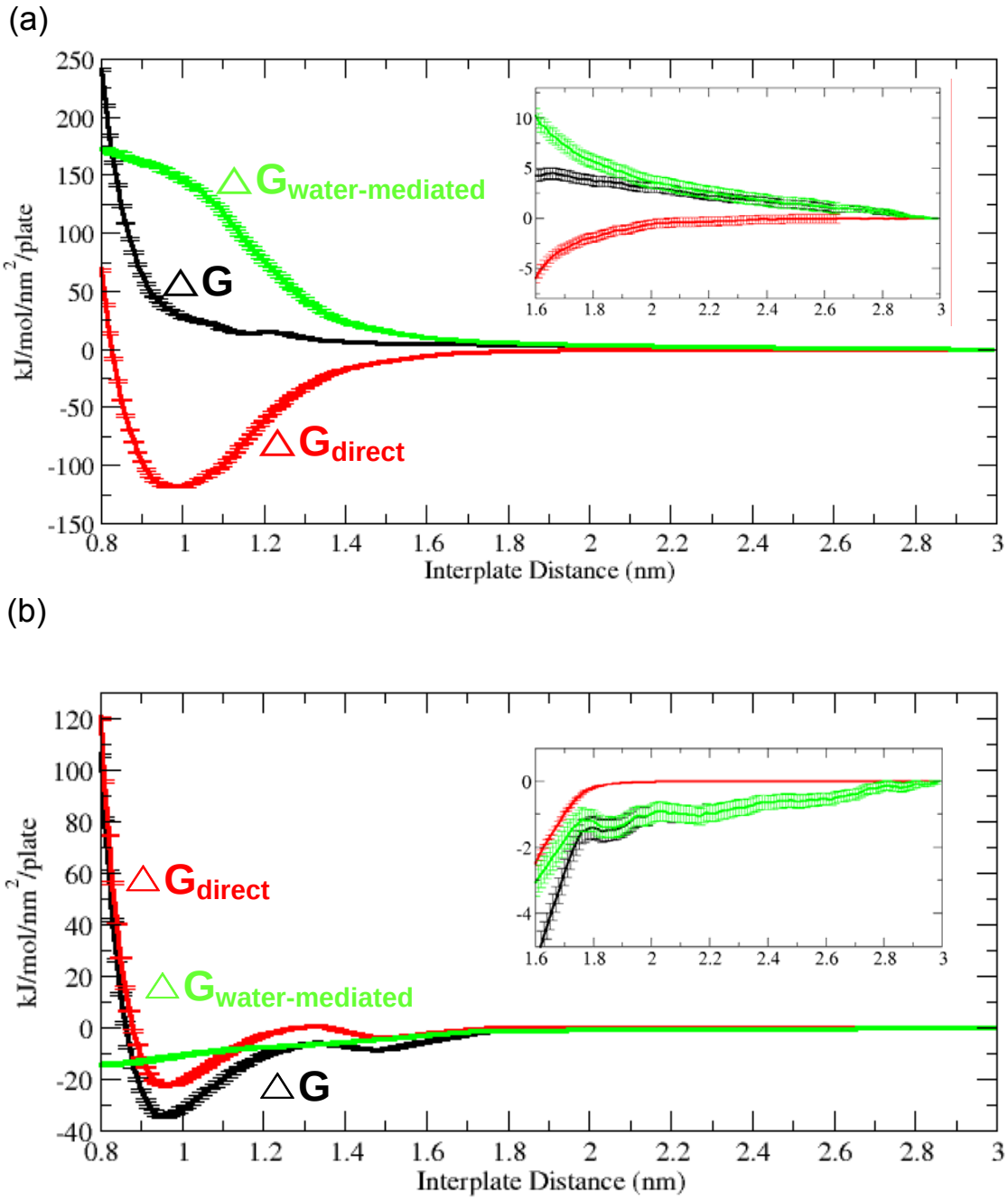

Figure 5-1. Decomposition of the PMF (black) into contributions from the direct interaction (red) and from the water-mediated interaction (green) between two PC-headgroup plates (a) and between two charge-removed PC-headgroup plate (b). Insets are for large interplate distances. Errors are represented by bars.

To find out how much the electrostatic interaction contributes to the potential energy of interaction between the plates and water, we calculated the electrostatic and the LJ interaction contributions and displayed them on Figure 5-2. As we can see from this Figure, the energy due to electrostatic interaction is dominant. This confirms our suggestion that the electrostatic interaction between polar headgroups and water molecules is so strong, that it requires work to remove water molecules when the two

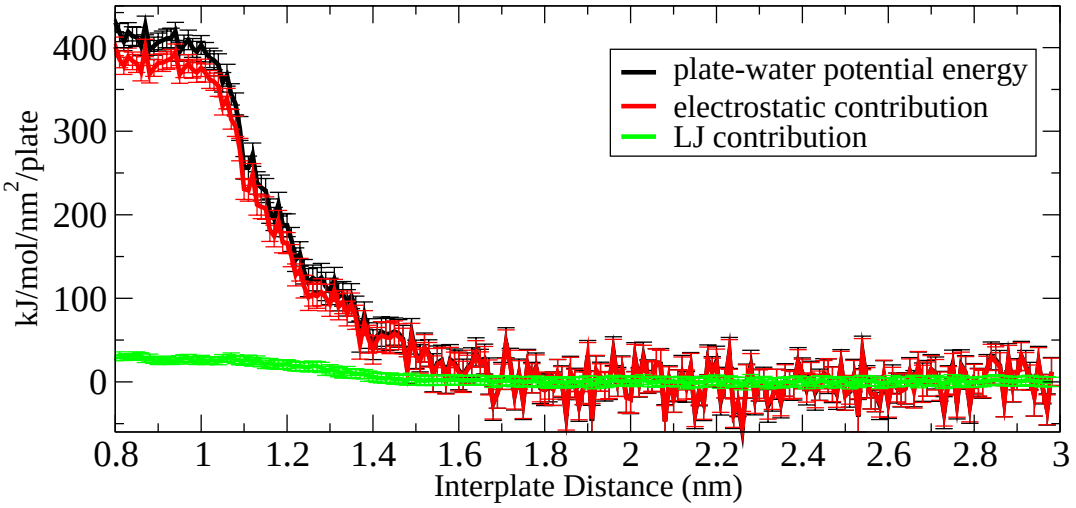

Figure 5-2. Contributions of electrostatic (red) and Lennard-Jones (green) interactions to the potential energy interaction between the PC-headgroup plates and water molecules (black). The electrostatic and Lennard-Jones energy changes between the plates and water molecules were directly calculated from MD simulations and by summing up we obtained total potential energy change. This plate-water potential change is exactly the same with the one calculated via another route within numerical errors (see Figure 3-4.). The error bars represent the standard deviations.

5.3.2 Hydrophilic interaction vs. hydrophobic interaction

Since the electrostatic interaction is crucial for generating repulsive interactions between PC-headgroup plates, we expect that if we remove the water-headgroup electrostatic interaction, the repulsive character of interbilayer interaction would disappear. To test this idea, we use our PC-headgroup plate again, but this time we remove all electric charges from the plate and then calculate the interplate interaction. Obviously, since the electrostatic interaction between the plate and water is absent now, this weakens the water-plate interaction compared to the original hydrophilic plate. As expected, the PMF for the interplate interaction between the charge-removed plates case is not repulsive, but attractive (see Figure 5-1b). From the decomposition of the PMF we notice that the attractive water-mediated interaction is responsible for the dramatic change of the nature of PMF. As we discussed this in the Introduction, since the water-mediated interaction is attractive, we can consider the interaction between CRPC plates to be hydrophobic. Moreover, in fact, the overall shape of the PMF in Figure 5-1b looks like the typical shape observed in other interaction with hydrophobic interaction. [43,78,110]

Besides performing the energetic analysis, we also examined the character of the dewetting transition in the charge-removed case, which is considered to be another signature of a hydrophobic interaction.[57] In order to do that, we calculated the average number of water molecules confined between the two CRPC plates. The result is shown in Figure 5-3a. It suggests that the dewetting transition actually occurs in the shaded narrow region (d=1.74~1.8 nm). In addition, the changes in instantaneous number of water molecules in the confined space and the snapshots from the simulations provide us with more clear evidence of the transition existence, as Figures 5-3b and 5-3c show. The

transition does not seem to be complete, just partial. Particularly, we observe from Figure 5-3c that a large cavity forms inside the interplate space, and the thickness of the cavity along the axis perpendicular to the plates is large enough to accommodate approximately two layers of water molecules.

(a)

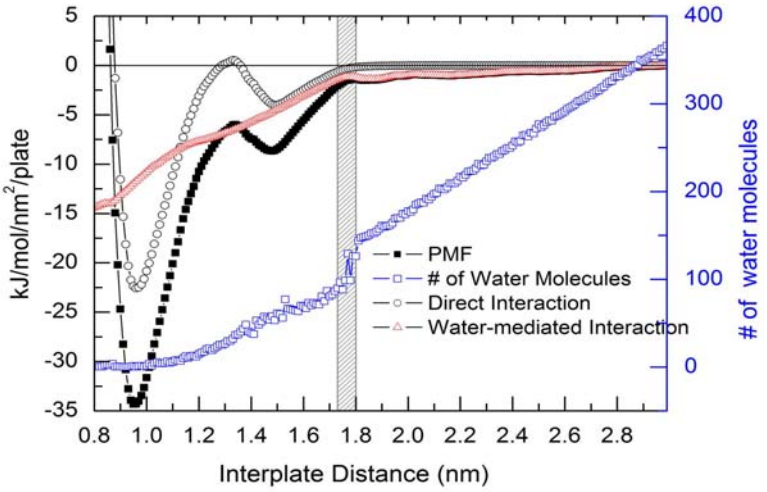
kJ/mol/nm²/plate
# of water molecules
PMF
# of Water Molecules
Direct Interaction
Water-mediated Interaction
Interplate Distance (nm)

(b)

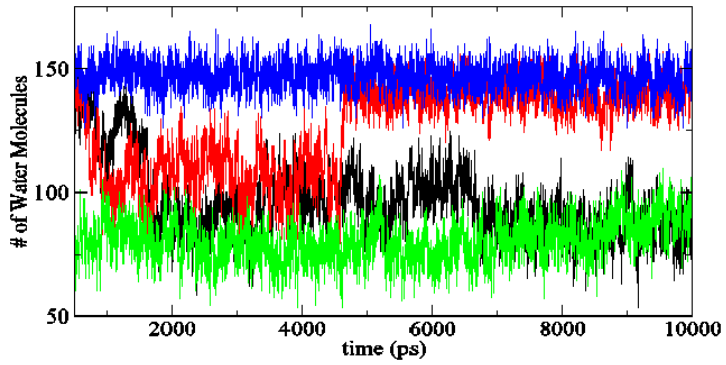
# of Water Molecules
time (ps)

(c)

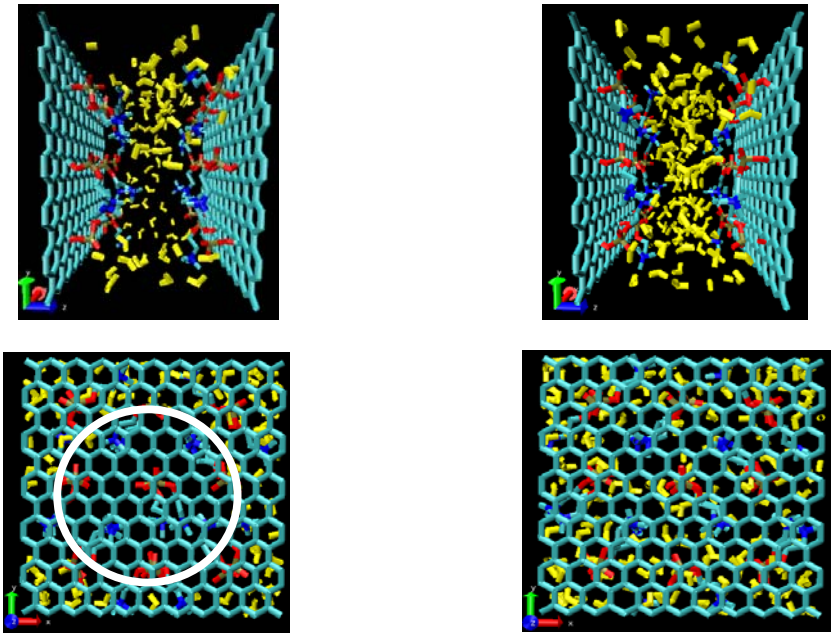

Figure 5-3. (a) Average number of water molecules in the confined space between two CRPC plates, the total PMF, the contribution of direct interaction into PMF, and the contribution of water-mediated interaction. (b) Changes in the number of water molecules in the confined space as functions of time at the distances of 1.82 nm (blue), 1.79 nm (red), 1.74 nm (black) and 1.7 nm (green). (c) For the case of an interplate distance of 1.79 nm, two snapshots taken at t = 3500ps (left) and t = 7800ps (right). Carbon and united carbon with hydrogen, nitrogen, phosphorus, and oxygen are colored in cyan, blue, tan and red, respectively. For clear representation, water molecules are represented by yellow.

5.3.3 "Carbon" plates as reference hydrophobic plates.

Our CRPC plates containing flexible non-polar headgroups can be considered as rough and flexible hydrophobic surfaces. To understand better how roughness and flexibility affect the hydrophobic interaction, we compare this system with the system containing two "carbon" plates that represent smooth and rigid surfaces. The reason why we choose systems with "carbon" plates, including graphene plates, as our reference systems is that they have been relatively well-studied.[22,43,59] Thus, such a comparison study can help us to understand the common features characteristic for plates that interact through hydrophobic interactions and unique properties of the charge-removed plates, due to their roughness and flexibility of the attached groups.

Besides a graphene plate, for a systematic comparison, we considered six other "carbon" plates, which have the same geometry as the graphene plate, but different interaction strength for the water-plate interaction. The graphene plate we considered is

not a typical hydrophobic plate since the contact angle for water with such a plate is around 90°[111] and the water-mediated interaction between such plates is not purely attractive[43,90]; moreover, the dewetting transition for water between graphene plates is hardly observable.[90] The way we adjust the interaction strength for water-plate interaction, or the plate hydrophobicity, is through variation in the value of ε_{CC}, as described in Methodology section. It was shown by Choudhury and Pettitt[22] that it is possible to induce a pronounced dewetting transition for water between two graphene-like plates by reducing the LJ parameter of "carbon"-water interaction. They performed their study only at a particular interplate distance of 6.8 Å, but it suggested that by controlling water-plate interaction we may also control the strength of hydrophobic interaction.

To understand the dependence of the hydrophobic interaction on water-"carbon" interaction strength, as well as the character of the character of the dewetting transition, we previously performed MD simulations for a certain range of water-plate interactions and for a range of interplate distances.[90] Figure 5-4a shows the PMFs and the average numbers of water molecules in the confined space for different strengths of "carbon"-"carbon" interaction. From the figure we see that as the value of ε_{CC} decreases from the value of 1.00 kJ/mol to 0.05 kJ/mol, the water-mediated interaction becomes more attractive, indicating stronger hydrophobic interaction acting between plates. Also, the reduction of water-plate interaction strength affects the behavior of the average number of water molecules. That is, the dewetting transition regions or vapor-liquid equilibrium regions, characterized by the rapid changes in the number of water molecules (left shaded region in Figure 5-4a), are getting broader and they shift towards larger distances. When the "carbon"-water interaction is reduced (this corresponds to ε_{CC} values of 0.10 and 0.05

kJ/mol) the dewetting region and the transition region between one and two layers of water (right shaded region in Figure 5-4a) are merged into one big region. For pure repulsive potential (WCA) case, the transition occurs at much larger interplate distance. Overall, the analysis of the average number of water molecules shows that as the "carbon"-water interaction decreases, the character of hydrophobic interaction between "carbon" plates increases and the dewetting transition regions become larger and the region gets shifted towards larger interplate distances.

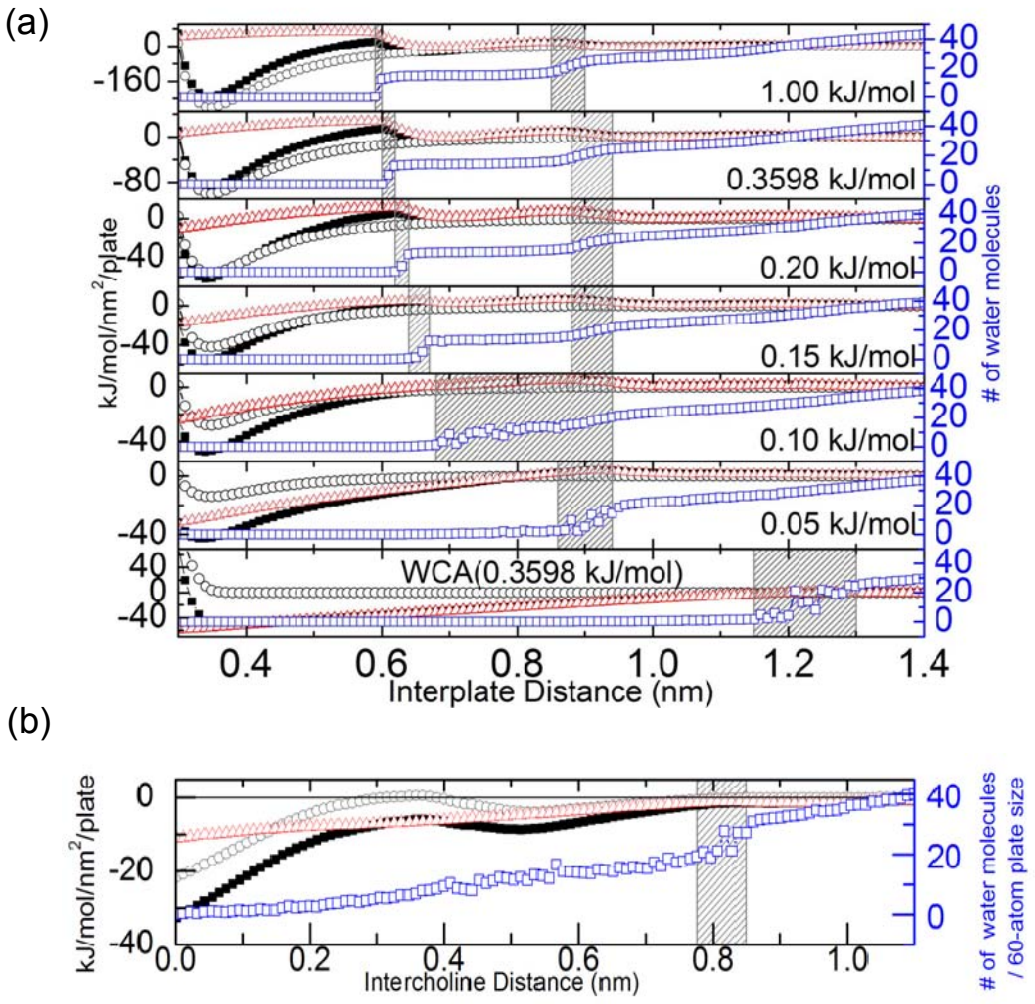

Figure 5-4. (a) PMF (black filled square), direct interaction (black open square), and water-mediated interaction (red triangle) of "carbon" (graphene-like) plates with different water-plate interaction strength. The number in each panel represents ε_{CC}. The blue squares are for the average numbers of water molecules in the confined space. (b) The PMF, its components and the number of water molecules as a function of distance between CRPC plates. The interplate distance is replaced by the intercholine distance.

5.3.4 Hydrophobicity of the charge-removed PC-headgroup plate

For an appropriate comparison between CRPC plate and reference "carbon" plates we calculate the number of water molecules per unit area of the "carbon" plate. Furthermore, we calculate the distance between the CRPC plates as the distance between opposing choline groups. This distance represents a better choice since the headgroups are also parts of the plate and, as we observed, water hardly penetrates inside the headgroups, in contrast to the case of PC-headgroup plate. Therefore, we determined that the relationship between the interplate distance x (in nm) and intercholine distance y (in nm) is $y = 1.046x - 1.034$ with the correlation coefficient of 0.99. Using this relationship we present in Figure 5-4b the PMF and the number of confined water molecules as a function of the intercholine distance.

From the comparison of Figures 5-4a and 5-4b we notice that the interaction between CRPC plates is similar to the interaction between "carbon" plates with a weak "carbon"-water interaction (ε_{CC}=0.05 kJ/mol), although the dewetting in charge-removed case is only partial. This partial dewetting is due to the presence of water molecules at the edges of the plate (see Figure 5-3c). Therefore, if we disregard this boundary effect

and focus only on the central confined space (circled space in Figure 5-3c), the dewetting transition can be considered as full dewetting transition.

To investigate the similarity furthermore, we calculated the averaged Lennard-Jones potential energy between a plate and a single water molecule (Figure 5-5). For this we performed a series of NVT simulations on a system containing 252-atom "carbon" plate, so that its size is exactly the same, as the one used in the simulations of plates with headgroups attached. In the case of the CRPC-headgroup plate we took an average of the LJ interaction over the 200 ps trajectory keeping water at a given distance, because the headgroups are fluctuating and so is the LJ interaction. In our calculations the plate-water distance along the z-axis (perpendicular to the plate) in case of a "carbon" plate was defined as the distance between the center of mass of the plate and the water molecule, while the distance between the CRPC-headgroup plate and water it was the average distance between the choline group and the water along the z-axis (see Figure 5-5a). Since the surfaces of plates are inhomogeneous on the atomic scale, we considered five different x-y positions of the water molecule (see Figure 5-5b) and calculated the average of the LJ interactions over these configurations (Figures 5-5c and 5-5d). The results show that when a water molecule approaches the CRPC plate, it is weakly interacting with the plate. As a matter of fact, up to the comparable distance (~ 0.34 nm), the behavior of the energy curve for the CRPC-water interaction is very similar to the behavior of the curve for the LJ interaction between "carbon" plates and water, when "carbon" plates interact weakly with water (ε_{CC} =0.05 and 0.10 kJ/mol), as Figure 5-5d shows. This result is consistent with the results obtained from consideration of PMFs and dewetting transitions. Note that the energy calculation we described is a rather crude calculation to understand

hydrophobicity in terms of energy, since we considered only five different positions of the water molecule.

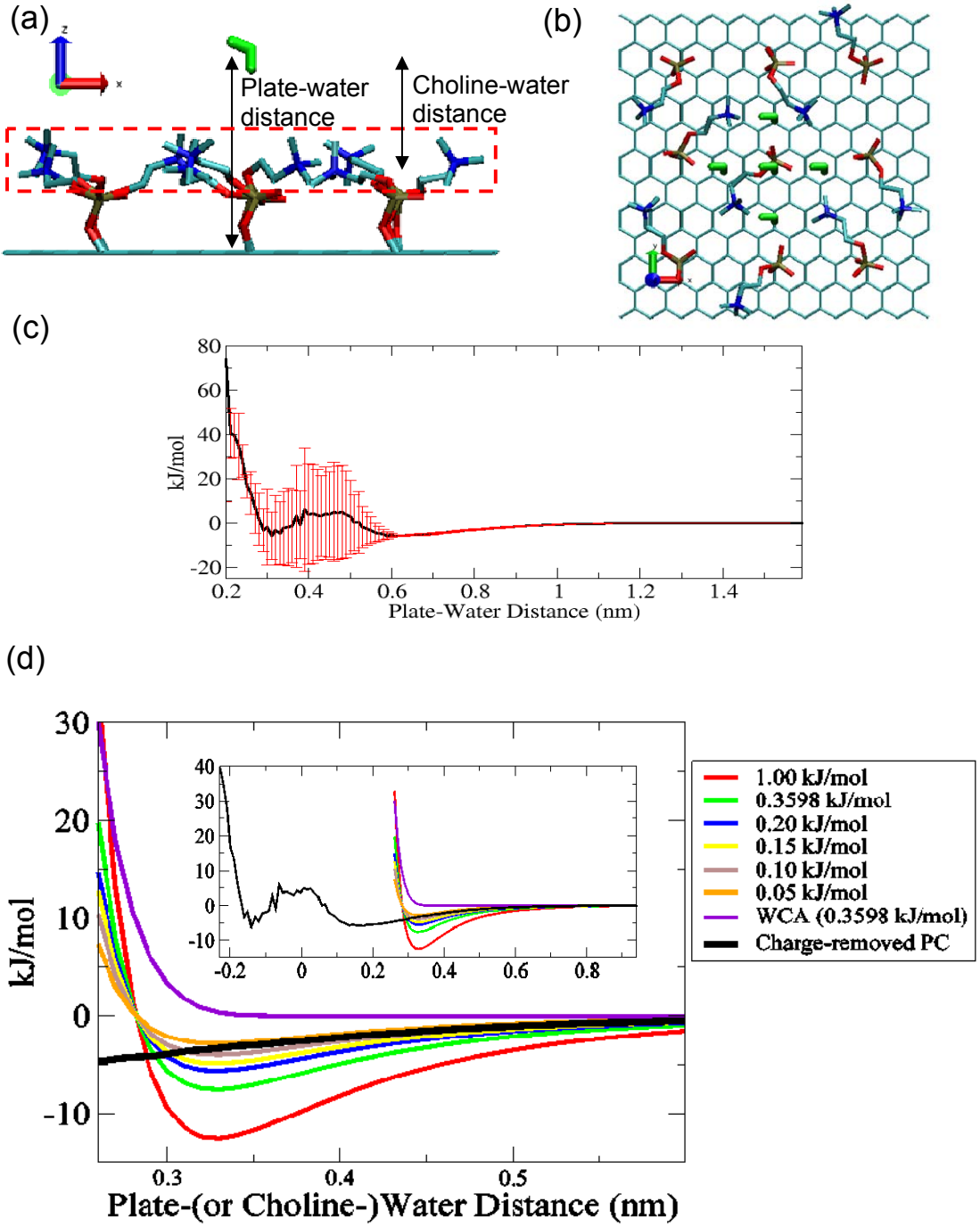

Figure 5-5. Plate-water Lennard-Jones (LJ) interaction. For a direct comparison with the CRPC plate, we increased the plate size of "carbon" plates so that their area is the same with the graphene plate of the CRPC plate, which is 4.7 times larger than the "carbon" plate used in Figure 5-4a. (a) An initial configuration at a water-plate distance of 1.01 nm, in which a water molecule is placed on the top of the center of the plate. (b) Five different positions for sampling in the CRPC plate. The same sampling was also applied to each case of "carbon" plate. (c) Plate-water LJ interaction of the CRPC plate as a function of plate-water distance. The errors are obtained by calculating the standard deviation from five samples. (d) Plate-water LJ interactions as a function of the distance between the plate and a water molecule for the "carbon" plates, and as a function of the distance between the cholines and a water molecule for the CRPC plate. Inset is for showing plate-water LJ interaction for smaller distances of the CRPC plate.

Finally, through the comparisons of the interaction between rough and flexible CRPC-headgroup plates with seven cases of interaction between smooth and fixed "carbon" plates, we conclude that the CRPC plate interaction is similar to a case with a strong hydrophobic interaction between "carbon" plates. Thus, due to the attachment of non-polar headgroups to a graphene plate, the hydrophobicity of the graphene plate is significantly enhanced. However, before we discuss the roles of roughness and flexibility due to the non-polar headgroups in detail, we want to discuss the correlation between number density of the confined water and water-mediated interaction.

5.3.5 Number density of the confined water and water-mediated interaction

The comparison among the "carbon" plates themselves shows an interesting aspect regarding the correlation between the change in the water-mediated interaction and the change in the average number of water molecules. The detailed visual inspection on Figure 5-4a suggests that when the system passes through the barriers in water-mediated interaction (red triangles), it always bring to relatively rapid decreases in the average number of water molecules (blue squares). For example, in the second top panel of Figure 5-4a for the realistic graphene model with ε_{CC} =0.3598 kJ/mol, the water-mediated interaction has two barriers and these barrier regions are clearly associated with the transition regions in the number of water molecules (the two shaded regions). Similarly, for the model with ε_{CC} =0.05 kJ/mol (second panel from the bottom), the system has one barrier in the water-mediated contribution and therefore, one corresponding transition region. Particularly, the transition in the latter case (ε_{CC} =0.05 kJ/mol) is known as a typical dewetting transition, in which an empty space is observed, where at least one or two layers of water can fit in that space.[110] Interestingly, this correlation is also noticed in the CRPC plate (see Figure 5-3a or 5-4b). This may imply that such a correlation is one of the general features appeared in hydrophobic system.

To explain this correlation in a simplest way, we may use the following equation for the average number of water molecules in the carbon nanotube (CNT), derived under the assumption that water molecules in the CNT is in equilibrium with bulk water. [18,112]

$$\langle \mathrm{N} \rangle = \rho_{bulk} \cdot \mathrm{V} \cdot e^{-\beta(\mu^{ex} - \mu^{ex}_{bulk})},$$

where N is the number of water molecules inside the CNT and ρ_{bulk} is the number density of bulk water and V is the volume inside the CNT. μ^{ex} and μ^{ex}_{bulk} are the local excess chemical potentials defined as the negative free energy of removing a water molecule from the inside of CNT and the bulk chemical potential, respectively. $\beta = 1/\mathrm{k}_B T$, where k_B and T are the Boltzmann constant and temperature, respectively. In the derivation, since it does not depend on the particular geometry of CNT, we can apply this to our situation, in which water molecules are confined by two planar surfaces. However, since in this case, we are interested in $\langle N \rangle$ as a function of d, interplate distance, we can simply generalize the equation in the following way.

$\langle N \rangle(\mathrm{d}) = \rho_{bulk} \cdot \mathrm{d} \cdot \mathrm{A} \cdot e^{-\beta(\mu^{ex}(\mathrm{d}) - \mu^{ex}_{bulk})}$,

Here, we use the fact that the volume (V) is the product of the area (A) of graphene-like plate and the interplate distance (d). First, let us consider a simple case, where the excess chemical potential of water in the confined space is equal to the one of bulk water. In this case, the slope, $\langle N \rangle(\mathrm{d})/\mathrm{d}$, is simply $\rho_{bulk} \cdot \mathrm{A}$ and it is the same with the slope when we consider the imaginary same space in bulk water. Probably, this corresponds to the case when two plates are very largely separated and the confined water is essentially bulk-like. Moreover, at these large separations, the water-mediated contribution to the PMF is negligible. However, when the separation is small enough, $\langle N \rangle(\mathrm{d})$ depends on $\mu^{ex}(\mathrm{d}) - \mu^{ex}_{bulk}$. Specifically, for example, if $\mu^{ex}(\mathrm{d}) > \mu^{ex}_{bulk}$, $\rho_{confined} := \langle N \rangle(\mathrm{d})/(\mathrm{d} \cdot \mathrm{A}) < \rho_{bulk}$, which means as the excess chemical potential increases more water molecules are removed compared to the corresponding bulk case, so that the

density is lower than the bulk density. Accordingly, this increase of excess chemical potential ($\mu^{ex}(\mathrm{d}) > \mu^{ex}_{bulk}$) can affect the water-mediated interaction in the following way.

The water-mediated interaction has a contribution, $G^{confined}_{water-mediated}$, from the $\langle N \rangle$ confined water molecules in a confined volume V and it can be expressed as $\sim \mu_{confined} \cdot \langle N \rangle$, where $\mu_{confined}$ is the chemical potential of the confined water. By further manipulating it with the above expression for $\langle N \rangle(\mathrm{d})$, we can obtain the following expression.

$$G^{confined}_{water-mediated} \sim \mu_{conined} \cdot \langle N \rangle = \left(\mu^{ex}_{confined} + \mu^{id}_{conined}\right) \cdot \langle N \rangle$$

$$= \left(\mu^{ex}_{confined} + \mu^{id}_{confined} + \mu^{ex}_{bulk} - \mu^{ex}_{bulk}\right) \cdot \langle N \rangle$$

$$= \left(\mu^{ex}_{confined} - \mu^{ex}_{bulk} + \mu^{id}_{confined} + \mu^{ex}_{bulk}\right) \cdot \langle N \rangle$$

$$= \left(\mu^{ex}_{confined} - \mu^{ex}_{bulk} + \mu_{bulk}\right) \cdot \langle N \rangle$$

$$= \left(-\frac{1}{\beta} \ln \frac{\rho_{confined}}{\rho_{bulk}} + \mu_{bulk}\right) \cdot \langle N \rangle$$

Here, we used the definition of excess chemical potential μ^{ex}: $\mu = \mu^{ex} + \mu^{id}$, where μ^{id} is the chemical potential of an ideal gas under the same conditions. And, obviously, $\mu^{id}_{confined} = \mu^{id}_{bulk}$.

To understand this equation, again let us consider an ideal case of $\mu^{ex}(\mathrm{d}) = \mu^{ex}_{bulk}$ (or $\rho_{confined} = \rho_{bulk}$). In this case, $G^{confined}_{water-mediated}$ is nothing but $\mu_{bulk} \cdot \langle N \rangle$. This is corresponding to the free energy of bulk water in the imaginary volume V. In this sense, the term $\mu_{bulk} \cdot \langle N \rangle$ can be denoted by $G^{bulk-like}_{water-mediated}$.

In fact, the quantity of $G^{confined}_{water-mediated}(\mathrm{d}) - G^{bulk-like}_{water-mediated}(\mathrm{d})$ is directly related to our calculation of water-mediated contribution to the PMF, $G_{water-mediated}(\mathrm{d}) - G_{water-mediated}(\infty)$, as we can see below.

$$G^{confined}_{water-mediated}(\mathrm{d}) - G^{bulk-like}_{water-mediated}(\mathrm{d})$$

$$= G^{confined}_{water-mediated}(\mathrm{d}) + (G^{bulk}_{water-mediated}(\mathrm{d}) - G^{bulk}_{water-mediated}(\mathrm{d})) - G^{bulk-like}_{water-mediated}(\mathrm{d})$$

$$= (G^{confined}_{water-mediated}(\mathrm{d}) + G^{bulk}_{water-mediated}(\mathrm{d})) - (G^{bulk}_{water-mediated}(\mathrm{d}) + G^{bulk-like}_{water-mediated}(\mathrm{d}))$$

$$= G_{water-mediated}(\mathrm{d}) - (G^{bulk}_{water-mediated}(\mathrm{d}) + G^{bulk-like}_{water-mediated}(\mathrm{d}))$$

$$= G_{water-mediated}(\mathrm{d}) - (G^{bulk}_{water-mediated}(\infty) + G^{bulk-like}_{water-mediated}(\infty))$$

$$= G_{water-mediated}(\mathrm{d}) - G_{water-mediated}(\infty)$$

Note that $G^{bulk}_{water-mediated}(\mathrm{d})$ and $G^{bulk-like}_{water-mediated}(\mathrm{d})$ are different in that the former is the water-mediated contribution of free energy due to the bulk water outside the confined space, which is defined by d and V, and the latter is the water-mediated contribution when the confined water is bulk-like. Also, here, the symbol ∞ represents the reference distance and we simply consider that $G_{water-mediated}(\mathrm{d}) = G^{confined}_{water-mediated}(\mathrm{d}) + G^{bulk}_{water-mediated}(\mathrm{d})$. And we used that if the confined water is truly bulk-like water, the total water-mediated interaction does not depend on the interplate distance d.

By combining all things together, we are able to obtain the following expression for water-mediated contribution.

$$G_{water-mediated}(\mathrm{d}) - G_{water-mediated}(\infty) = \left(-\frac{1}{\beta} \ln \frac{\rho_{confined}}{\rho_{bulk}} \right) \cdot \langle N \rangle$$

Note that this relation works only when water molecules are in equilibrium with the bulk; for example, in the case that the water molecules are strongly bound to the plate, those

water molecules should be considered as a part of plate, not confined water molecules we are discussing here.

Finally, by using this last equation, we can understand the inverse correlation between density change and water-mediated contribution change. For example, if $\mu^{ex}(\mathrm{d}) > \mu^{ex}_{bulk}$, then the slope of the plot of $\langle N \rangle$ versus d is greater than the slope of bulk water and $\rho_{confined} < \rho_{bulk}$ and $\Delta G_{water-mediated}(\mathrm{d}) \equiv G_{water-mediated}(\mathrm{d}) - G_{water-mediated}(\infty) > 0$ (see Figure 5-6b). In the same way, if $\mu^{ex}(\mathrm{d}) < \mu^{ex}_{bulk}$, then the slope is less than the bulk water slope and $\rho_{confined} > \rho_{bulk}$ and $\Delta G_{water-mediated}(\mathrm{d}) < 0$ (see Figure 5-6c). However, after dewetting transition or in a vapor-liquid equilibrium, the relation does not hold. This is because the water molecules in the confined space are not in equilibrium with the bulk and they are thermodynamically unstable. In fact, the water number fluctuation is so large that the statistics is significantly deviated from Gaussian statistics.[90] In other words, the dewetting transition begins when the relation is broken.

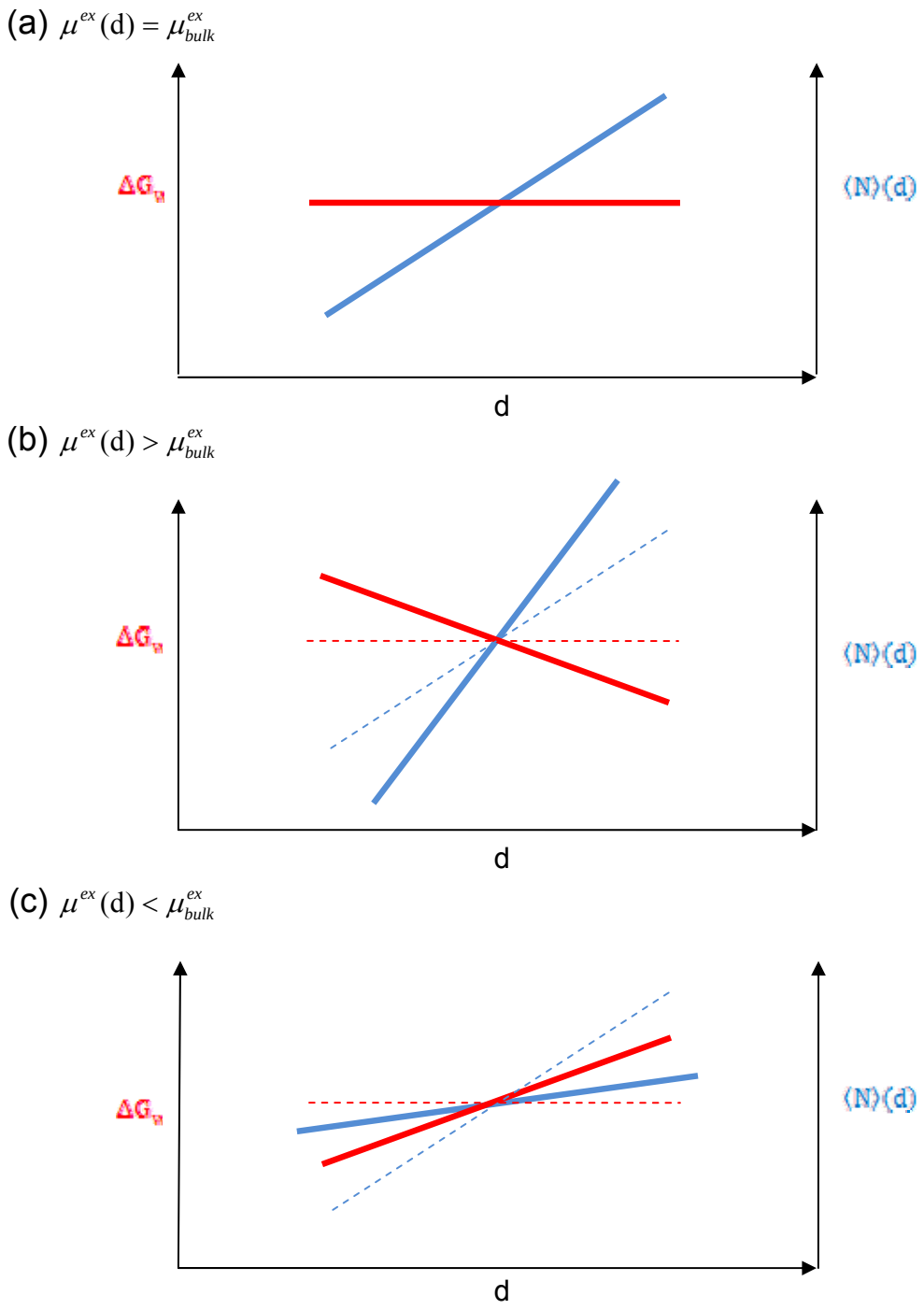

Figure 5-6. Schematic diagrams showing an inverse correlation between the changes in $\Delta G_V :\equiv G_{water-mediated}(\mathrm{d})$ (red line) and $\langle N \rangle(\mathrm{d})$ (blue line), in the cases of $\mu^{ex}(\mathrm{d}) = \mu^{ex}_{bulk}$ (a), $\mu^{ex}(\mathrm{d}) > \mu^{ex}_{bulk}$ (b) and $\mu^{ex}(\mathrm{d}) < \mu^{ex}_{bulk}$ (c).

5.3.6 Role of roughness due to non-polar headgroups

Let us now discuss the effects of roughness due to the presence of non-polar headgroups attached to the CRPC plate. As we can see from Figure 5-4, the water-mediated attraction is stronger in the presence of the headgroups than in the case of bare graphene plates. Moreover, the dewetting transition or vapor-liquid equilibrium takes place when the interplate fluid space is larger (~ 0.8 nm in Figure 5-4b) in case of CRPC plates compared to case of graphene plates (~0.6 nm in Figure 5-4a). Thus, as we already mentioned, the roughness enhances hydrophobic interaction, and a proper comparison can be made with plates containing "carbon" atoms with a low strength of water-plate interaction (in our case for ε_{CC} =0.05 kJ/mol).

To get more insight of why this is happening, we consider the snapshots of water and calculate the water density profiles, especially in a region that is close to the dewetting transition. The density profiles are shown in Figure 5-7a. Note that the change of density profiles in the dewetting transition regime (d=1.74~1.8 nm) is correlated with the large change in the average number of water molecules depicted in Figure 5-3a. After the partial dewetting transition is completed (d < 1.74 nm), the water density in the middle is significantly reduced and it forms a plateau, indicating the existence of some residual water molecules. From the snapshots in Figure 5-3c, we understand that these residual waters are the waters at the boundary of the confined space, which are interacting with the bulk water. Because of this contribution, the density profiles of CRPC plate for the confined space are quite different from the ones observed for the systems with smooth graphene-like plates and shown in Figure 5-7b. However, since this portion of density profile due to boundary water molecules (blue dotted rectangle in

Figure 5-7a) is not of our main concern, we can disregard it and only concentrate on the change in the middle region that is represented by a red dotted rectangle in Figure 5-7a.

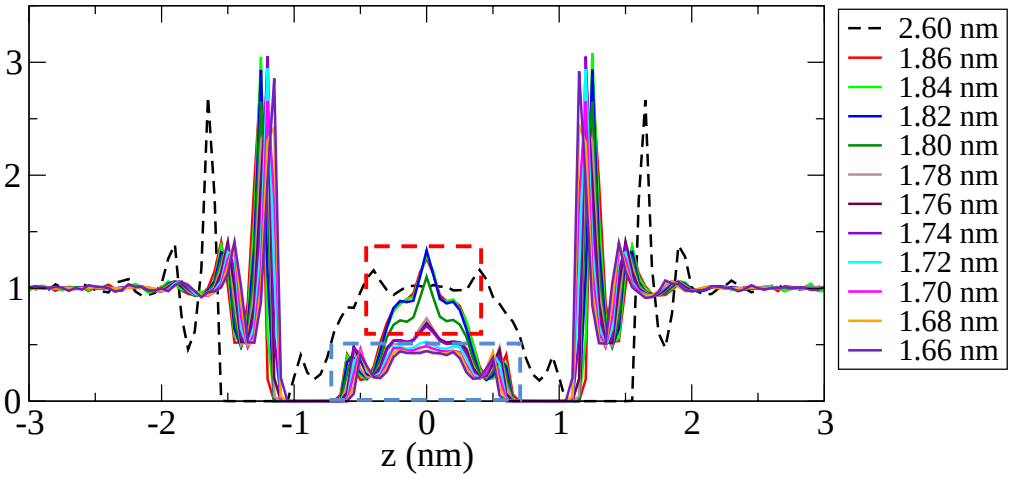
2.60 nm
1.86 nm
1.84 nm
1.82 nm
1.80 nm
1.78 nm
1.76 nm
1.74 nm
1.72 nm
1.70 nm
1.68 nm
1.66 nm
z (nm)

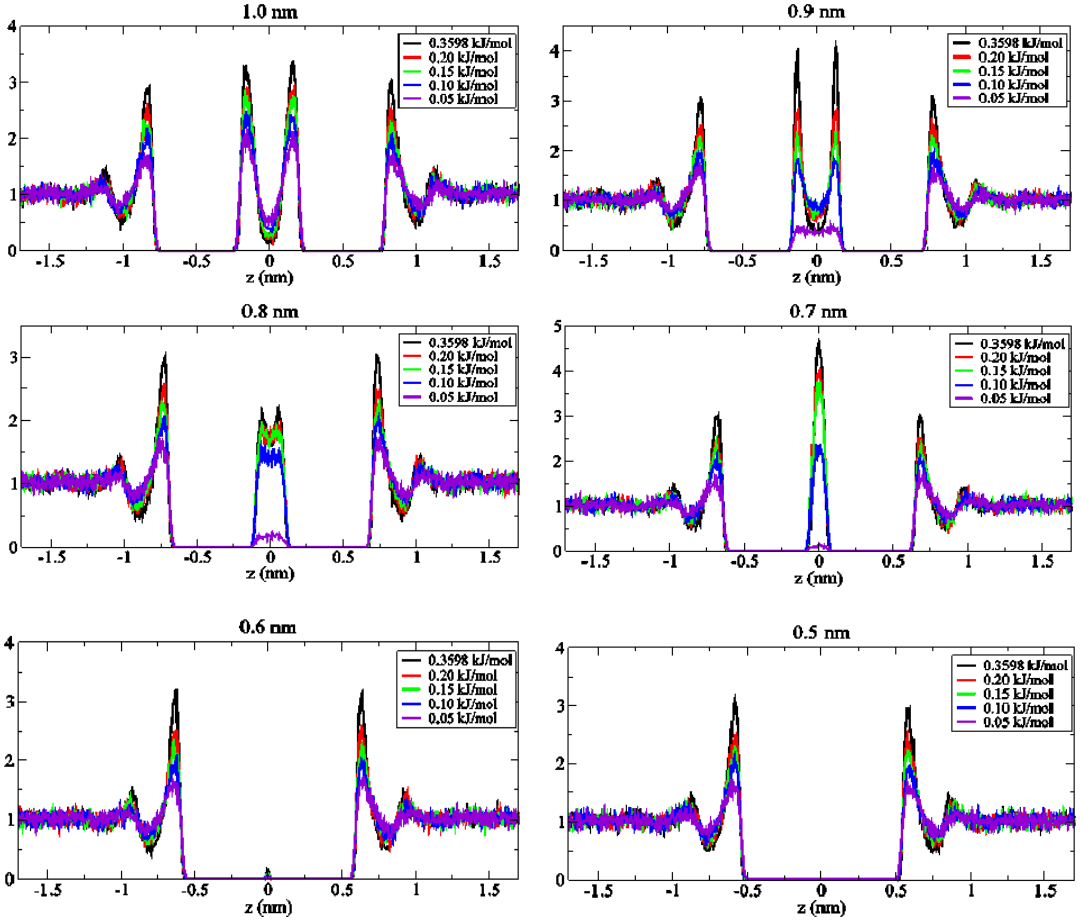
1.0 nm
0.9 nm
0.8 nm
0.7 nm
0.6 nm
0.5 nm
0.3598 kJ/mol
0.20 kJ/mol
0.15 kJ/mol
0.10 kJ/mol
0.05 kJ/mol
z (nm)

Figure 5-7. Water number density profiles for the system containing the CRPC plate (a) and "carbon" plates (b). For clarity, only the water molecules in the x-y dimensions of the plates are taken into account. The density profiles are normalized so that the values in bulk water region are 1 and the z coordinate of middle point in the confined space is set to be zero.

From Figure 5-7b we observe that water between the graphene plates (black, ε_{CC} =0.3598 kJ/mol) shows a strong layering structure, as the distance between plates decreases. However, water between the CRPC plates does not show layering. Probably, this is happening because the non-polar headgroups significantly disturb the smooth geometry of the graphene plate (and thus water hydrogen bonding network next to the plate) and do not allow stable water layers to form, as this is happening in the case of smooth graphene plates. Water between "carbon" plates with ε_{CC} =0.05 kJ/mol and between the CRPC plates show a similar behavior in the dewetting transition regime; compare the changes depicted in the red box in Figure 5-7a and the changes of profiles in the confined space from Figure 5-7b (d ≤ 0.9 nm).

As we already observed, the presence of uncharged headgroups decreases water-plate interaction, leading to a strong hydrophobicity. To investigate this in more detail, we examine the snapshots again. The sideviews in Figure 5-3c clearly demonstrate that water molecules do not penetrate inside the hydrophobic environment created between graphene plates and the headgroups. For a quantitative analysis, we calculate the density profiles for headgroups in Figure 5-8 and superpose them with the water density profiles in Figure 5-7, to understand where water molecules are located. As we can see from

Figures 5-8a and 5-8b, the density of water molecules close to carbon atoms of the plates is low in case of the CRPC plates, when compared to the density in case of PC-headgroup plates(compare the density peaks of water at z=-0.6nm). Thus, water molecules in the center of the confined space between the CRPC plates cannot strongly interact with the graphene parts (red box in Figure 5-8a) of the plates, and, therefore, the plate-water interaction is relatively weak. The distance between the closest water to the graphene part of the plate is around 0.5 nm (arrow in Figure 5-8a), which is much larger than σ_{CO} (~0.33 nm). The reason why water is staying away from the graphene parts of the CRPC plates is that there is no driving force to break water-water hydrogen bonds; for the case of PC-headgroup case, this driving force is the strong electrostatic interaction between water and the polar headgroup, which produces a relatively high water density next to the graphene parts (see Figure 5-8c and 5-8d). Thus, water essentially does not interact with the graphene parts of the plates, which results in the reduction of the strength of the plate-water interaction in the CRPC plate case, compared to the pure graphene case.

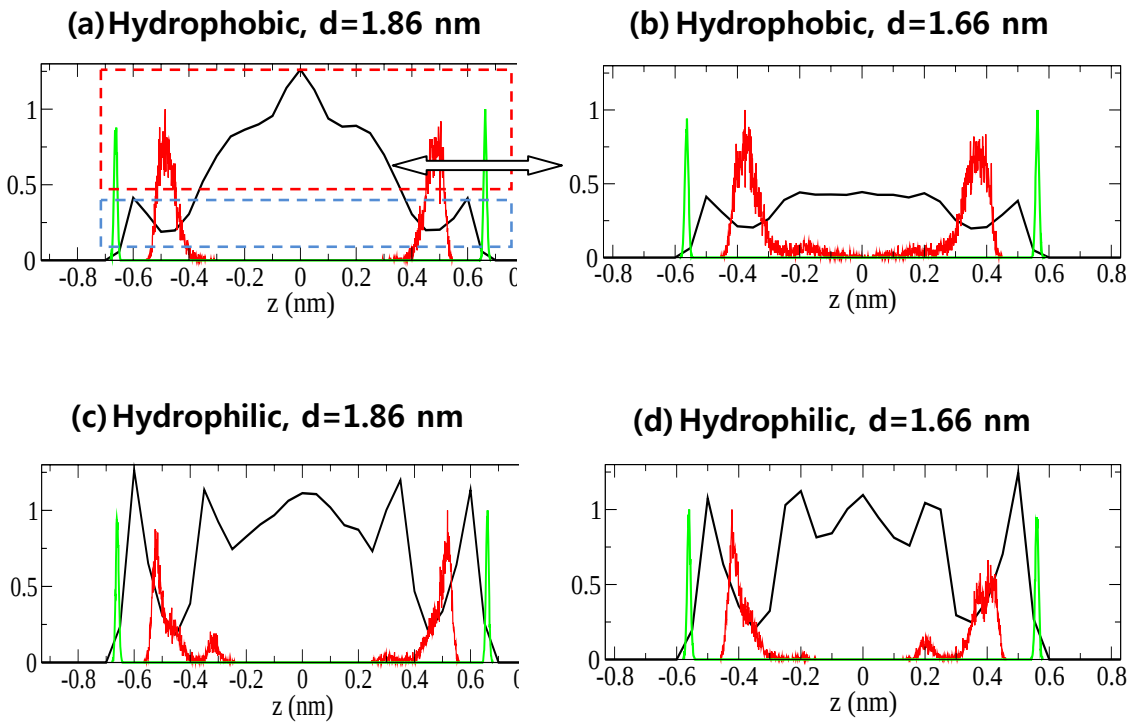

Figure 5-8. Profiles for the number of water molecules represented by oxygen atom (black), the center of mass (COM) of three end carbons of choline (red), and the COM of phosphates (green) along the z axis (perpendicular to the graphene plates) of four cases. (a) CRPC plates at an interplate distance of 1.86 nm, when water wets the plates. (b) CRPC plates at 1.66 nm, when the system is a partially dry state. (c) PC-headgroup plates at 1.86 nm. (d) PC-headgroup plates at 1.66 nm. Here, the profiles associated with cholines and phosphates are normalized, so that the maximum values are 1, whereas for water the plots are normalized by the number density of bulk water. The red and blue dotted boxes in (a) indicate the regions where contributions from water molecules located inside and outside of the spherical boundary region shown in Figure 5-3c. Note that in each case the plates are located at the both ends of the z axis in the plots.

In fact, this situation strongly reminds us of a Cassie-Baxter state[19,93] used to describe wetting of the rough solid surface. Cassie-Baxter state occurs when the contact area between the surface and water molecules is reduced due to roughness of the surface that effectively interacts with water molecules decreases. Assuming that we deal with the Cassie-Baxter-like states in our situation, we can quantify the degree of an effective interaction of the surface with water by defining a simplified measure of an effective interaction strength, as an intrinsic quantity of the plate. This measure, S_{eff}, is estimated to be the total strength of interaction between the plate and water divided by the total area of the plate.

$$S_{eff} = \frac{total\ strength}{area} = \frac{\sum_i total\ \#\ of\ particles\ of\ type\ i \times \varepsilon_{particle(i)-O}}{area},$$

where $\varepsilon_{particle(i)-O}$ is the LJ parameter for interaction between the particle of type i belonging to the plate and the oxygen atom of water. We calculated the values of S_{eff} for our systems and the results are summarized in Table 5-1. Although our calculations represent just a rough estimate, the numbers we get show that indeed for CRPC plates the S_{eff} is relatively small, and corresponds to a value for which "carbon" plates are strongly hydrophobic.

Model	S_{eff} (kJ/mol/nm^2)
"carbon"plate (ε_{CC}=1.00 kJ/mol)	40.0
graphene plate (ε_{CC}=0.3598 kJ/mol)	23.7
"carbon" plate (ε_{CC}=0.20 kJ/mol)	17.7
"carbon" plate (ε_{CC}=0.15 kJ/mol)	15.3
"carbon" plate (ε_{CC}=0.10 kJ/mol)	12.5
"carbon" plate (ε_{CC}=0.05 kJ/mol)	8.9
CRPC plate	11.6*

*In this calculation, the graphene part is excluded and the entire headgroups are included.

Table 5-1. Effective interaction strength for our model plates.

5.3.7 Role of local flexibility due to non-polar headgroups

Since the length of a headgroup (composed of 11 of atoms and united atoms) is relatively small compared to the graphene plate size and the one end atom of the headgroup is fixed because it is attached to the plate, the effect of flexibility is relatively small. However, we are able to capture this effect in the PMF curve. Specifically, it is clearly seen in the shape of the curve for the direct interaction contribution to the PMF. As we can notice from Figure 5-3a, the direct interaction between CRPC plates has, besides the global minimum, a local minimum around d=1.5 nm, while the correspoidng direct interaction between graphene plates does not have such a minimum (see open circles in Figure 5-4a). To understand the existence of this minimum, we looked at some snapshots from the simulations. These snapshots, shown in Figure 5-9a, indicate that the minimum in the direct interaction curve is associated with the change of relative orientations of the headgroups protruding from one plate with respect to the headgroups of the other plate.

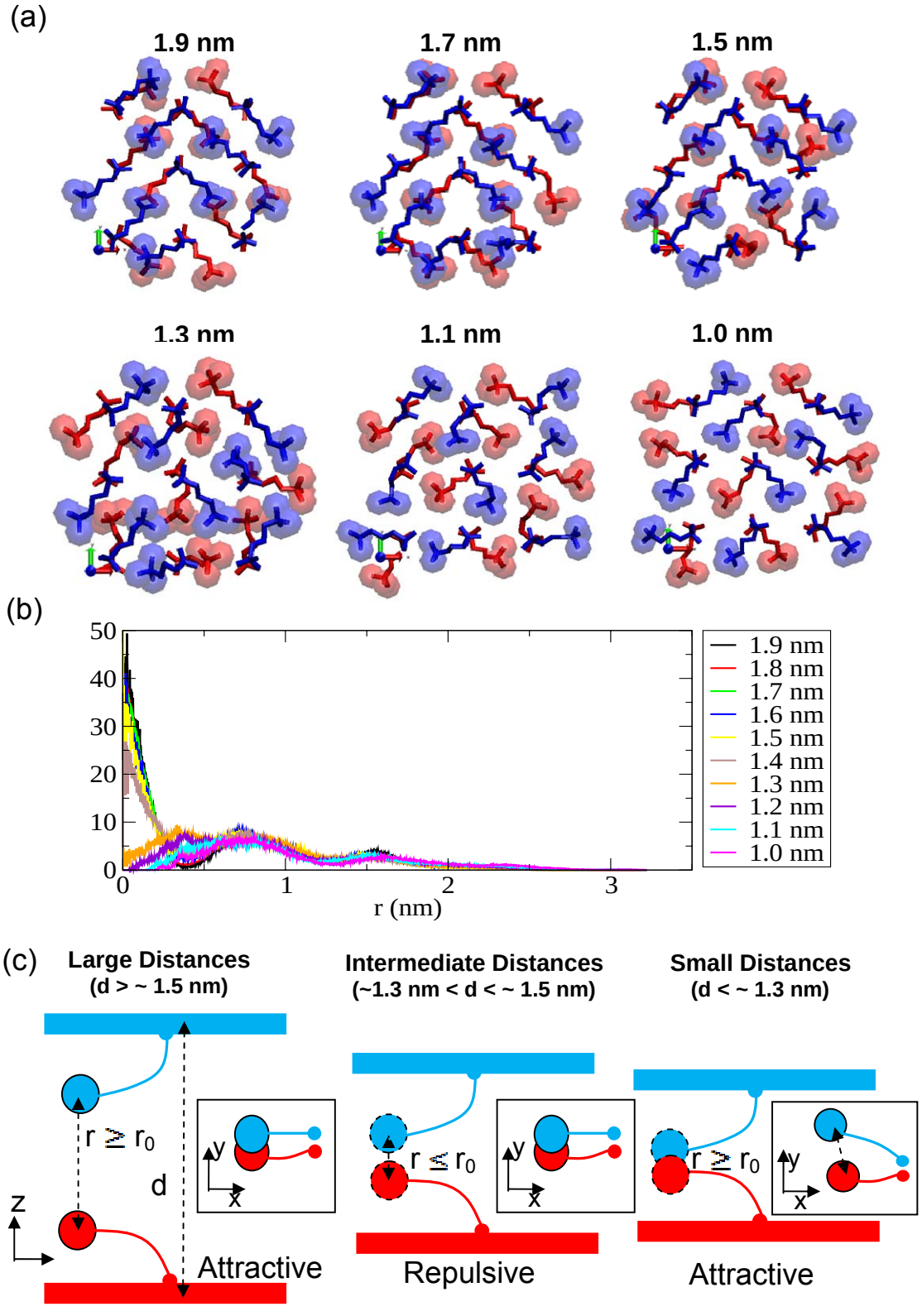
(a)
1.9 nm
1.7 nm
1.5 nm
1.3 nm
1.1 nm
1.0 nm
(b)
50
40
30
20
10
0
0
1
2
3
r (nm)
1.9 nm
1.8 nm
1.7 nm
1.6 nm
1.5 nm
1.4 nm
1.3 nm
1.2 nm
1.1 nm
1.0 nm
(c)
Large Distances
(d > ~ 1.5 nm)
Intermediate Distances
(~1.3 nm < d < ~ 1.5 nm)
Small Distances
(d < ~ 1.3 nm)
r ≥ r0
d
z
y
x
Attractive
r ≤ r0
y
x
Repulsive
r ≥ r0
y
x
Attractive

Figure 5-9. (a) Snapshots taken at 1 ns for some selected interplate distances. The perspective is perpendicular to the graphene plates. United carbon atoms (methyl groups of choline moieties) are represented by van der Waals spheres. To distinguish two types of the united atoms, depending on which plate they belong to, we use red and blue colors. The graphene plates are parallel to the paper. (b) xy-dimensional radial distribution functions of the red united carbon atoms of the bottom plate, with respect to the blue united carbon atom of the top plate. (c) Schematic diagrams for explaining why direct interaction has a small barrier between1.3 nm and 1.5 nm. r_0 is a critical distance for the repulsion between non-polar headgroups corresponding to the σ parameter in LJ interaction.

For a quantitative analysis of this reorientational motion we calculated a xy-dimensional pair correlation function between the two groups of headgroups (specifically, methyl groups of choline moieties; blue and red spheres in Figure 5-9a). The result is shown in Figure 5-9b. It is clear that there is a conformational change when the distance between CRPC plates is in the interval between 1.3 nm and 1.5 nm. Note that at these distances the partial dewetting already took place and water does not play a significant role. At larger separations ($d > \sim 1.5$ nm), the preferable configuration is such that blue and red headgroups overlap in the xy plane, to maximize the van der Waals interaction between them. Also, for the same reason, the headgroups in a dewetted state are a little bit stretched along the z axis (see the red plots in Figure 5-8b). However, when the headgroups are close enough ($d < \sim 1.3$ nm), such configuration is not preferable any more, due to steric repulsion. Thus, in the regime of the intermediate separations, the

headgroups change their relative orientations, so they can avoid repulsion acting between them. As a result, the overlaps in the xy plane disappear. This is explained using cartoons in Figure 5-8c. Thus, due to flexibility of the headgroups, the system can reach a deeper minimum in the direct interaction part of PMF.

5.4 Summary and Conclusions

This study was initiated to understand the contribution of the electrostatic interaction into a repulsive hydration force acting between two lipid bilayers. In order to do this we studied the interaction between model lipid bilayers called PC-headgroup plates and we directly calculated the contribution of electrostatic interaction to the potential energy of interaction between these model bilayers and water molecules. The latter interaction, as we previously established, is crucial in understanding the thermodynamic origin of the hydration interaction.[88] As another evidence for this conclusion, we removed the electric charges from headgroup atoms and calculated the free energy as a function of distance between the two now non-polar model bilayers. Contrary to the case of the original model bilayers, the interbilayer interaction became attractive. Therefore, we can firmly conclude that the repulsive interaction between the PC-headgroup plates is originated from the electrostatic interaction between polar headgroups and water molecules.

To understand how hydrophobic the interaction between our CRPC plates is, we compared the results from the simulations with these plates to the results obtained from simulations where the interaction between smooth plates containing "carbon" atoms was varied by varing the strength of "carbon"-water interaction. The comparison showed that our CRPC plates are strongly hydrophobic. Attachment of hydrophobic groups to smooth plates increased the plate hydrophobicity, because the groups created voids between water and graphene surface and water molecules were not able to fill up these voids. Therefore the state of water in our simulations with CRPC plates was similar to the Cassie-Baxter state and this contributed to the increase of hydrophobicity of the interplate

interaction. The flexibility of the plate headgroups also influenced the interaction, mostly the direct interaction between the plates.

In this study and our previous studies on this subject,[56,88,90] we did not calculate the contract angle between the water droplet and our plates to determine the hydrophobic (hydrophilic) character of the plate. We did not do it because our plates are small, and it is very difficult to calculate accurately the microscopic contact angle of a water nanodroplet. For example, in the 1 ns NVT simulations with 300 water molecules placed on the plate at 298 K, a water nanodroplet moves around on the plate surface and sometimes stays on the edges of the plate, instead of being in the middle of the plate (see Figure 5-10b). This is most often happening in cases of strongly hydrophobic plates. However, the snapshots shown in Figure 5-10 can give us an idea that the water nanodroplet on the plate beads up or reduces its spread over the surface, as the "carbon"-water interaction decreases. The shape of the water droplet on the charge-removed PC-headgroup plate is similar to the shape in the cases of strong hydrophobic "carbon" plates (see Figures 5-10b and 5-10f). Importantly, this trend of hydrophobicity on a single plate is consistent with the trend of hydrophobic effects observed in interplate interaction and dewetting transition between two plates.

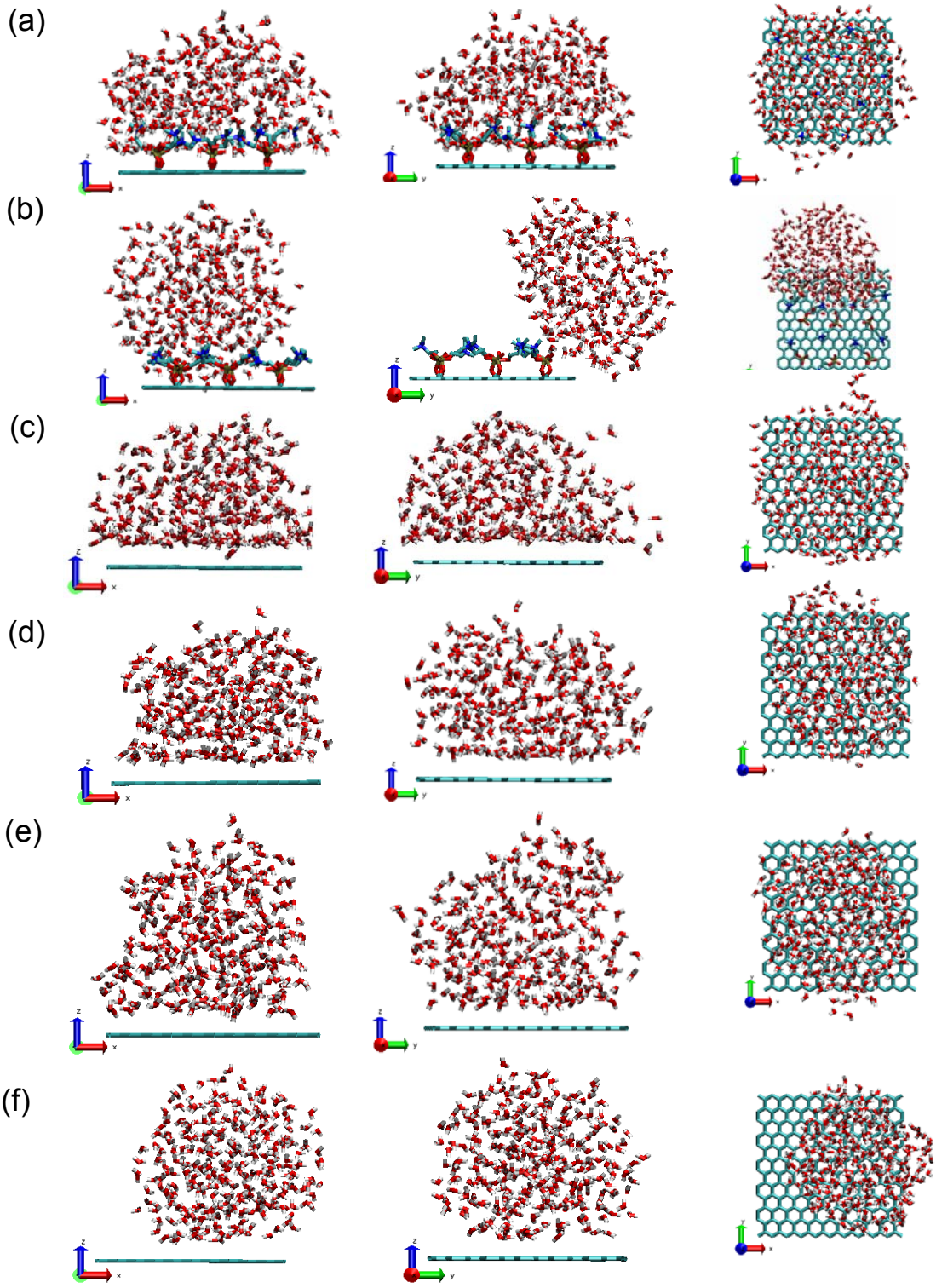
(a)
(b)
(c)
(d)
(e)
(f)

Figure 5-10. Snapshots taken at 1 ns for a water nanodroplet on the PC-headgroup plate (a), the CRPC plate (b), the "carbon" plates with ε_{CC} = 1.00 kJ/mol (c), ε_{CC} = 0.3598 kJ/mol (d), ε_{CC} = 0.10 kJ/mol (e), and ε_{CC} = 0.05 kJ/mol (f). For each case, the middle snapshot is obtained by rotating the system in the left one by 90° around the z axis. The rightmost snapshot represents a view from the top. According to the conventional criterion based on the contact angle, it seems the plates of (b), (e) and (f) are hydrophobic, while the plates of (a), (c) and (d) are hydrophilic.

Finally we would like to mention that the systems we studied here and previously,[56,88,90] especially the system containing the CRPC plates, may seem to be somewhat artificial. Nevertheless, by systematic study of such systems and their hierarchy (graphene plates, "carbon" plates with different water-"carbon" interaction strength, dressing up the plates with zwitterionic headgroups, removing charges on the headgroups) allowed us to understand the role of important factors in the phenomena of hydrophobic and hydrophilic interactions.

References

(1) Chaplin, M. *Nature Reviews Molecular Cell Biology* **2006**, *7*, 861.

(2) Ball, P. *Chemical Reviews (Washington, DC, United States)* **2008**, *108*, 74.

(3) Ball, P. *ChemPhysChem* **2008**, *9*, 2677.

(4) Westhof, E. *Annual Review of Biophysics and Biophysical Chemistry* **1988**, *17*, 125.

(5) Levy, Y.; Onuchic, J. N. *Proceedings of the National Academy of Sciences of the United States of America* **2004**, *101*, 3325.

(6) Papoian, G. A.; Ulander, J.; Eastwood, M. P.; Luthey-Schulten, Z.; Wolynes, P. G. *Proceedings of the National Academy of Sciences of the United States of America* **2004**, *101*, 3352.

(7) Fitter, J. *Biophysical Journal* **1999**, *76*, 1034.

(8) Volkhard, H. *ChemPhysChem* **2007**, *8*, 23.

(9) Levy, Y.; Onuchic, J. N. *Annual Review of Biophysics and Biomolecular Structure* **2006**, *35*, 389.

(10) Frauenfelder, H.; Fenimore, P. W.; Chen, G.; McMahon, B. H. *Proceedings of the National Academy of Sciences* **2006**, *103*, 15469.

(11) Schwabe, J. W. R. *Current Opinion in Structural Biology* **1997**, *7*, 126.

(12) Ladbury, J. E. *Chemistry & Biology* **1996**, *3*, 973.

(13) Phillip, Y.; Carmi, A.; Schreiber, G. *Biochemistry* **2007**, *47*, 1051.

(14) Tanford, C. *Science* **1978**, *200*, 1012.

(15) Zhang, Y. *Current Opinion in Structural Biology* **2008**, *18*, 342.

(16) Granick, S.; Bae, S. C. *Science* **2008**, *322*, 1477.

(17) Godawat, R.; Jamadagni, S. N.; Garde, S. *Proceedings of the National Academy of Sciences of the United States of America* **2009**, *106*, 15119.

(18) Hummer, G.; Rasaiah, J. C.; Noworyta, J. P. *Nature* **2001**, *414*, 188.

(19) Hirvi, J. T.; Pakkanen, T. A. *Journal of Physical Chemistry B* **2007**, *111*, 3336.

(20) Giovambattista, N.; Debenedetti, P. G.; Rossky, P. J. *Proceedings of the National Academy of Sciences of the United States of America* **2009**, *106*, 15181.

(21) Giovambattista, N.; Lopez, C. F.; Rossky, P. J.; Debenedetti, P. G. *Proceedings of the National Academy of Sciences of the United States of America* **2008**, *105*, 2274.

(22) Choudhury, N.; Pettitt, B. M. *Journal of the American Chemical Society* **2007**, *129*, 4847.

(23) Ben-Naim, A. *Molecular Theory of Water and Aqueous Solutions*; World Scientific Publishing Co. Pte. Ltd., 2009.

(24) Leneveu, D. M.; Rand, R. P.; Parsegian, V. A. *Nature* **1976**, *259*, 601.

(25) Leikin, S.; Parsegian, V. A.; Rau, D. C.; Rand, R. P. *Annual Review of Physical Chemistry* **1993**, *44*, 369.

(26) Israelachvili, J. N.; Wennerstrom, H. *Langmuir* **1990**, *6*, 873.

(27) Israelachvili, J.; Wennerstrom, H. *Nature* **1996**, *379*, 219.

(28) Mcintosh, T. J.; Simon, S. A. *Biochemistry* **1993**, *32*, 8374.

(29) Marcelja, S.; Radic, N. *Chemical Physics Letters* **1976**, *42*, 129.

(30) Manciu, M.; Ruckenstein, E. *Langmuir* **2001**, *17*, 7582.

(31) Gruen, D. W. R.; Marcelja, S. *Journal of the Chemical Society-Faraday Transactions Ii* **1983**, *79*, 225.

(32) Schiby, D.; Ruckenstein, E. *Chemical Physics Letters* **1983**, *95*, 435.

(33) Attard, P.; Batchelor, M. T. *Chemical Physics Letters* **1988**, *149*, 206.

(34) Besseling, N. A. M. *Langmuir* **1997**, *13*, 2113.

(35) Kornyshev, A. A.; Leikin, S. *Physical Review A* **1989**, *40*, 6431.

(36) Essmann, U.; Perera, L.; Berkowitz, M. L. *Langmuir* **1995**, *11*, 4519.

(37) Raghavan, K.; Reddy, M. R.; Berkowitz, M. L. *Langmuir* **1992**, *8*, 233.

(38) Pertsin, A.; Platonov, D.; Grunze, M. *Journal of Chemical Physics* **2005**, *122*.

(39) Pertsin, A.; Platonov, D.; Grunze, M. *Langmuir* **2007**, *23*, 1388.

(40) Lu, L.; Berkowitz, M. L. *Journal of Chemical Physics* **2006**, *124*.

(41) Lu, L.; Berkowitz, M. L. *Molecular Physics: An International Journal at the Interface Between Chemistry and Physics* **2006**, *104*, 3607

(42) Leikin, S. *Journal of Chemical Physics* **1991**, *95*, 5224.

(43) Choudhury, N.; Pettitt, B. M. *Journal of the American Chemical Society* **2005**, *127*, 3556.

(44) Nose, S. *Journal of Chemical Physics* **1984**, *81*, 511.

(45) Hoover, W. G. *Physical Review A* **1985**, *31*, 1695.

(46) Parrinello, M.; Rahman, A. *Journal of Applied Physics* **1981**, *52*, 7182.

(47) Essmann, U.; Perera, L.; Berkowitz, M. L.; Darden, T.; Lee, H.; Pedersen, L. G. *Journal of Chemical Physics* **1995**, *103*, 8577.

(48) Berendsen, H. J. C.; Grigera, J. R.; Straatsma, T. P. *Journal of Physical Chemistry* **1987**, *91*, 6269.

(49) Lindahl, E.; Hess, B.; van der Spoel, D. *Journal of Molecular Modeling* **2001**, *7*, 306.

(50) Chandler, D. *Nature* **2005**, *437*, 640.

(51) Mcintosh, T. J.; Simon, S. A. *Annual Review of Biophysics and Biomolecular Structure* **1994**, *23*, 27.

(52) Rand, R. P.; Parsegian, V. A. *Biochimica Et Biophysica Acta* **1989**, *988*, 351.

(53) Leikin, S.; Kornyshev, A. A. *Journal of Chemical Physics* **1990**, *92*, 6890.

(54) Berkowitz, M. L.; Raghavan, K. *Langmuir* **1991**, *7*, 1042.

(55) Perera, L.; Essmann, U.; Berkowitz, M. L. *Langmuir* **1996**, *12*, 2625.

(56) Eun, C.; Berkowitz, M. L. *Journal of Physical Chemistry B* **2009**, *113*, 13222.

(57) Berne, B. J.; Weeks, J. D.; Zhou, R. H. *Annual Review of Physical Chemistry* **2009**, *60*, 85.

(58) Lum, K.; Chandler, D.; Weeks, J. D. *Journal of Physical Chemistry B* **1999**, *103*, 4570.

(59) Choudhury, N.; Pettitt, B. M. *Journal of Physical Chemistry B* **2006**, *110*, 8459.

(60) Nagle, J. F.; Tristram-Nagle, S. *Biochimica Et Biophysica Acta-Reviews on Biomembranes* **2000**, *1469*, 159.

(61) Pandit, S. A.; Bostick, D.; Berkowitz, M. L. *Biophysical Journal* **2003**, *84*, 3743.

(62) Marrink, S. J.; Tieleman, D. P.; vanBuuren, A. R.; Berendsen, H. J. C. *Faraday Discussions* **1996**, 191.

(63) Iuchi, S.; Chen, H. N.; Paesani, F.; Voth, G. A. *Journal of Physical Chemistry B* **2009**, *113*, 4017.

(64) Jedlovszky, P.; Brodholt, J. P.; Bruni, F.; Ricci, M. A.; Soper, A. K.; Vallauri, R. *Journal of Chemical Physics* **1998**, *108*, 8528.

(65) Hess, B. *Journal of Chemical Physics* **2002**, *116*, 209.

(66) Zangi, R.; Berne, B. J. *Journal of Physical Chemistry B* **2008**, *112*, 8634.

(67) Bhide, S. Y.; Berkowitz, M. L. *Journal of Chemical Physics* **2005**, *123*, 224702.

(68) Pal, S.; Balasubramanian, S.; Bagchi, B. *Journal of Physical Chemistry B* **2003**, *107*, 5194.

(69) Bruce, C. D.; Senapati, S.; Berkowitz, M. L.; Perera, L.; Forbes, M. D. E. *Journal of Physical Chemistry B* **2002**, *106*, 10902.

(70) Senapati, S.; Berkowitz, M. L. *Journal of Chemical Physics* **2003**, *118*, 1937.

(71) Lee, S. H.; Rossky, P. J. *Journal of Chemical Physics* **1994**, *100*, 3334.

(72) Kjellander, R.; Marcelja, S. *Chemical Physics Letters* **1985**, *120*, 393.

(73) Stillinger, F. H. *Journal of Solution Chemistry* **1973**, *2*, 141.

(74) Hummer, G.; Garde, S.; Garcia, A. E.; Paulaitis, M. E.; Pratt, L. R. *Journal of Physical Chemistry B* **1998**, *102*, 10469.

(75) Pratt, L. R. *Annual Review of Physical Chemistry* **2002**, *53*, 409.

(76) Ashbaugh, H. S.; Pratt, L. R. *Reviews of Modern Physics* **2006**, *78*, 159.

(77) Janecek, J.; Netz, R. R. *Langmuir* **2007**, *23*, 8417.

(78) Hummer, G.; Garde, S.; Garcia, A. E.; Pohorille, A.; Pratt, L. R. *Proceedings of the National Academy of Sciences of the United States of America* **1996**, *93*, 8951.

(79) Huang, D. M.; Geissler, P. L.; Chandler, D. *Journal of Physical Chemistry B* **2001**, *105*, 6704.

(80) Rajamani, S.; Truskett, T. M.; Garde, S. *Proceedings of the National Academy of Sciences of the United States of America* **2005**, *102*, 9475.

(81) Mittal, J.; Hummer, G. *Proceedings of the National Academy of Sciences of the United States of America* **2008**, *105*, 20130.

(82) Patel, A. J.; Varilly, P.; Chandler, D. *Journal of Physical Chemistry B* **2010**, *114*, 1632.

(83) Pohorille, A.; Wilson, M. A. *Theochem-Journal of Molecular Structure* **1993**, *103*, 271.

(84) Sarupria, S.; Garde, S. *Physical Review Letters* **2009**, *103*, 037803.

(85) Pratt, L. R.; Chandler, D. *Journal of Solution Chemistry* **1980**, *9*, 1.

(86) Chandler, D.; Weeks, J. D.; Andersen, H. C. *Science* **1983**, *220*, 787.

(87) Israelachvili, J. N.; Wennerstrom, H. *Journal of Physical Chemistry* **1992**, *96*, 520.

(88) Eun, C.; Berkowitz, M. L. *Journal of Physical Chemistry B* **2010**, *114*, 3013.

(89) Hua, L.; Zangi, R.; Berne, B. J. *Journal of Physical Chemistry C* **2009**, *113*, 5244.

(90) Eun, C.; Berkowitz, M. L. *Journal of Physical Chemistry B* **2010**, *114*, 13410.

(91) Giovambattista, N.; Debenedetti, P. G.; Rossky, P. J. *Journal of Physical Chemistry B* **2007**, *111*, 9581.

(92) Wenzel, R. N. *Industrial & Engineering Chemistry* **1936**, *28*, 988.

(93) Cassie, A. B. D.; Baxter, S. *Transactions of the Faraday Society* **1944**, *40*, 546.

(94) Yang, C.; Tartaglino, U.; Persson, B. N. J. *Physical Review Letters* **2006**, *97*.

(95) Lafuma, A.; Quere, D. *Nature Materials* **2003**, *2*, 457.

(96) Carbone, G.; Mangialardi, L. *European Physical Journal E* **2005**, *16*, 67.

(97) Patankar, N. A. *Langmuir* **2004**, *20*, 7097.

(98) Dupuis, A.; Yeomans, J. M. *Langmuir* **2005**, *21*, 2624.

(99) Barthlott, W.; Neinhuis, C. *Planta* **1997**, *202*, 1.

(100) Neinhuis, C.; Barthlott, W. *Annals of Botany* **1997**, *79*, 667.

(101) Gao, X.; Jiang, L. *Nature* **2004**, *432*, 36.

(102) Nakajima, A.; Hashimoto, K.; Watanabe, T. *Monatshefte fuer Chemie* **2001**, *132*, 31.

(103) Lundgren, M.; Allan, N. L.; Cosgrove, T.; George, N. *Langmuir* **2003**, *19*, 7127.

(104) Lundgren, M.; Allan, N. L.; Cosgrove, T. *Langmuir* **2007**, *23*, 1187.

(105) Koishi, T.; Yasuoka, K.; Fujikawa, S.; Ebisuzaki, T.; Zeng, X. C. *Proceedings of the National Academy of Sciences of the United States of America* **2009**, *106*, 8435.

(106) Daub, C. D.; Wang, J.; Kudesia, S.; Bratko, D.; Luzar, A. *Faraday Discussions* **2010**, *146*, 67.

(107) Zwanzig, R. W. *Journal of Chemical Physics* **1954**, *22*, 1420.

(108) Meyer, S. L. *Data Analysis for Scientists and Engineers*; Wiley: New York, 1975.

(109) Taylor, J. R. *An Introduction to Error Analysis: The Study of Uncertainties in Physical Measurements* 2nd ed.; University Science Books: Sausalito, California, 1997.

(110) Wallqvist, A.; Berne, B. J. *Journal of Physical Chemistry* **1995**, *99*, 2893.

(111) Werder, T.; Walther, J. H.; Jaffe, R. L.; Halicioglu, T.; Koumoutsakos, P. *Journal of Physical Chemistry B* **2003**, *107*, 1345.

(112) Rasaiah, J. C.; Garde, S.; Hummer, G. *Annual Review of Physical Chemistry* **2008**, *59*, 713.